Paradigmes de conception auto-adaptative pour le développement de structures à haute performance : du processus de fabrication au contrôle des vibrations en temps réel

Jessé Augusto dos Santos Paixão

THÈSE DE DOCTORAT DE L'ÉTABLISSEMENT UNIVERSITÉ BOURGOGNE FRANCHE-COMTÉ

PRÉPARÉE A L'UNIVERSITÉ DE FRANCHE-COMTÉ

École doctorale n° 37

Sciences Pour l'Ingénieur et Microtechniques

Doctorat de Mécanique

Par

Jessé Augusto DOS SANTOS PAIXAO

Paradigmes de conception auto-adaptative pour le développement de structures à haute performance : du processus de fabrication au contrôle des vibrations en temps réel

Self-adaptive design paradigms for the development of high-performance systems: from the manufacturing process to real-time vibration control

Thèse présentée et soutenue à Besançon, le 24 Novembre 2023

Composition du Jury :

Christophe Collette	Professeur des universités, Université de Liège	Président du jury
Marcelo Areias Trindade	Professeur des universités, Université de São Paulo	Rapporteur
Manuel Collet	Directeur de recherche, CNRS, École Centrale de Lyon	Rapporteur
Frédéric Demoly	Professeur des universités, UTBM	Examinateur
Peter Green	Maître de Conférences, Université de Liverpool	Examinateur
Scott Cogan	Chargé de recherche, CNRS	Directeur de thèse
Emmanuel Foltête	Professeur des universités, SUPMICROTECH-ENSMM	Codirecteur de thèse
Emeline Sadoulet-Reboul	Maître de Conférences, UFC	Invitée
Gaël Chevallier	Professeur des universités, UFC	Invité

Remerciements

C'est avec beaucoup d'émotion et de bons souvenirs que j'écris ce dernier chapitre, qui clôt une phase importante de ma vie, une aventure intense de trois ans à Besançon. Durant cette période, j'ai rencontré de nombreuses personnes qui ont participé de près ou de loin à cette aventure et qui ont marqué ma vie. J'essaierai de mettre des mots sur les sentiments de gratitude que j'éprouve à l'égard de chacune d'entre elles.

Je tiens tout d'abord à remercier les membres du jury pour leur participation à la soutenance de ma thèse, qui en a fait une expérience mémorable. Un grand merci aux rapporteurs Marcelo Trindade et Manuel Collet pour leurs lectures attentives du manuscrit et leurs suggestions très constructives. J'adresse également ces remerciements à Cristophe Collette, président du jury, et aux examinateurs Frédéric Demoly et Peter Green. Les échanges qui ont suivi la soutenance, les remarques et les suggestions précises ont été très enrichissants.

Je tiens à exprimer ma profonde gratitude envers mon équipe encadrante, Scott, Emmanuel, Emeline et Gaël, qui ont fait de cette aventure une belle expérience, agréable et enrichissante, tant sur le plan professionnel que personnel. J'ai eu l'immense privilège d'apprendre de vous vos différentes visions sur les problèmes scientifiques à travers vos expériences et vos spécialités, qui sont très complémentaires et qui ont été fondamentales pour atteindre les objectifs de cette thèse. Scott, toutes nos discussions, vos conseils pendant la thèse et les voyages à l'IMAC ont marqué cette expérience. Ta façon d'aborder les problèmes avec beaucoup de recul, tes idées originales et ton côté très humain m'ont beaucoup appris. Manu, je te remercie pour tes encouragements tout au long de la thèse dans les moments difficiles, lorsque la motivation manquait face à un problème sans solution apparente, tu avais toujours un mot d'encouragement qui me donnait la force de continuer. Ta façon particulière de voir la dynamique des structures, tant sur le plan théorique qu'expérimental, m'a toujours impressionné, merci beaucoup pour tes enseignements. Emeline, je me souviens encore du premier jour où Giovanna et moi sommes arrivées à Besançon, en plein confinement, et où tu es venue nous chercher à la gare Viotte. Tu t'es assurée que nous étions bien installés et tu nous as présenté la ville. C'était très réconfortant d'avoir ce soutien quand je suis arrivée dans un nouveau pays en pleine pandémie pour commencer mon doctorat. Je voudrais te remercier pour tous tes enseignements sur la modélisation de la dynamique des structures et de l'acoustique, qui m'ont beaucoup aidé, et pour nous avoir toujours orientés dans la bonne direction lors des réunions. Gaël, ce fut un plaisir de travailler avec toi, ta bonne humeur, ton enthousiasme pour chaque nouvelle idée ont rendu l'expérience plus agréable et ta vision pluridisciplinaire des différents problèmes explorés tant d'un point de vue théorique qu'expérimental a été riche d'enseignements. Je suis reconnaissant d'avoir eu le privilège de travailler avec chacun d'entre vous et je suis sûr que j'emporterai vos visions et vos enseignements avec moi dans chaque nouveau défi.

Je souhaite adresser mes sincères remerciements à l'ensemble du personnel du DMA qui ont contribué d'une manière ou d'une autre à cette thèse. Tout d'abord, à mes col-

lègues doctorants, avec qui j'ai eu le plaisir de partager de bons moments, des discussions, quelques parties de pétanque et de nombreuses tasses de café. Un merci tout particulier à mes amis du bureau 37H, avec qui j'ai eu le privilège de passer du temps au quotidien pendant cette période : Jamal, Lobna, Rafael Teloli, Haythem, Liam, Thibaud et Darian. Je garderai précieusement nos bonnes discussions, nos repas partagés et nos pauses café. Merci à Robin et Francesco pour l'aventure aux États-Unis pour l'IMAC. Merci aussi à Océane pour les moments partagés à l'école d'été de Toulouse. Merci à Shakiba et Johann pour les bonnes discussions lors des expériences réalisées au laboratoire. Un grand merci à Rafael Raqueti, Rafael Teloli (et Dani), João Pedro (et Cynthia) et Arthur, mes compatriotes, pour les bonnes discussions et les rigolades, qui ont apporté un peu du soleil brésilien même pendant les froides journées d'hiver à Besançon. Merci également à Delphine, Isabelle et Christine qui m'ont aidé dans toutes les tâches administratives avec beaucoup de patience. Merci à Thomas et Pierre pour leur aide dans la réalisation de certaines pièces mécaniques. Je tiens à remercier David Vernier pour toute son attention et son aide dans la réalisation des bobines. J'aimerais également remercier l'équipe informatique, en particulier Jérôme et Vugar, qui m'ont beaucoup aidé à résoudre certains problèmes techniques. Je tiens également à remercier les professeurs Morvan, Nouredinne et Vincent Walter avec qui j'ai eu le plaisir de côtoyer, tout au long de cette période.

J'aimerais aussi adresser mes remerciements à certaines des personnes que j'ai rencontrées à Besançon en dehors du laboratoire et qui ont marqué cette période. Je pense notamment à Gilson, Shirley et leurs fils Caleb, Nathan et Eli, avec qui nous avons partagé de nombreux bons week-ends et qui ont été comme une famille pour moi et Giovanna. Je tiens également à remercier Jacques et Françoise Roffidal, nos grands-parents français, qui nous ont beaucoup appris sur les particularités de la langue et de la culture française. Je suis également reconnaissant pour l'amour fraternel que nous avons trouvé chez les personnes que nous avons rencontrées à l'église baptiste de Besançon. Je tiens également à remercier nos amis Enzo et Concetta, qui nous ont aidés dans la préparation du cocktail après la soutenance, ainsi que Carl, Martine et Robert, qui sont venus me voir lors de la soutenance. Merci beaucoup pour tout votre soutien et vos encouragements.

Pour terminer, je voudrais remercier ma famille. Mes parents Marisa et José pour leur amour, leurs encouragements et leurs conseils tout au long de ma vie. Mes sœurs Mirian et Josiane pour leur soutien dans tous mes rêves. Mes beaux-parents Walter et Rosana et mon beau-frère Gustavo, pour leur soutien, même à distance. Enfin, je voudrais terminer en remerciant Giovanna, mon épouse bien-aimée qui n'a pas hésité à s'embarquer avec moi dans cette aventure dans un nouveau pays, à qui je dédie ce travail, pour tout son amour, sa patience et son précieux soutien quotidien, qui ont été fondamentaux pour moi lors de la réalisation de ce travail !

Contents

List of Figures

List of Tables

Chapter 1

Introduction

Contents

1.1 Context

Human beings have always designed things. A fundamental characteristic of humans is their ability to create a wide variety of tools and artifacts tailored to their needs [2]. As these needs evolve and individuals consider existing artifacts, improvements are introduced to refine them. Occasionally, entirely new types of artifacts are imagined and created in response to these changing purposes. This process has evolved from the creation of simple tools to today's complex engineering structures and systems, such as bridges, buildings, and airplanes.

In traditional craft-based societies, the design of objects was inherently intertwined with their manufacturing, and there was typically no preliminary step of drawing or modeling before the actual crafting of the artifact begins [2]. The design of the object usually would evolve over the course of its manufacturing through trial and error. For example, archers, who made bows for ancient archery, carved and shaped bows from wooden staves, refining the design by feel and testing the bow's performance by trial and error. In contrast, in modern industrial societies, the steps of designing and manufacturing products are usually separate in a sequential process. Typically, the process of manufacturing a product cannot begin until the design process has been completed. The manufacturing process then seeks to reproduce the defined design as accurately as possible. In this context, most of the important design decisions that will affect the final performance of the product are concentrated in the design stage, which tends to be longer the more complex the product. For example, the design phase of an airplane can take many years, whereas the manufacturing phase of each individual airplane can be completed in a matter of months. This traditional product development life-cycle is illustrated in Figure 1.1. While this was a major breakthrough, opening up the possibility of large-scale production and cost reduction, it brought with it the challenge of how to deal with the uncertainties that affect each step of the process from designing to operation.

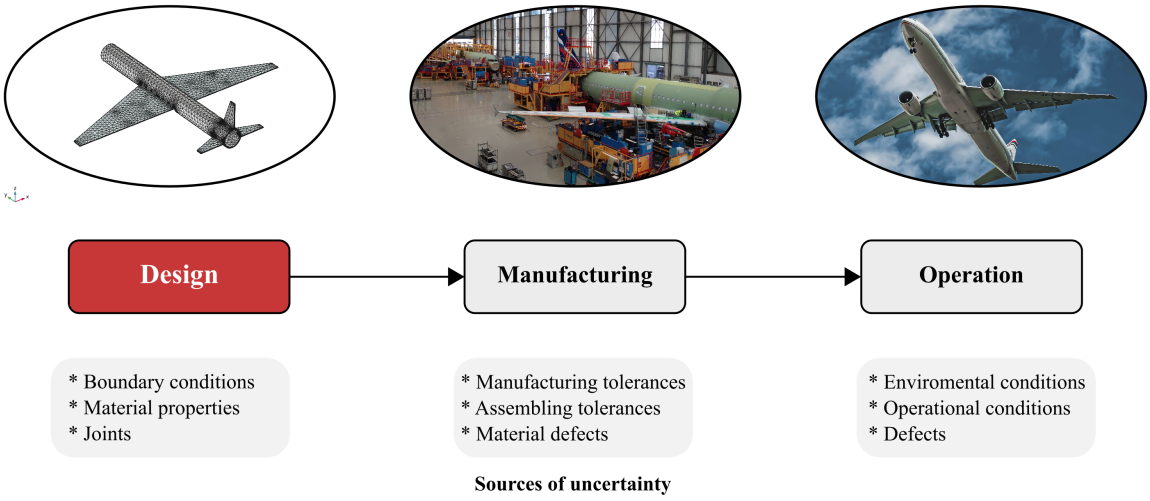

Figure 1.1: Traditional paradigm for development of structures and sources of uncertainties.

Sources of uncertainty are diverse in the development of engineering structures but generally fall into two categories: *aleatory* due to random process and *epistemic* resulting from a lack of knowledge [3]. These uncertainties may have a substantial impact on the final performance of the manufactured structure and may even jeopardize its operation. Although epistemic uncertainties can be reduced by increasing knowledge about the system and are therefore known as reducible, aleatory uncertainties are generally treated as irreducible due to their random nature. Therefore, a major challenge for the engineer is to ensure that the manufactured structure performs satisfactorily despite these unavoidable uncertainties.

In this context, robust design has emerged as a dominant strategy to improve product quality and reliability in industrial engineering by ensuring statistically acceptable performances of the manufactured products [4]. A product is said to *robust* when it is insensitive to the effects of sources of uncertainty, even through the sources themselves have not been eliminated [5]. The main steps of this design paradigm can be summarized as follows:

- define the design space with its design variables, objectives, constraints, and uncertainty models;
- leverage high fidelity physics-based models to specify product design providing acceptable performance under uncertainty;
- manufacture nominally identical or standardized products to design specifications.

While this paradigm based on the concept of robustness is omnipresent in engineering applications where complex and generally multiphysical systems must be designed and fabricated, it has a number of important drawbacks:

- the necessity of accurate modelling of all dominant sources of uncertainty to ensure reliable performance [6];
- the high cost of reducing manufacturing tolerances and modeling errors;
- an inescapable trade-off between performance and robustness to uncertainty [7].

The last point is of particular importance for high performance applications since for a given candidate design, changes introduced to guarantee acceptable performance under uncertainty translate to suboptimal designs with degraded performance. Moreover, it is very difficult to satisfy equality design constraints in a robust-design approach.

In this context, this thesis seeks to propose a paradigm shift to overcome the above limitations in the development of high-performance engineering structures. This paradigm shift relies on a modification of the traditional life cycle of structure development to introduce the bio-inspired concept of developmental plasticity, which will be discussed in more detail below. Although this paradigm shift addresses general engineering applications, in this thesis it will be explored specifically for applications in structural dynamics.

1.2 Robustness and developmental plasticity

Robustness is a concept that is relevant to many scientific disciplines, from engineering to biology [8]. In biology, it can be defined as the ability to generate identical phenotypes in the face of environmental perturbations and genetic variation. It is not only important for maintaining the function of an organism under challenging conditions, but it can also accelerate evolution by enabling the accumulation of cryptic genetic variation [9]. In engineering, although a unique definition does not exist, the term usually refers to the insensitivity to the effects of sources of uncertainty [10]. Despite their vastly different substrates, time-scales, and mechanistic implementation, biological and engineering systems share many similarities regarding the robustness concept [8]. An interesting analysis of these similarities, which goes beyond the scope of this thesis, is presented by Khammash [11] in his comparison between electronic amplifiers and gene expression circuits.

In the context of engineering, robust design methods were pioneered by Taguchi in the 1950s and early 1960s to meet the challenge of producing high-quality products in the Japanese manufacturing sector and have since been successfully applied to a wide range of sectors, including electronics, automotive, photographic and telecommunications [5]. Taguchi's robust design method is based on direct experimentation. The aim of the Taguchi's method is to identify the factors that have the greatest impact on the performance of a product or process and then optimize these factors to minimize the effects of variation. The fundamentals of robust design established by Taguchi have served as the basis for the development of so-called robust design optimization methods by taking into account uncertainties into the traditional structural design optimization problem. There is a vast literature on this topic that finds applications in various areas of engineering, in which it is possible to find many different formulations [12–16]. In this work, however, the focus will be on structural dynamics applications.

Robust design optimization methods have been widely investigated for structural dynamics applications in recent decades with the aim of improving the dynamic performance of structures in some of the classic problems like noise and vibration reduction, structural modification and energy harvesting. Dell'Elce et al [17] have proposed recently a robust equal-peak method for the design of tuned mass dampers considering a scenario approach, a general-purpose numerical method for robust optimization [18]. This method can significantly improve the performance on vibration attenuation of these devices in uncertain mechanical systems compared to the traditional method based on Den Hartog's equal-peak method [19]. Kim et al [20] investigated the robust design optimization of the design of a fixed-fixed beam piezoelectric energy harvester to maximize the power generated taking into account manufacturing uncertainties. Adamson et al [21] proposed a receptance-based robust method to improve the robustness of the design of mechanical systems with assigned natural frequencies in relation to identification uncertainties on the transfer function identification. Although all of the aforementioned meth-

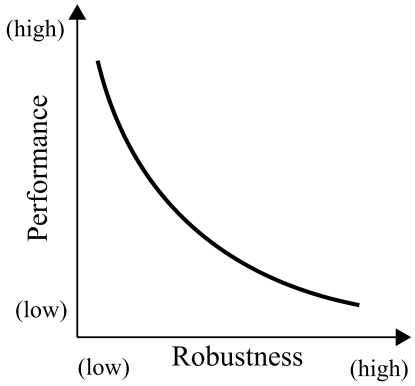

Figure 1.2: Illustrative example of the robustness and performance trade-off curve.

ods demonstrate a significant gain in the final performance of manufactured mechanical systems by adequately accounting for uncertainties in the design of structures, they are all based on the robust design paradigm and therefore are subject to limitation: an inescapable trade-off between performance and robustness to uncertainty, as illustrated in Figure 1.2. This means that in order to improve the performance of the structure, the designer must inevitably sacrifice robustness. While this compromise can be managed for certain applications where the level of uncertainty or performance requirements are low, it is extremely complicated in the context where high-performance structures are sought in the presence of a high uncertainty.

Biological systems face a similar trade-off scenario to survive in uncertain environments and rely on the concept of developmental plasticity to respond to changing environmental conditions during their growth. This concept, known as developmental plasticity, refers to a feature of development in which identical genetic backgrounds produce different traits in response to changing environmental conditions [22]. Consequently, developmental plasticity implies that a sensitivity to the environment, in contrast to the concept of robustness that suggests resistance to environmental changes, can actually accelerate the evolutionary process. This is achieved by eliminating selective constraints through conditional expression (plasticity) and concealing mutations from selection pressures (robustness). Recent investigations into developmental plasticity in both plants and animals have unveiled new insights into the underlying molecular mechanisms. These findings suggest that plasticity can facilitate adaptive changes, enhance diversity, and drive the emergence of novel traits in the evolutionary process [9].

Plants in particular have a unique potential to respond to changing environmental conditions during the development and formation of roots, stems, branches, leaves, and flowers. Despite being genetically encoded, they have a developmental plasticity that is critical for their survival as sessile organisms [23]. For example, genetically identical trees growing under different conditions of wind exposure will present stem thickening on the leeward side [24]. Moulia et al [25] investigated the mechanisms underlying this

mechanosensitive control of plant growth and broke it into the four processes illustrated in Figure 1.3: (1) bearing the load, (2) sensing the effect of the load distribution, (3) transducing the signal, and (4) responding by retuning the growth rate and direction. From an engineering viewpoint of the plant growth mechanism, the developmental plasticity of the system can be associated with the ability to modify its shape (design) during its growth (manufacturing) based on the transduction of signals from the environment in an interconnected process. This allows the system to perform optimally even in uncertain environments.

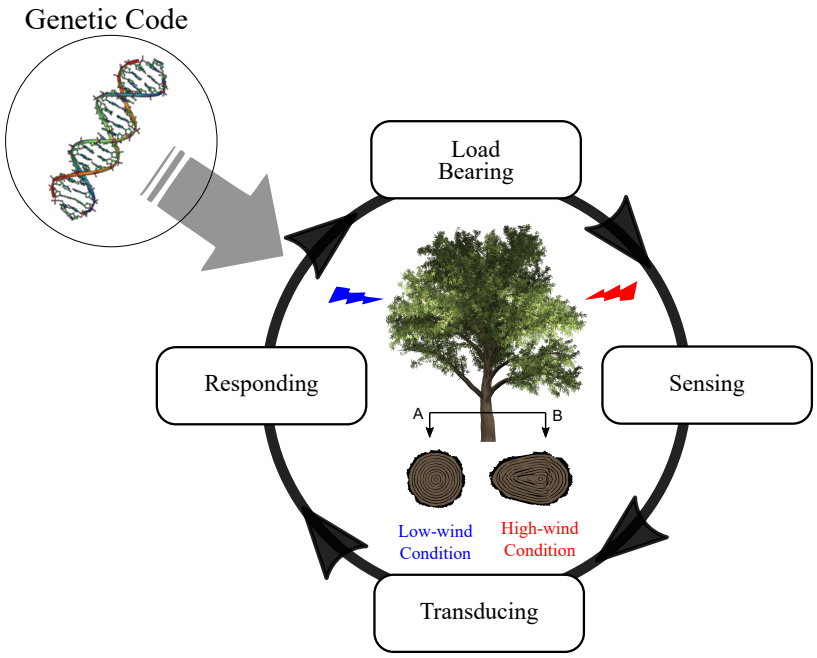

Figure 1.3: Schematic representation of the biological mechanism of mechanosensitive control of plant growth. Moulia (2015) presented a theoretical division of plants response to mechanical loads into four processes : load bearing, sensing, transducing and responding.

In this context, a paradigm shift is proposed herein to explore the concept of developmental plasticity in the fabrication of high-performance engineering structures with the aim of overcoming the previously discussed limitations of the traditional paradigm based on the concept of robustness.

1.3 A paradigm shift in the development of high performance dynamic structures

The thesis proposed in this work is that the analogy of the biological concept of developmental plasticity to applications in the development of engineering structures requires a paradigm shift that involves changes in two aspects: (1) in the way uncertainties are dealt with; and (2) in the sequential life cycle of design, manufacturing and operation. With respect to the first aspect, the key idea is to make the manufacturing of the struc-

ture sensitive to sources of uncertainty affecting the structure performance and provide it with the capacity to respond to this through design changes. This requires integrating the design and manufacturing stages in a closed loop, thus changing the traditional sequential process. In biological systems, this responsiveness can be observed throughout their life. For engineering structures, however, it is necessary to make a distinction between the development stage involving design and manufacture and the operation stage, since the design of a structure can hardly be modified in operation. To take this distinction into account, the term operational plasticity is proposed, which is applied at the stage of the structure's operation, when it is no longer possible to change its design. Therefore, two paradigms are proposed, schematically illustrated in Figure 1.4: the self-design manufacturing paradigm, which seeks to address uncertainties in the development phase; and the self-adaptive structures paradigm, which seeks to address uncertainties related to the operation of the structure.

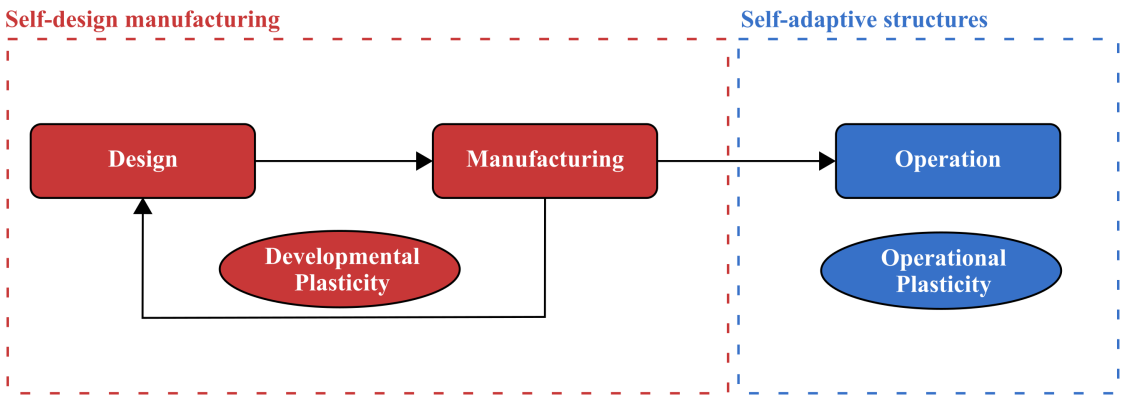

Figure 1.4: Schematic representation of the proposed paradigm shift based on the concepts of developmental and operational plasticity.

1.3.1 Self-design manufacturing paradigm

The self-design manufacturing paradigm translates the developmental plasticity based on a closed loop between the design and manufacturing process, taking advantage of physical intelligence to guide design changes *in situ*. The introduction of feedback loops in engineering applications is of course not new. Simple mechanical devices (e.g. water level control or centrifugal speed control [26]), active controllers (e.g. shape control [27]), metamaterials [28] , and self-programming networks [29], are just a few examples that implement closed loop processes to attain a sought after functionality. Living organisms display a rich variety of self-regulating or self-adapting processes, including homostasis [30], thigmomorphogenesis in trees growth [31], and Wolff's law for bone growth [32] to name but a few. These biological mechanisms are the embodiment of physical intelligence wherein information concerning the local state of an organism drives biological processes (e.g. targeted cell growth) to better meet the organisms performance require-

ments (e.g. zero stress gradients). Although physical intelligence has been observed in many living organisms, this concept has only recently been explored for engineering application, particularly focused in the robotic field for creation of autonomous machines. Sitti [33] defined it as 'physically encoding sensing, actuation, control, memory, logic, computation, adaptation, learning and decision-making into the body of an agent'. In the proposed paradigm, physical intelligence is derived from in-situ measurements and leveraged to drive with hardware-in-the-loop the manufacturing process.

1.3.2 Self-adaptive structures paradigm

The paradigm of self-adaptive structures seeks to provide operational plasticity for a structure in operation. In this phase, it is considered that the design of the structure can no longer be altered through a manufacturing process, but through functional mechanisms such as passive, active or semi-passive control. Although the concept of adaptive structures in the field of structural dynamics has already been explored in the literature with similar control mechanisms, the idea is fundamentally different in the sense that the latter seek to reduce sensitivity to uncertainties based on the concept of robustness, whereas the paradigm proposed here is based on the biological concept of plasticity and seeks to exploit this sensitivity through the capability of self-adaptation for the structure to adapt to the uncertainties affecting its operation. This idea can be compared to the adaptability explored in morphing structures, which has received much attention in the literature [34]. In morphing aircrafts, for example, the goal is to improve the aerodynamic performance of the aircraft for different flight conditions by adapting the shape of the wing during the mission [35, 36].

1.4 Objectives and outline of the thesis

The main objective of this thesis is to propose a paradigm shift in the development of high dynamic performance structures through the introduction of bio-inspired developmental plasticity. This general objective can be divided into the following specific objectives related to the scientific contributions described respectively.

- **Development of a methodology and experimental setup for implementing the self-design manufacturing paradigm in a demonstration case:**
  The proposed paradigm shift based on the concept of developmental plasticity depends on the integration of the manufacturing process, a real-time measurement system and a decision algorithm for modifying the initial design in a closed loop. Therefore, the implementation of this concept, which is being explored for the first time in the literature in the context of engineering applications, requires the development of a complex experimental setup.

- **Investigate decision-making algorithms to guide the modification of the structural design:**
  The key element to guide the process of modification of the structure to provide developmental or operational plasticity is the decision algorithm. The choice of the type of algorithm, the input data and its integration into the process is a challenging point. Therefore, one objective of this thesis is to investigate the performance of different algorithms.

- **Propose methodological and experimental solutions for implementing the self-adaptive structures paradigm:**
  The application of the self-adaptive structure paradigm is based on the concept of operational plasticity, which requires a mechanism and methodology capable of modifying the properties of the structure in operation. This is therefore one of the specific objectives of this thesis.

In accordance with the objectives listed above, this manuscript is divided into the following chapters:

Chapter 2 presents a methodology for implementing the self-design manufacturing paradigm in a demonstration case of manufacturing a vibration absorber. A brief review of absorber design methods is provided to support the simplified decision algorithm proposed to guide the design modification. A description of the experimental setup developed integrating a laser vibrometer inside a 3D printer is presented. Then, the experimental results of manufacturing some samples of a plate with the beam-like vibration absorber are discussed. This experimental application demonstrates the feasibility of the proposed methodology based on the self-design manufacturing paradigm. One of the main limitations of the proposed methodology is the simplified decision algorithm, which allows only two types of modification in pre-defined regions of the absorber, a problem that is addressed in the next chapter.

Chapter 3 investigates a new algorithm to guide the design modification of the self-adaptive manufacturing paradigm based on more than one source of information. The problem of assigning multiple natural frequencies to a plate-like structure with high accuracy is explored by numerically simulating the experimental application scenario of the proposed methodology, where design modification by additive manufacturing and *in-situ* vibration measurements at some points of the structure are considered. The results of the application of the proposed decision algorithm, which combines the methods of topological optimization and modal expansion to guide the process of modifying the design of the structure to assign the desired natural frequencies, are discussed.

At last, Chapter 4 proposes a methodology for applying the self-adaptive structures paradigm to the problem of vibration attenuation of harmonically excited structures using piezoelectric vibration absorbers with resonant shunts. The operational plasticity of the shunt circuit is achieved through a newly proposed semi-passive resonant shunt with

tunable inductance. A machine learning control method based on a Gaussian process regression model is used to drive the tunable inductance based on minimizing the time-averaged RMS response of the structure. The experimental application of the proposed strategy is presented to attenuate a single-mode of a simplified aircraft fuselage demonstrative structure.

1.5 Publications and communications

The research contributions of this thesis resulted in the publications and communications listed below. It should be noted that the preparation of this manuscript was based on the listed articles.

Journal Articles

- J. Paixao, E. Sadoulet-Reboul, E. Foltête, G. Chevallier, S. Cogan : **Leveraging physical intelligence for the self-design of high performance engineering structures**. – *Scientific Reports*, July 2022 (Published)
- J. Paixao, E. Sadoulet-Reboul, E. Foltête, G. Chevallier, S. Cogan : **Self-design Manufacturing for Assignment of Natural Frequencies via Online Topological Optimization**. – *Structural and Multidisciplinary Optimization*, (In Preparation)
- J. Paixao, E. Sadoulet-Reboul, E. Foltête, G. Chevallier, S. Cogan : **Self-adaptive piezoelectric vibration absorber with semi-passive tunable resonant shunt**. – *Journal of Sound and Vibration*, (In Review)

Conferences

- J. Paixao, E. Sadoulet-Reboul, E. Foltête, G. Chevallier, S. Cogan: **A Paradigm for Self-design Manufacturing: Application to a Tuned Mass Damper**. – *Journées Jeunes Chercheurs Acoustique vibration et Bruit*, November 2021, Compiègne, France
- J. Paixao, E. Sadoulet-Reboul, E. Foltête, G. Chevallier, S. Cogan: **Self-Design Manufacturing for Enhanced Structural Dynamic Performance**. – *IMAC XL*, February 2022, Orlando, USA
- J. Paixao, E. Sadoulet-Reboul, E. Foltête, G. Chevallier, S. Cogan: **Self-design Manufacturing for Assignment of Natural Frequencies via Online Topology Optimization**. – *IMAC XLI*, February 2023, Austin, USA
- J. Paixao, E. Sadoulet-Reboul, E. Foltête, G. Chevallier, S. Cogan: **Self-design Manufacturing Paradigm: Application to a Vibration Absorber**. – *SIM-AM*, July 2023, Munich, Germany

Chapter 2

Leveraging Physical Intelligence for the Self-design of High Performance Engineering Structures

Contents

2.1 Introduction

The analogy of the concept of developmental plasticity for engineering applications is attained by closing the loop between the design and manufacturing processes by allowing real-time product behavior to participate in its own design, and consequently by providing a developmental plasticity. The proposed bio-inspired self-design paradigm focuses here on the load bearing structural components of a complex engineering system and it can be divided in a similar way to the mechanosensitive control of plant growth process presented in the previous chapter (see Figure 2) into the four steps shown in Figure 2.1, summarized as follows : (i) manufacturing process - fabricate the nominal design; (ii) online testing - combine the manufacturing process with in situ testing – the physical intelligence - to drive real physical design modifications; (iii) decision algorithm - evaluate the system performance and decide to continue or stop the loop; (iv) design modification - propose the modification of the design based on data from the online testing to improve the system's performance.

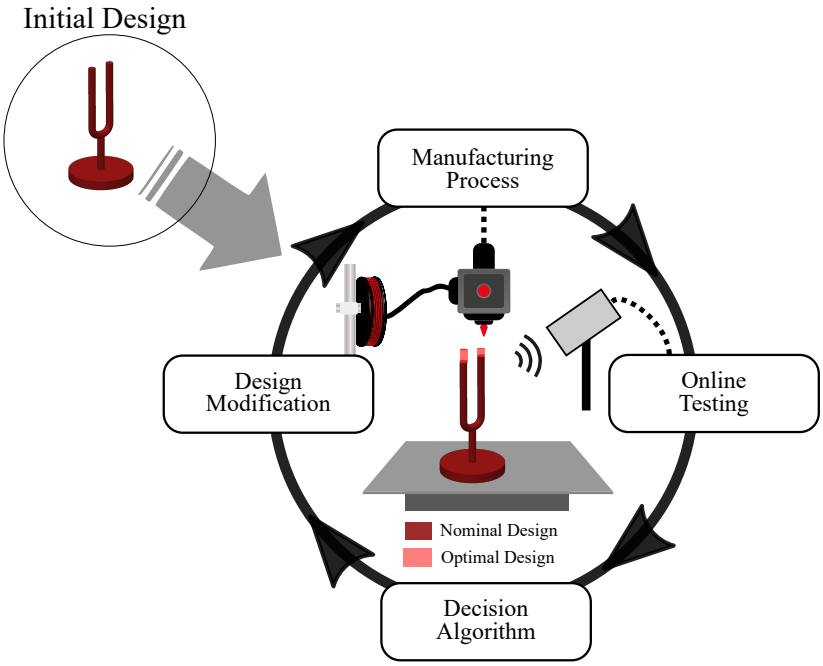

Figure 2.1: Schematic representation of the self-design manufacturing paradigm inspired by the biological mechanism of mechanosensitive control of plant growth.

The proposed self-design paradigm starts with an initial nominal design, which is modified along the closed-loop process, in order to manufacture tailored products with enhanced performance with respect to their standardized counterparts. In contrast to the model-based design approach, the main advantages of the self-design paradigm are: combine mass production approach with physical intelligence via real-time *in situ* performance measurements to yield optimal performances; circumvents robustness-performance trade-off by taking into account the true real-time behavior of the structure that implicitly depends on the specific realization of a statistical population under test; alleviates

the need for high fidelity models; guarantees enhanced performance with respect to a robust design based on computational intelligence; and leads to unique tailored designs. The bio-inspired self-design manufacturing paradigm proposed in this work is aligned with perspectives of the so-called fourth industry revolution which takes advantage of information from both the virtual and physical worlds (cyber-physical systems) combined with advanced manufacturing technologies to achieve flexible, smart, and reconfigurable manufacturing processes for the production of high-performance individualized products [37, 38]. Therefore, it is proposed in this work a new strategy for producing high-performance systems that circumvents the traditional practice of model-based design under uncertainty by directly observing the *in-situ* system response and adapting the design accordingly. This paradigm is particularly attractive in the current technological environment with availability of advanced information flow from cyber-physical systems and emerging manufacturing technologies. Additive manufacturing is particularly promising due to its versatility and ability to fabricate a product from scratch by continually adding material. However, uncertainties concerning the quality of additive manufactured products severely compromise its adoption in many industry sectors [39]. In this context, given the relatively high material and geometric uncertainties associated with this process, the proposed self-design paradigm is very attractive. Recently, some studies have explored the idea of a closed-loop quality control process to detect or correct defects to improve the reliability of manufactured parts, but based on the control of manufacturing process parameters, which is fundamentally different from the paradigm shift proposed in this work based on the developmental plasticity of the structure [40–42]. Herein, it is presented a demonstration case involving the design and additive manufacturing of a structure with an integrated device for vibration attenuation, a vibration absorber, whose performance is known to be very sensitive to mistuning. To the authors' knowledge, constraints on structural dynamic performance have not yet been introduced within a closed-loop design-manufacturing process.

2.1.1 Demonstration case

In order to demonstrate the potential of the self-design paradigm, the problem of vibration attenuation in mechanical structures was explored. Although has been intensively explored over the last century it remains an important challenge in engineering applications ranging from machinery to satellites [43]. A traditional method for suppressing vibration is through the use of vibration absorbers. This type of device was proposed by Frahm [44] to reduce the rolling motion of ships and essentially consists of an undamped mass-spring system, the absorber also called dynamic vibration absorber, whose parameters may be tuned at a specific frequency to attenuate the motion or vibration of the host structure where the device is connected. Later, Ormondroyd and Den Hartog [19] proposed to add a damper element to improve the vibration attenuation of the absorbers. In

this case, the vibration absorber is commonly named as tuned mass damper. Vibration absorbers are especially useful for mitigating narrow bandwidth vibration, and they must be designed in order to finely tune the operating frequency. Although, they have been used in numerous real-life structures due to their simplicity, effectiveness and low-cost, this kind of device presents a major drawback related to the high sensitivity to mistuning, which can degrade their efficiency in the presence of uncertainty and limit their application in the context of high-performance structures [17].

The effectiveness of a vibration absorber relies on tuning its resonance frequency and damping properties for a given primary structure, such that significant kinetic energy is transferred from the vibrating primary structure to the absorber. A very insightful real-life case concerning absorber tuning is found in the application of tuned mass dampers for the attenuation of lateral wind-induced vibration in tall buildings, such as Chifley Tower, Taipei 101 and Shanghai Tower [45, 46]. In this type of application, a pendulum-like vibration absorber consisting of a suspended mass is installed close to the top of the building. Although the device is designed based on a numerical model to achieve a maximum vibration attenuation of the fundamental lateral mode shape, due to the absorber high-sensitivity to mistuning and uncertainties related to the model and construction/installation of the device, a frequency adjustable mechanism is necessary. To make the absorber meet the expected design requirements in the installation process, the suspended mass is lifted with cables whose lengths are adjustable to ensure that the absorber frequency is consistent with that of the main structure. This adjustable mechanism allows a finely tuning of the absorber resonance frequency iteratively going from an initial cable length to a modified cable length to achieve an acceptable vibration attenuation performance.

A demonstration case consisting in the design and manufacturing of a beam-like absorber inserted into a plate for the vibration attenuation of its first mode, shown in Figure 2.2a, is presented in this work. Similar structures have been explored recently in the literature [47–49].The finite element simulation of the first mode of vibration of the simply-supported plate without and with the beam-like vibration absorber, shown in Figure 2.2b and Figure 2.2c, illustrates the effects of vibration attenuation caused by the insertion of this device into the host structure, which by destructive interference attenuates the targeted resonance frequency at the expense of two additional resonances, and a high amplitude of vibration of the absorber [50].

2.1.2 Vibration Absorber Tuning

This section briefly reviews the theory of vibration absorber tuning using a simple lumped mass model of the proposed demonstration case. The first vibration mode of the system, consisting in the plate with the beam-like absorber, can be modeled as two mass-spring-damper systems connected in series as shown in Figure 2.3a. The larger mass represents

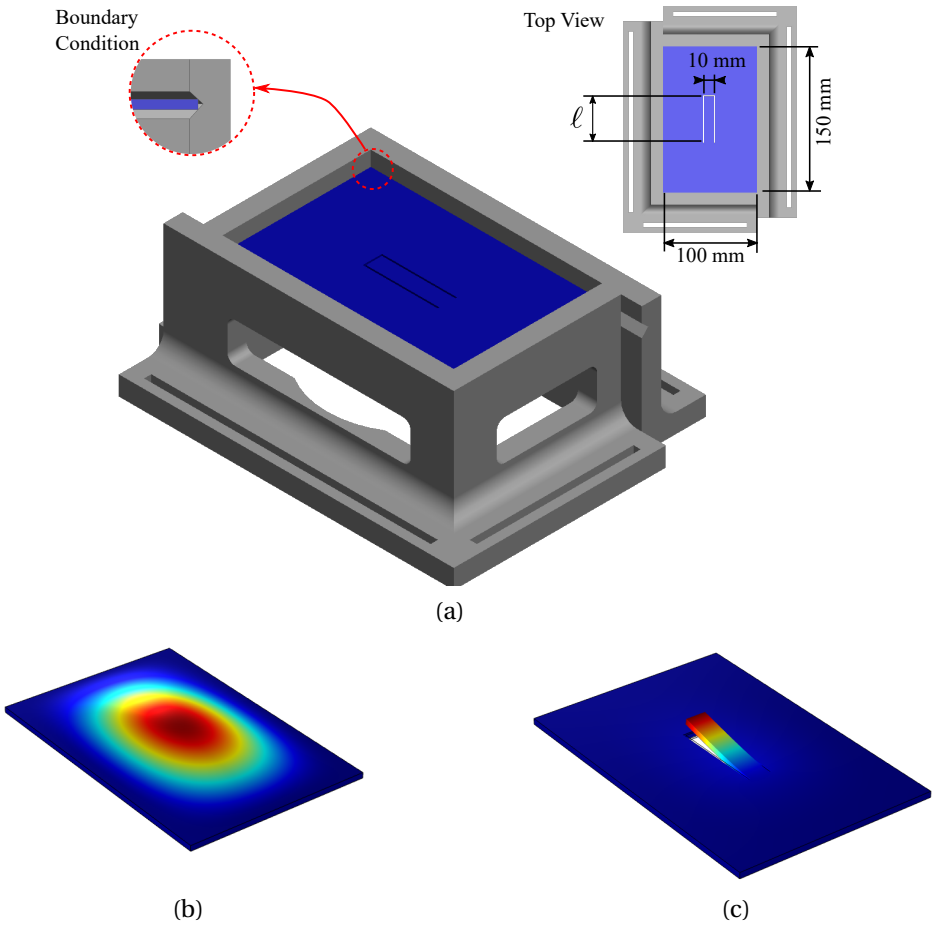

Figure 2.2: (a) 3D-view of the plate with beam-like absorber and the support structure and the first vibration mode shapes of the plate without (b) and with the beam-like absorber (c).

the host structure or primary system, the plate, and the smaller mass represents the absorber. The equations of motion in the frequency domain of the coupled system are :

$$\begin{bmatrix} k_1 + k_2 + i\omega(c_1 + c_2) - \omega^2 m_1 & -(k_2 + i\omega c_2) \\ -(k_2 + i\omega c_2) & k_2 + i\omega c_2 - \omega^2 m_2 \end{bmatrix} \begin{Bmatrix} X_1 \\ X_2 \end{Bmatrix} = \begin{Bmatrix} F(\omega) \\ 0 \end{Bmatrix} \tag{2.1}$$

where m_1, k_1 and c_1 denote the mass, spring and damper of the host structure; m_2, k_2 and c_2 their analagous of the absorber; and $X_1(\omega)$ and $X_2(\omega)$ are the displacements of the harmonically-forced host system and of the absorber.

The design of the absorber for vibration attenuation of a specific mode can be formalized as an optimization problem involving the minimization of the maximum amplitude ratio of the primary system's response to the excitation force, i.e., $G(\omega) = X_1(\omega)/F(\omega)$, the receptance. Although there is still a small amount of material damping in the beam-like absorber, which is inherent to the whole structure and represented in the lumped mass model by the damper elements, it can not be controlled for the vibration absorber tuning. This system behaves then more like an undamped vibration absorber than a tuned mass damper. Thus, if we consider the dampers of the system fixed and the mass and stiffness of the absorber the variables to be tuned, the tuning ratio between the resonance

frequencies of the absorber and the primary system can be used as the design variable and the optimization problem is posed as follows:

$$\gamma^{\star} = \arg\left[\min_{\gamma\in\mathbb{R}^{+}} \|\mathrm{G}(\omega \mid m_1, c_1, k_1, m_2, c_2, k_2)\|_{\infty}\right] \tag{2.2}$$

where $\gamma = \sqrt{k_2/m_2}/\sqrt{k_1/m_1}$ is the tuning ratio, $\|\mathrm{G}(\omega)\|_{\infty}$ represents the *H-infinity* norm of the receptance frequency response function (FRF) of the primary system, which means its maximum amplitude. Den Hartog [19] addressed this problem nearly a century ago when he proposed the equal-peak method based on the existence of two invariant points independent of absorber damping for the case of undamped primary system, which is widely used in many practical applications today. This method established the foundations of the equal-peak design by providing an approximate solution for stiffness and damping of a tuned mass damper. Surprisingly, an exact closed-form solution to this classic problem has only recently been discovered [51]. The equal-peak design can be extended for cases where the primary system is damped by adding hypothesis that the optimal solution satisfies the condition of two equal peaks about the targeted frequency, but requires numerical solution [52]. In this case, the problem is to find the design variables that will produce equal peaks around the targeted frequency, which depend on the tuning ratio between the host structure and the absorber damping. Although the original formulation of the equal-peak design is based on the minimization of the receptance, it can also be applied for mobility ($\mathrm{M}(\omega) = \dot{\mathrm{X}}_1(\omega)/\mathrm{F}(\omega)$) and accelerance ($\mathrm{H}(\omega) = \ddot{\mathrm{X}}_1(\omega)/\mathrm{F}(\omega).$), which are simple variations of the receptance case.

For the purpose of illustration, the receptance of the primary system ($m_1 = 10\,\mathrm{kg}$, $k_1 = 10\times10^3\,\mathrm{N\,m^{-1}}$ and $c_1 = 500\,\mathrm{N\,s\,m^{-1}}$) without the absorber and after its introduction considering different tuning ratios are presented in Figure 2.3b. The introduction of the absorber splits the single peak of the primary system without the device into two peaks corresponding to the vibration modes of the coupled system by causing an important reduction in the maximum amplitude of the receptance function and consequently to the vibration of the structure. The optimal solution for the tuning ratio of the absorber assuming mass and damping ratio are constant, is represented by the receptance with two equal peaks and it was obtained by the numerical optimization. Slight deviations from this optimal tuning ratio can significantly degrade the absorber performance by increasing one of the peaks depending on the deviation direction.

The two peaks, designated here by P and Q, represent respectively the first and second peaks observed about the targeted frequency. Figure 2.3c shows the behavior obtained by the numerical simulation of amplitude at these two peaks varying according to the tuning ratio, which reveals one point of intersection between the two curves, corresponding to the solution obtained by the equal-peak design. The relation between these two peaks provides information about the optimal design solution. If we represent this relation in

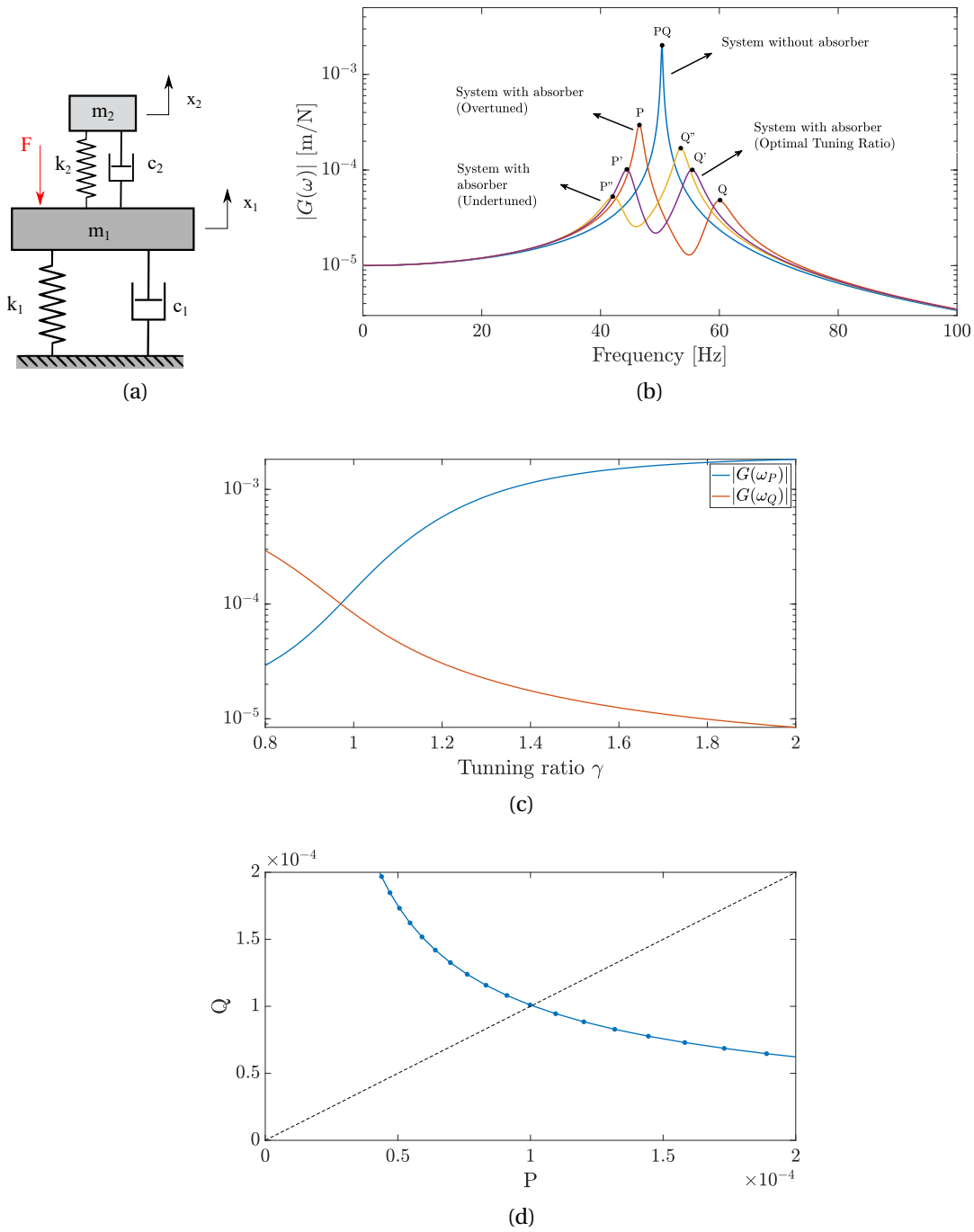

Figure 2.3: (a) One-dimensional lumped mass model of host structure coupled with a vibration absorber. (b) FRF for the primary system without the absorber (blue) and with the absorber considering different tuning ratios : undertuned (orange), optimal (purple) and overtuned (yellow). The two-peaks are identified sequentially as P and Q for the FRF of the system with the absorber and as PQ for the single peak for the FRF of the system without the absorber. (c) FRF peaks P and Q of the primary system versus tuning ratio γ. (d) Representation of FRF peaks into PQ space for tuning ratio varying from 0.8 to 1.2 .

a two-dimensional space, as shown in Figure 2.3d by plotting the amplitude of the first peak P by the second peak Q, a simple interpretation of the equal-peak design emerges, represented by the diagonal line where the amplitudes of the two peaks are equal. Hence,

the optimal design is achieved along the diagonal line. Design points in the PQ space located in the region above the diagonal present a tuning ratio lower than the optimal and those located below the diagonal have a higher tuning ratio. This representation will be further explored in the application of the self-design for the proposed demonstration case.

The solution of the optimization problem expressed in Equation 2.2 using deterministic methods is very sensitive to uncertainties which can degrade significantly the attenuation vibration performance of the manufactured vibration absorber. A robust design approach has been proposed to circumvent this issue by formulating the absorber design as a worst-case optimization problem. The key idea is to minimize the maximum response amplitude of the primary system among all possible outcomes over the uncertain set. The formulation of the robust design approach for the lumped mass model illustrated here taking into account uncertainties in the stiffness of the primary system is given by:

$$\gamma^{\star} = \arg\left[\min_{\gamma\in\mathbb{R}^{+}}\left(\max_{k_1\in\Delta}\|\mathrm{G}\,(\omega \mid m_1, c_1, k_1, m_2, c_2, k_2)\|_{\infty}\right)\right] \tag{2.3}$$

Dell'Elce et al [17] addressed this problem recently for a tuned mass damper, where the damping ratio of the absorber is also considered as design variable and they demonstrated that it can be solved numerically using the scenario approach, a general-purpose numerical method for robust optimization [53]. However, it is solved by means of a relaxed version of the problem, because the problem is generally unfeasible in the uncertain domain Δ, which can be a dense set and present an infinite number of constraints. Then, the problem is solved in a feasible subset of Δ of size defined based on the user-defined risk parameter ϵ, for which, the case $\epsilon = 1$ represents the solution of the deterministic problem formulated in Equation 2.2 and the case $\epsilon = 0^{+}$ represents the solution of the robust equal-peak design. The scenario approach is used here to solve the problem posed in Equation 2.3 using classical optimization algorithms with the associated confidence level β in the subset Δ_s which contain n instances or scenarios randomly extracted from the original uncertain set; the solution is only guaranteed with probability $1-\beta$ such that a realization of the uncertain quantities belongs to this subset is larger than a desired threshold $1-\epsilon$ [17].

The robust equal-peak design can significantly reduce a degradation in the vibration attenuation performance due to uncertainties when compared with the deterministic-based equal-peak design, as illustrated in Figure 2.4a. In this case, uncertainty was introduced in the stiffness of the primary system by sampling it from a uniform marginal distribution bounded between ± 20 % of its initial stiffness. For the designs based on the two approaches, deterministic and robust, 10000 random samples were generated considering the stiffness distribution, represented by the sample envelopes shown by the blue and red shaded regions in Figure 2.4a. Although, the robust equal-peak design attenuates the

effects of uncertainties in the FRF maximum amplitude, it presents an important drawback illustrated in Figure 2.4b, an unavoidable trade-off between the robustness and performance. The extreme case associated with the risk level $\epsilon = 100\%$ is associated with the solution of the problem considering the deterministic approach, where uncertainties are neglected. As the risk level decreases, there is an increase in the maximum amplitude of the FRFs of the of envelope of samples, since the effects of the presence of uncertainty are taken into account. Thus, there is a reduction in the attenuation performance of the absorber as the level of uncertainty considered increases, which characterizes the mentioned trade-off between robustness and performance.

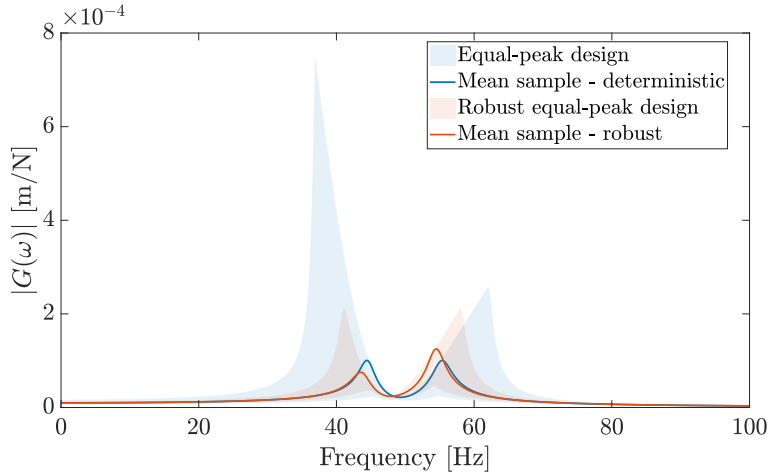

(a)

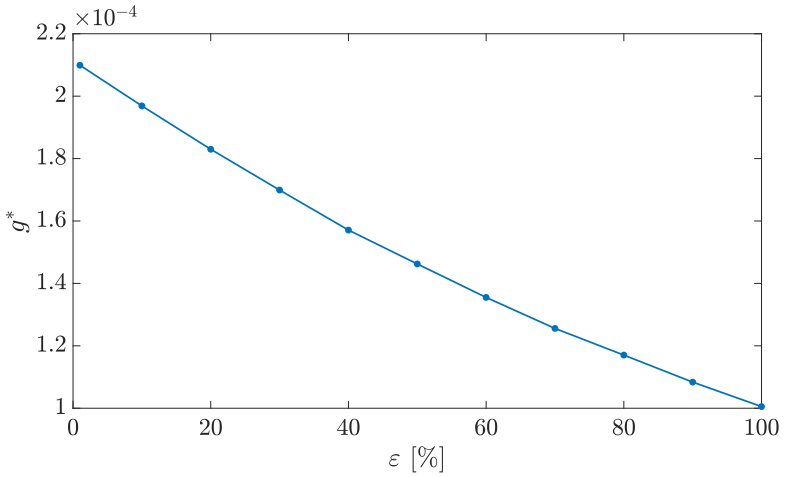

(b)

Figure 2.4: (a) Uncertainty propagation effects on the FRF of primary system for the vibration absorber design solution using the equal-peak (deterministic) and robust equal-peak (stochastic) approaches and the mean samples of FRFs. The blue and red shaded regions define the sample envelopes for the design based on the equal-peak and robust equal-peak methods, respectively. (b) Maximum amplitude of the FRF (g^*) in the envelope of samples considering the propagation of uncertainties using the robust optimization scenario approach as function of the risk level (ε). This function illustrates the trade-off between the performance and robustness in the robust-based approaches.

2.2 Results

2.2.1 Self-design manufacturing approach

The flowchart of the proposed approach for application of the self-design manufacturing paradigm in the demonstration case is illustrated in Figure 2.5. It starts with the initial design of the structure to be manufactured followed by the main loop containing the four steps of the self-design manufacturing paradigm – manufacturing process, online testing, decision making and design modification – until to obtain the final structure. Each step of this approach is discussed in the detail in the following sub-sections.

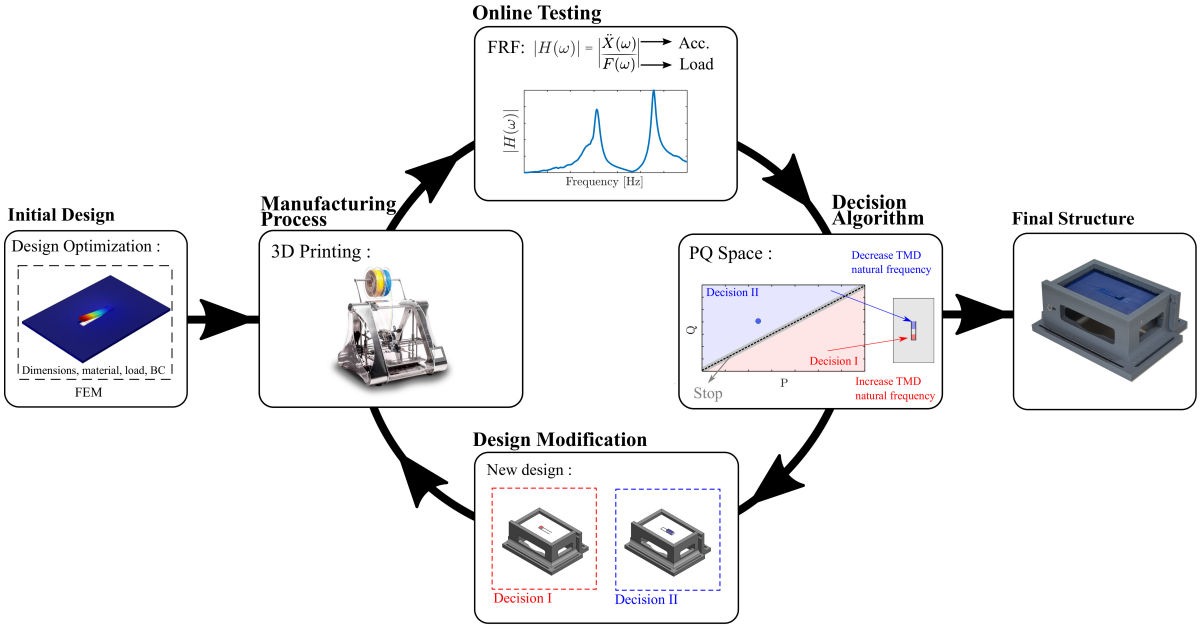

Figure 2.5: Flowchart of the proposed approach for the application of self-design manufacturing paradigm applied to the design of the vibration absorber

.

2.2.2 Initial Design

The proposed approach begins with the initial design of a beam-like absorber on a simply supported beam. The objective function is represented by the accelerance's maximum amplitude of the plate and the design variable is the length of the beam ℓ, which can be used to control the working frequency of the vibration absorber. Then, the design optimization problem is defined mathematically as follows :

$$\ell^{\star} = \arg\left[\min_{\ell \in [L_{min}, L_{max}]} \|H(\omega|\ell)\|_{\infty}\right] \tag{2.4}$$

where $\|H(\omega)\|_{\infty}$ represents the H-infinity norm of the accelerance FRF of the plate, and L_{min} and L_{max} are respectively the minimum and maximum length of the beam defined to guarantee its feasibility.

This problem is addressed by coupling finite element analysis with a gradient-based optimization method to iteratively update the beam length of the absorber from the initial guess to the optimal design, represented by the equal-peak design. The finite element model to simulate the structure was constructed using COMSOL. The plate was modeled with shell-elements using a mixed interpolation of tensorial components, with dimensions of 100x150x3 mm and the four edges simply-supported. This boundary condition was ensured by means of a V-groove supporting frame of the plate which prevents translation movements, but allows rotation in the perpendicular direction of the main vibration of the plate, an effective design solution for emulating simply-supported boundary conditions with thin plates, as recently demonstrated by Dumond et al [54]. The material properties were assumed to be linear elastic possess Young's modulus of 2174 MPa, density of 1120 kg/m^3 and Poisson's ratio of 0.35, values provided in the data sheet of the ABS material, manufactured by PolyLite. Modal damping values of 1.93 % and 2.10 % associated respectively with the first and second vibration modes of the structure were assumed based on identification with sacrificial samples.

The sequential quadratic programming algorithm, a gradient-based optimization approach, was used to solve the formulated design optimization problem. The objective function was defined as the *H-infinity* norm of accelerance FRF in frequency range selected between 50 Hz and 400 Hz, close to the targeted frequency. The position of the beam was defined as the center of the plate. Its width was set to 10 mm so that its first natural frequency was close to the first mode of the plate for a feasible length range. A gap of 1 mm was defined as the distance between the beam and the plate to allow the free part of the beam to vibrate without contacting the plate. The accelerance FRF of the plate considering the measurements at the point indicated in Figure 2.5 was obtained by the finite element model simulation. For the numerical optimization, the length of the beam was limited between lower and upper bounds defined respectively as 10 mm and 90 mm to ensure a feasible solution that is not larger than the dimensions of the plate and is not too small. The optimal beam length obtained by the optimization was 46.07 mm, for which the finite element model provides the accelerance FRF with two equal peaks, in agreement with the equal-peak design. The dimensions of the nominal design for the solution obtained are shown in detail in Appendix A1.

2.2.3 Integration of Manufacturing Process and Online Testing

The implementation of the proposed approach requires integrating the manufacturing process and the online testing system, so as to allow the real-time performance evaluation of the structure and modifications of the manufactured design. Additive manufacturing by fused filament fabrication with the 3D printer ZMorph model VX was used as manufacturing process. To perform the *in situ* online testing of the structure inside the 3D printer, a non-contact excitation and acquisition system was coupled to the 3D printer as shown

in Figure 2.6a. This system consists of a loud-speaker positioned below the structure to excite it and a vibrometer placed on the top of the 3D printer to measure the vibration of the plate at the measurement point indicated.

Figure 2.6b presents a schematic diagram of the experimental setup. The acquisition and generation of the signals are managed by a MATLAB script. The structure is acoustically excited by the loud-speaker TECTRON using a logarithm sine sweep signal varying from 10 Hz to 1500 Hz generated at a sampling frequency of 10 240 Hz by the computer's sound board and amplified into the BSK-1000 amplifier. The National Instrument board 9234 is used for the synchronized acquisition of the velocity measured by the vibrometer PDV-100 from Polytec and the voltage signal sent to the loud-speaker at the output of the amplifier. The signal processing of input voltage in the loud-speaker and plate's velocity measured at the measurement point is performed in real-time to estimate the accelerance FRF based on the H1 estimator. The sampling frequency and the duration of the acquisition signal provide a frequency resolution of 0.1 Hz, which allows the adequate identification of the natural frequencies and maximum amplitudes of the FRF of the structure for the proposed demonstration case.

The 3D printer communicates with the computer via an ethernet cable using the Telnet protocol. The machine is controlled by the MATLAB script developed to convert the geometry to be printed into the G-code programming language used by the 3D printer. Then, the initial design of the structure can be modified by printing new geometries over the structure. This requires just a calibration step of the initial position of the extruder in a point of reference of the structure. In this demonstration case, the reference point used to calibrate the position of the extruder is the vertex at tip of the beam. The MATLAB script described in this section to manage the experimental setup is available into the github repository [1]. Further details of the experimental setup are given in Appendix A1.

2.2.4 Decision algorithm and design modification

The simple decision algorithm proposed in this demonstration case is based on the equal-peak design represented in the PQ space. Although the initial design of the structure theoretically yields the maximum performance in vibration attenuation, this optimal point proves inadequate due to uncertainties affecting the manufacturing process, environmental conditions and the model, as well as the absorber high-sensitivity to the mistuning. The decision algorithm will use the experimental evaluation of the structure performance obtained from the online testing system to decide if a design modification could improve the vibration attenuation performance of the absorber in order to achieve the requirements specified by the user.

The equal-peak design provides the condition for the absorber's optimal performance and it will be the basis for the decision algorithm. In the PQ space, the equal-peak de-

[1] https://github.com/jessepaixao/EASER

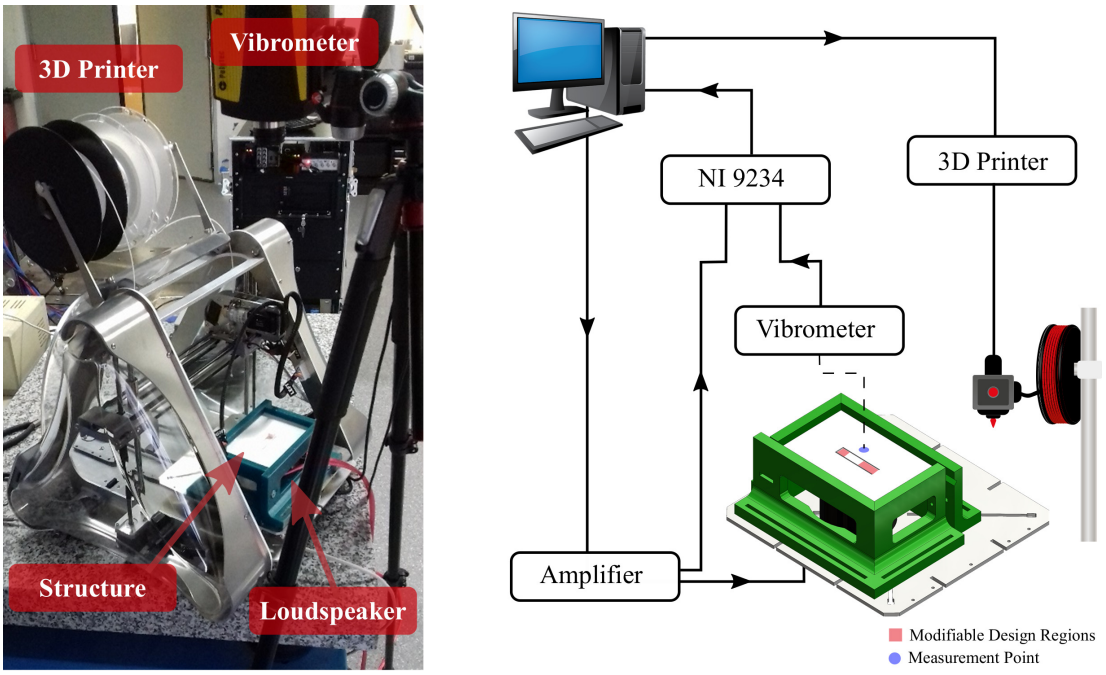

(a) (b)

Figure 2.6: Setup used to implement the self-design approach for the additive manufacturing of the proposed structure. (a) Photograph of the system, (b) Schematic representation of the experimental setup.

sign is represented by the diagonal line in the plane. Then, the main goal of the decision algorithm is to move the point representing the structural design in the PQ space closest to this diagonal line. If the point is close enough based on a user defined threshold value (T_h), no design modification is required and the decision algorithm can stop. The diagonal line divides the PQ space into two regions indicated in Figure 2.5, one represented by the blue color, associated with the absorber resonance frequency lower than the optimal and another represented by the red color, associated with absorber resonance frequency higher than the optimal. Then, according to the location of the point in the PQ space a decision of the design modification will be defined in order to achieve the main goal.

The problem of improving the vibration attenuation performance of the structure can be seen as the absorber resonance frequency tuning. Because the absorber is a beam, it simplifies the definition of the design modifications to change its resonance frequency. To decrease the resonance frequency of the beam-like absorber we defined the first design modification as adding mass at the free-end of the beam by means of the 3D printing of a 10x10 mm square with a height of 0.2 mm; and in the other sense, to increase the resonance frequency of the beam, we defined the second design modification as increasing the beam rigidity by adding mass in the form of a rectangle of 10x20 mm with a height of 0.2 mm at the beginning of the beam. The layer height of 0.2 mm was defined based on experimental tests of printing new layers on a sample with different thicknesses and for which it was found that the thickness of 0.2 mm was the minimum thickness for which

there was no defect of the layer detaching during printing. These two design modifications are illustrated in the Figure 2.5.

Thus, the decision algorithm can mathematically summarized as follows :

$$D = \begin{cases} \text{Decision I} & \text{if } P > Q + T_h \\ \text{Decision II} & \text{if } P < Q - T_h \\ \text{Stop} & |P - Q| \leqslant T_h \end{cases} \tag{2.5}$$

2.2.5 Application of self-design manufacturing approach

The vibration attenuation effect caused by the introduction of the beam-like absorber in the plate structure can be observed in Figure 2.7a by comparing the frequency response function of the samples of the plate without the absorber with those with the absorber. The samples of the plate without the absorber are identified as P1, P2 and P3; while the five samples of the plate with the beam-like absorber are identified as PB1, PB2, PB3, PB4 and PB5. Even though the samples manufactured present a unique nominal design, important differences can be observed between their frequency response functions regarding the resonant frequencies and the amplitudes. These differences are due to the uncertainties affecting the manufacturing process, material properties, environmental conditions, boundary conditions, etc. Each manufactured sample can be seen as an unique system that will converge to different equal-peak designs achieved via the self-design approach.

The representation of the data in the PQ space given in Figure 2.7b provides a more insightful interpretation of the vibration attenuation performance. As long as the frequency response function of the plate without the absorber has only one peak around the required frequency, it can be represented in PQ space using a one-dimensional space and then in the diagonal line. A comparison between the cluster of points from the samples without and with the absorber reveals an important attenuation of vibration. However, as can be seen, the points representing the plates with absorber are far from the diagonal line, which is a graphical representation of the equal-peak design and then of the optimal performance. This is expected due to uncertainties affecting the process and the high sensitivity of the vibration absorber to mistuning. The major purpose of using the self-design manufacturing approach is to attain the equal-peak design, which is represented visually as pushing the points closer to the diagonal.

The real-time evolution of the application of the self-design manufacturing approach in each one sample with the vibration absorber is presented from Figure 2.8a to Figure 2.8e by representing the frequency response function of three selected steps and H_∞ along all the steps until the algorithm stop. It can be observed an important reduction in the H_∞ from the initial step to the last step in all samples as the two peaks observed in the frequency response function approach the equal-peak condition. Specifically, the observed percentage reductions in the norm-infinity of the FRFs of each sample are respectively

22.6%, 15.3%, 30.6%, 1.6% and 8.6%.

The representation of the peaks of the accelerance FRF in the PQ space of samples manufactured presented in Figure 2.8f guided the decision algorithm along the main loop of the self-design manufacturing approach. The design modifications introduced in the strucures by using the simple decision algorithm proposed, moved the initial points of the samples into the PQ space to a region closer to the diagonal line, which represents the optimal performance for vibration attenuation of the absorber. Although one could expect a convergence of samples to the same performance and design modifications, it is worth noting that the uncertainties in the manufacturing process affects each sample differently, which explains the differences observed in each sample.

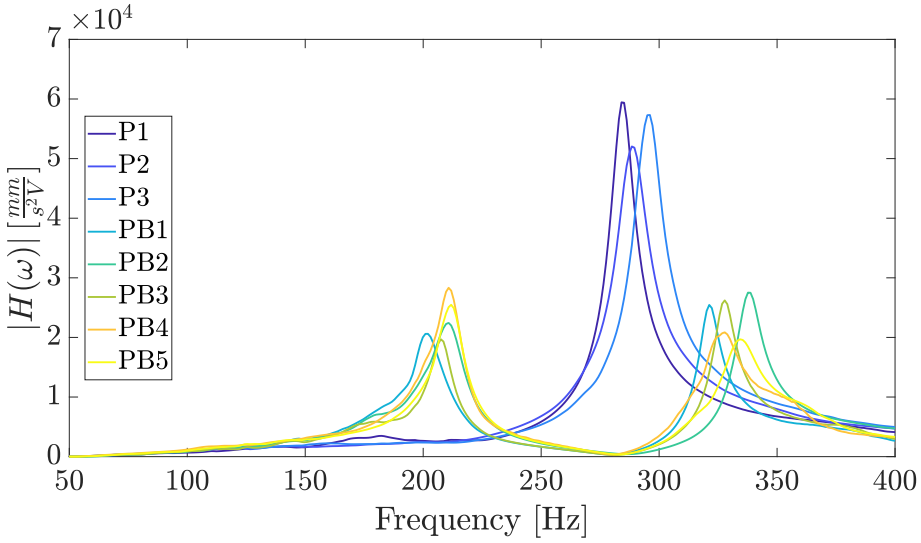

(a)

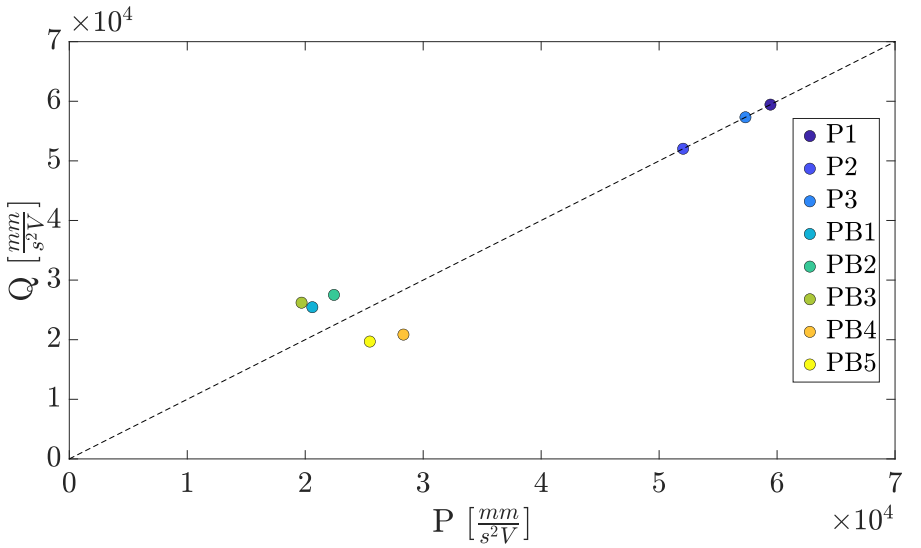

(b)

Figure 2.7: Frequency response function of nominal identical 3D-printed samples of the plate without the absorber and the plate with the beam-like absorber.

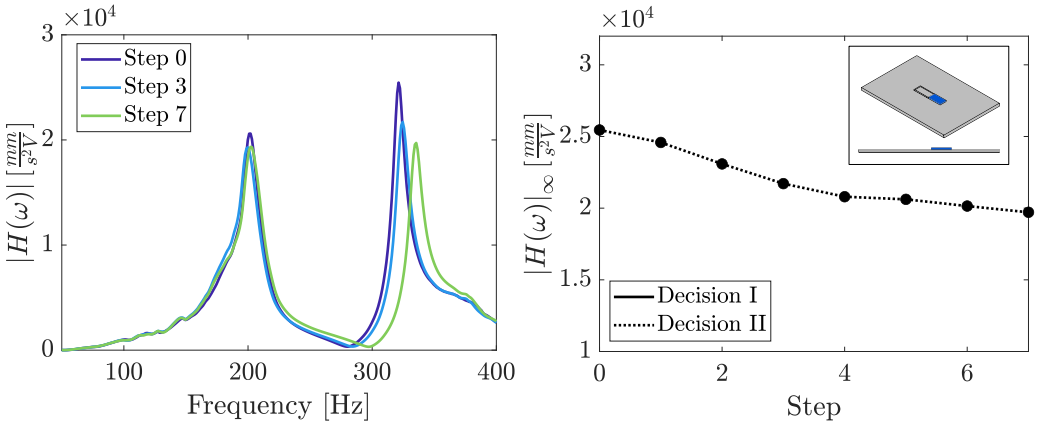

(a) PB1

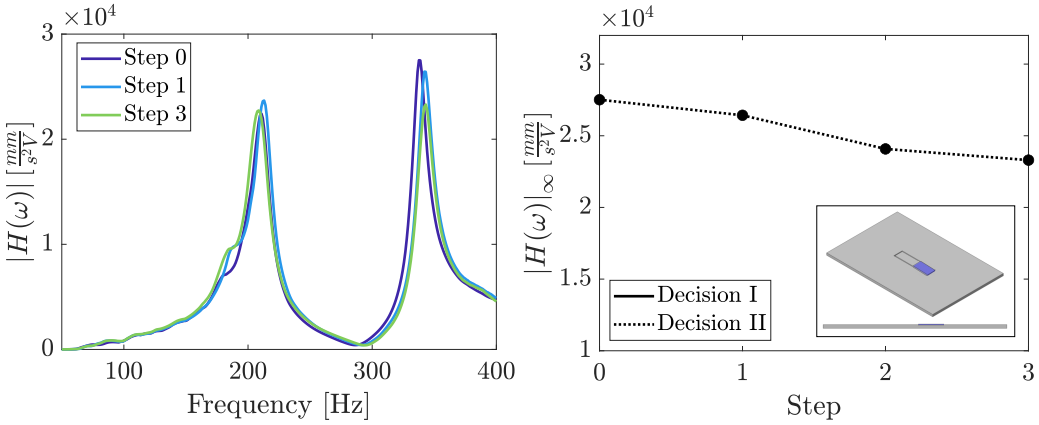

(b) PB2

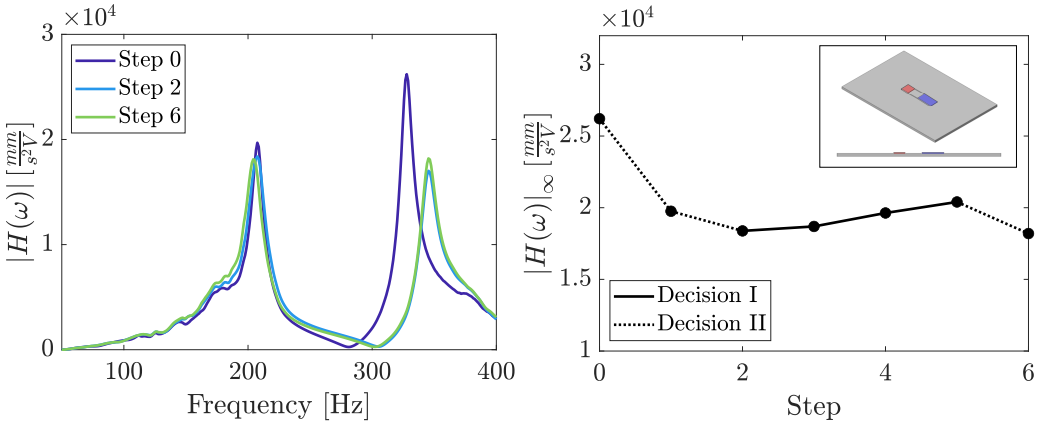

(c) PB3

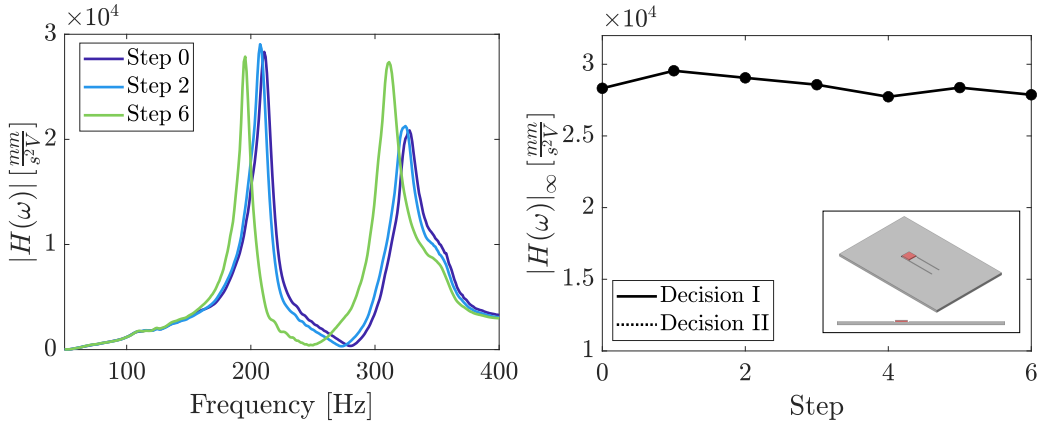

(d) PB4

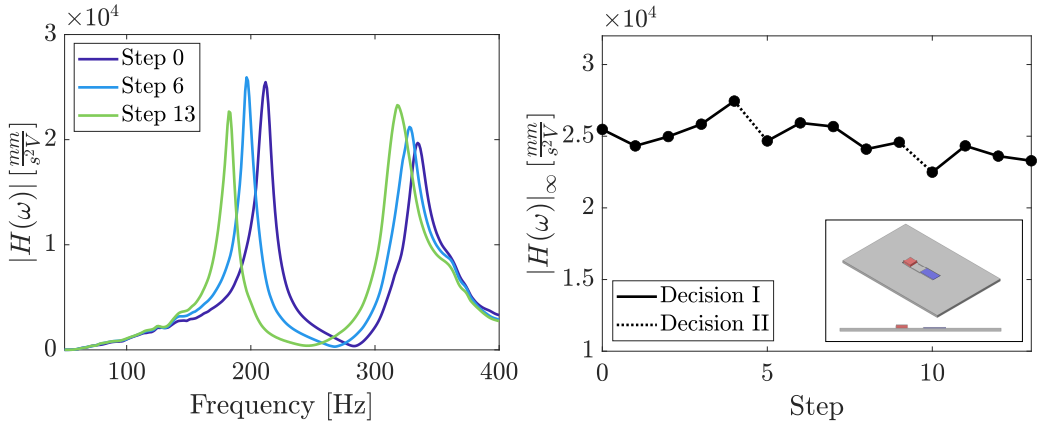

(e) PB5

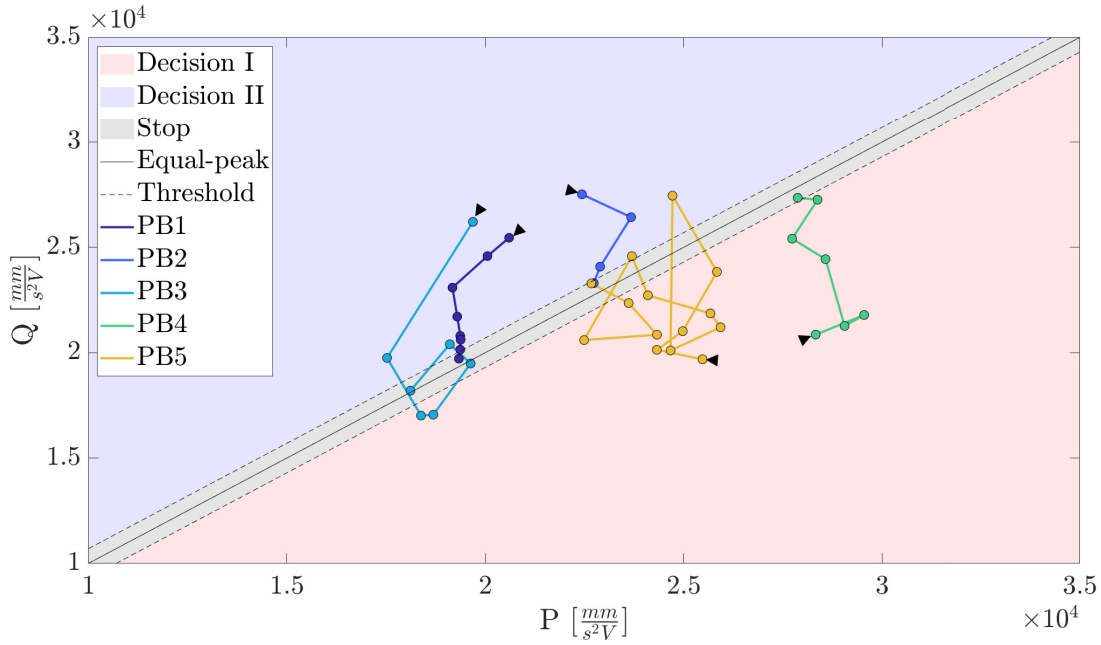

(f) PQ Space

Figure 2.8: Accelerance FRF and vibration attenuation performance index $|H(\omega)|_\infty$ evolution along the steps of the loop of the self-design manufacturing approach for the samples : (a) PB1, (b) PB2, (c) PB3, (d) PB4 and (e) PB5. (f) Representation of the FRF peaks evolution in the PQ space along the steps of the loop of the self-design manufacturing approach. The decisions made by the decision algorithm in each step are represented by the background colors corresponding to the point location. The threshold value for stop-decision are represented by the dashed diagonal lines and equal-peak design by the solid diagonal line.

2.3 Discussions

The vibration absorber application was specifically chosen here for its high sensitivity to manufacturing uncertainty and the inherent difficulty of achieving a high performance vibration attenuation with the traditional model-based robust-design approach. In the present case, five nominally identical but different samples served as a starting point for the self-design process. Each starting sample has different dynamic behaviors as seen in Fig. 2.7a. All structural modifications were restricted to the beam-like absorber and the final designs converged to different beam profiles. Meanwhile, the performance of each sample improved through the iterative closed-loop manufacturing process.

The emergence of the fourth industrial revolution embodying cyber-physical manufacturing technologies provides the necessary ingredients for deploying the proposed self-design manufacturing paradigm. By introducing a developmental plasticity in the manufactured structure, an enhanced performance can be achieved in the presence of uncertainty in the manufacturing process itself. Applications of greater complexity can be envisioned integrating different manufacturing processes, embedded sensors and more sophisticated decision algorithms.

The self-design manufacturing paradigm is particularly attractive for applications whose performance depends on satisfying equality design constraints can benefit from this new paradigm. There is a broad range of engineering applications where the self-design manufacturing paradigm is well adapted, in particular the production of high-performance customized products, including space observation applications, noise and vibration protection devices, sports equipment, musical instruments, medical prostheses, and optimized supports for passive and active metamaterials [55–58].

2.4 Conclusions

In this chapter, it was presented a new self-design manufacturing paradigm for engineering applications that closes the loop between design and manufacturing process by leveraging physical intelligence in the form of real-time experimental observations, thus providing design developmental plasticity to the manufactured product. The proposed shift provides a novel strategy to circumvent the unavoidable robustness-performance trade-off of traditional model-based robust-design approaches using a sequential design-manufacturing process. The potential of the proposed approach is illustrated in the design and 3D additive manufacturing of a beam-like absorber structure integrated in a plate whose sensitivity to uncertainty is well-known. The developmental plasticity inherent in the self-design approach yielded tailored designs for each sample, based on a simple decision algorithm, with a concomitant gain in the vibration attenuation ranging from 1.6 % to 22.6 %. This application demonstrates the effectiveness of the methodology in accounting for manufacturing uncertainties while reducing the dependency on costly

high-fidelity physics-based models. The self-design manufacturing paradigm requires a complex integration between the manufacturing process, the online testing system and the decision algorithm for design modification. Future challenges include managing a large number of design degrees of freedom, increasing the number of experimental observation points via full-field measurements or distributed embedded sensors, and decision making under non-unique design paths.

Chapter 3

Self-design Manufacturing for Assignment of Natural Frequencies via Online Topology Optimization

Contents

3.1 Introduction

The assignment of natural frequencies is an important problem in the design of engineering structures since it has a significant impact on the dynamic performance of the structure. In some cases, such as the design of airplanes, bridges and pipelines, it is sought to shift the natural frequencies away from their frequency range of excitation to reduce structural vibration and deformation in order to improve safety by avoiding resonances [59, 60]. In other cases, such as the design of vibration absorbers, resonators, and musical instruments, which are structures whose performance depends on the resonance of specific frequencies, the aim is to precisely tune the desired natural frequencies. This latter application scenario therefore requires tighter design tolerances in order to achieve the fabrication of a high-performance structure.

The problem of natural frequency assignment can be approached in two different stages of the development of a structure: (1) in the design stage, as an optimization problem of the nominal design; or (2) after manufacturing, as a problem of structural modification of an existing design. In the first approach, the assignment of natural frequencies is formulated as an optimization problem of the design variables of the structure based on the predictive modeling of the frequencies, in which methods of optimization of size, shape and topology stand out. Numerous works in the literature have investigated the application of multilevel optimization techniques with frequency constraints for size and shape in complex structures like aircrafts, cars and truss-like buildings [61, 62]. Recently, topology optimization methods have received a significant amount of attention driven by advances in additive manufacturing [63, 64]. Although the approach of assignment of natural frequencies in the design stage presents well-established methods, due to its high dependence on the model's prediction accuracy, they are mostly effective for the application scenario where it is desired just to shift natural frequencies away from a certain range, generally taking into account a safety margin translated by an *inequality* frequency constraint. As pointed out by Mottershead and Ram [65], for applications where it is desired to obtain structures with specific natural frequencies such as in vibration absorption problems, that requires an equality frequency constraint, this strategy is ineffective due to uncertainties affecting the modeling and manufacturing process. This challenging scenario requires an approach where the dynamics of the structure can be adjusted while it is built, for which the structural dynamics modification approach is particularly well suited.

The structural dynamics modification approach has been widely studied in this particular context through its inverse formulation, where the modification necessary on the structure is sought in order to assign the prescribed natural frequencies. This complex problem has been frequently addressed by receptance-based methods, originally proposed by Weissenburger [66]. It relies on point mass or stiffness modifications of the structure derived analytically to assign a set of eigenfrequencies of the receptance based on a matrix inversion problem. This method was later extended for damped structures

by Pomazal [67]. An important aspect of receptances is that they can be obtained directly from experimental identification. What makes it possible to predict the receptances of a modified system from the experimentally identified receptances of the original system, a technique known as pseudo-testing and widely used by Lallement and Cogan [68, 69]. Receptance-based structural modification methods are still a topic of intense research for dynamic performance assignment problems regarding natural frequencies, mode shapes and anti-resonances [70–72]. Although significant advances have been made in the applications of these methods over time, as pointed out by Balmes et al [73], they struggle with the main limitation of this methodology, which is that the modifications are considered as point masses or relative springs and dampers between nodes, very difficult to translate into physical modifications of the real structure.

In a novel way to address this limitation Balmes et al [73] have recently proposed a methodology combining structural dynamics modification and structural optimization approaches to get the best of both worlds: the ability to work with the real behavior of the structure extracted experimentally through its receptance from structural modification; with the high geometric resolution offered by the optimization of finite element models from structural optimization. They applied it to propose the structural modification of the thickness map of an industrial brake system with the aim of separating two modal frequencies to prevent brake squeal. To combine the two approaches, correlating the experimental measurements with the finite element model of the structure, they used modal expansion via the Minimum Dynamics Residual Expansion method. The results presented for a demonstration in a numerical model are promising reaching a frequency shift of 3% between two modes. However, it should be noted that in that work they performed the structural optimization by sensitivity analysis, only analyzing the direct effect of the structural modification. Also, they applied it in the context of maximizing the difference between the natural frequencies of two consecutive modes.

In this chapter we propose to combine structural dynamics modification with topology optimization method and apply it in the slightly more challenging context of assigning prescribed natural frequencies with high accuracy. As proposed by Balmes et al [73] we use modal expansion to correlate experimental data and a finite element model, but using a different technique of modal expansion [74]. It is important to note the subtle difference in the application of the topology optimization algorithm, which instead of being used to obtain the nominal design of the structure, is applied to guide the structural modification with a high geometric resolution. Moreover, combining it with modal expansion reduces the dependence on a high-fidelity model, since information from experimentally observed data is updated. As such, one of the main limitations of model-based structural optimization methods, which is the high dependence on the fidelity prediction can potentially be overcome. The application of the proposed methodology is presented numerically in a demonstration case where the goal is to obtain a simply supported plate with the first three resonance frequencies precisely assigned to defined values.

This chapter is organized as follows: in Section 3.2 the numerical demonstration case is first described, followed by the detailed presentation of the proposed methodology. Section 3.3 is dedicated to the analysis and discussion of the results; and finally the conclusions are summarized in Section 3.4.

3.2 Structural modification driven by topology optimization for natural frequency assignment

3.2.1 Case description

The problem of interest in this chapter is the assignment of natural frequencies in plate-like structures. To help illustrate the methodology and its challenges, the design case of a simply supported plate with multiple natural frequencies assigned with high precision is presented. The realization of such structures with frequency constraints is extremely useful in manipulating the dynamic characteristics in a variety of applications. The main goal in the case proposed here is to realize a thin plate of $100 \times 100 \times 2$ mm made of Acrylonitrile Butadiene Styrene (ABS) with its first three natural frequencies assigned with high precision. By considering the thickness profile of the plate as a design variable, the design to satisfy the desired natural frequencies can be obtained through structural optimization methods based on a finite element model of the structure (see Appendix A2.2 for an application example). However, current solutions for realizing this type of structure with precisely assigned natural frequencies using the traditional paradigm are extremely challenging due to the presence of modeling uncertainties and those related to the manufacturing processes due to the trade-off between robustness and performance, which in this case is related to the precision of the frequencies.

In this context, the self-design manufacturing paradigm, based on the concept of developmental plasticity, seems an appropriate solution to overcome the aforementioned limitations. Although the methodology proposed in the previous chapter for its application to the fabrication of absorbers proved to be effective, it relied on a simplified decision algorithm to guide the design plasticity with limited possibilities for structural modification. Hence, a new decision algorithm to guide the structural modification referred here as online topology optimization to address the proposed problem of assignment of natural frequencies will be investigated. The numerical demonstration case proposed here is formulated for future experimental application based on the experimental apparatus developed in Chapter 1 which employs an additive manufacturing process. It is therefore important to note that the structural modifications considered in the physical structure will be limited to adding material to the plate by modifying its thickness profile.

In the self-design manufacturing paradigm, the decision algorithm is responsible for proposing a modification to the design of an existing physical structure, based on experi-

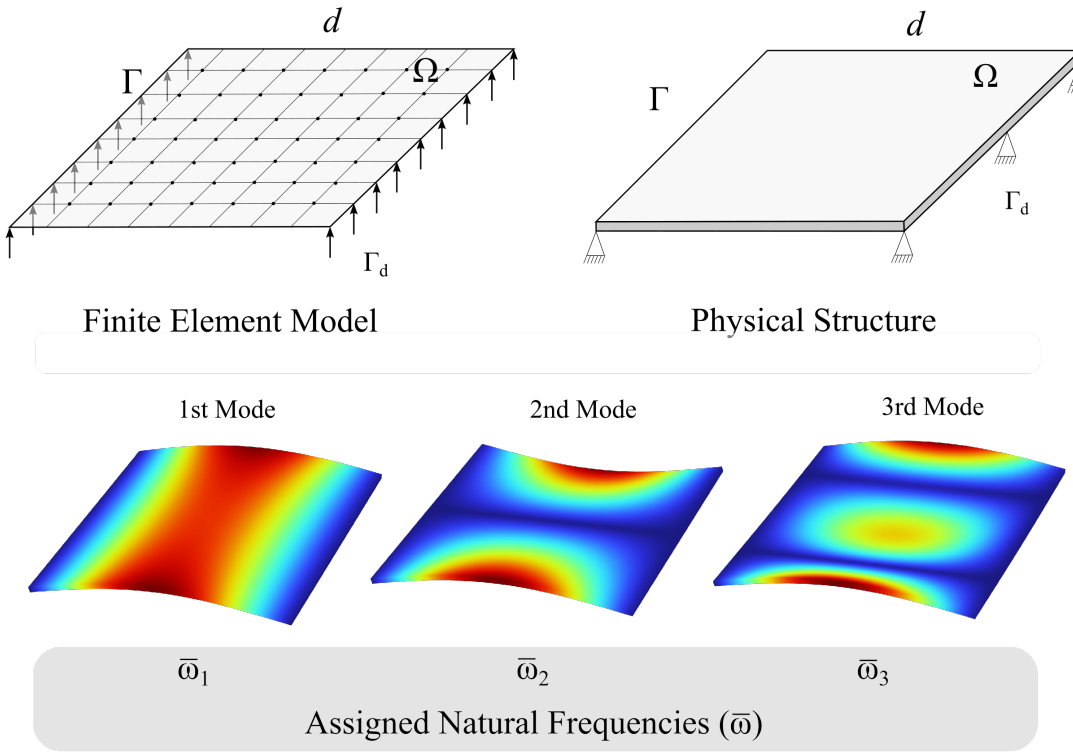

Figure 3.1: Problem statement of the proposed case of multiple natural frequencies assignment with high-precision in a plate-like structure.

mental data, with the aim of improving the performance of the structure to be manufactured. Therefore, the development of the algorithm is based on the scenario defined by three hypotheses. A first hypothesis considered is that the realization of an initial design of the structure already exists, thus the physical structure. A second hypothesis adopted is that a verified and validated finite element model of the structure with the nominal design is available. A third and last hypothesis is that the displacement of the physical structure can be experimentally observed at defined points, also observable in the FEM, in order to identify its natural frequencies and mode shapes. The hypotheses adopted here adequately represent, without loss of generality, the scenario of application of the structural dynamics modification approaches. Therefore, the developmental plasticity provided through the self-design manufacturing paradigm is addressed in this demonstration case based on the formulation of a structural dynamics modification problem, where the objective is to find the structural modification that will give the desired dynamic characteristics to the physical structure in a closed-loop process that can take multiple cycles to complete.

The detailed formulation of the methodology proposed for application in this demonstration case is constructed in the following section, accompanied by a brief theoretical review of the methods involved.

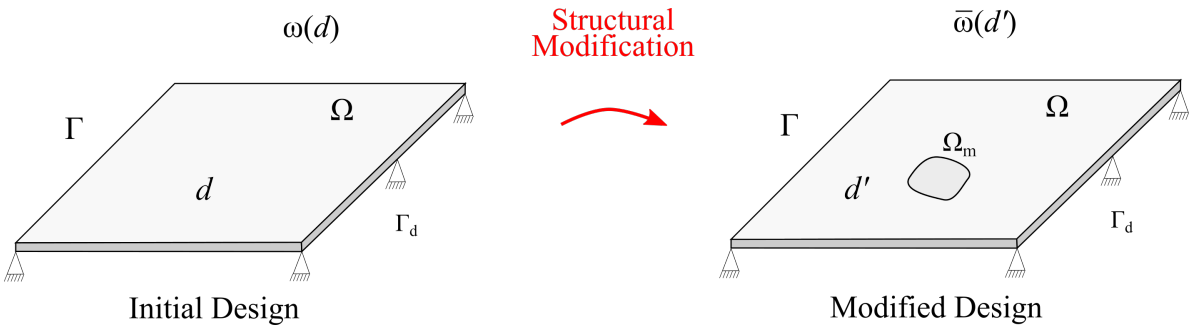

Figure 3.2: Schematic representation of structural dynamics modification scenario of a generic plate-like structure.

3.2.2 Natural frequency assignment problem based on structural dynamics modification

Consider the plate-like structure illustrated in Figure 3.2, which represented by an initial design d within the design domain Ω bounded by the boundary surface Γ. The structure is subjected to external forces acting on its boundary represented by the time-dependent vector $\mathbf{f}(t)$. The dynamic behavior of the structure with the initial design considering its discretization in a linear conservative model - finite element model or lumped mass model - is described by the differential equation of motion below:

$$\mathbf{M}\ddot{\mathbf{q}}(t) + \mathbf{K}\mathbf{q}(t) = \mathbf{f}(t) \tag{3.1}$$

where $\mathbf{K}$ and $\mathbf{M}$ are the stiffness and mass matrices, respectively; $\mathbf{q}$,$\ddot{\mathbf{q}}$ denote the vectors of displacement and acceleration.

The natural frequencies and mode shapes of the model of this structure are obtained by solving the eigenvalue value problem from the characteristic equation for its free response, which leads to the following equation:

$$\left(\mathbf{K} - \omega_i^2 \mathbf{M}\right) \boldsymbol{\phi}_i = 0 \tag{3.2}$$

for every natural frequency ω_i and corresponding eigenvector $\boldsymbol{\phi}_i$, also named mode shape. In its initial design, the resonance frequencies of the model are given by the vector $\boldsymbol{\omega}$. The natural frequencies and mode shapes obtained reveal important characteristics of the dynamic behavior of the conservative model.

The frequency assignment problem consists of finding a new design d' obtained from the transformation of the initial design that will assign the resonance frequencies to the defined values given by the vector $\overline{\boldsymbol{\omega}}$. Regardless of the method used to solve this problem, the solution will always be dependent on the prediction fidelity of the model. In this context, structural dynamics modification techniques, which allow to work directly with experimentally identified frequencies and mode shapes, which are therefore of higher fidelity, have an advantage over structural optimization techniques that rely exclusively on

predictive models.

The methods of structural dynamics modification are based on natural frequencies and eigenvectors identified from experimental modal analysis, which, despite generally providing a higher fidelity in the identification of natural frequencies and mode shapes, have a lower spatial resolution associated with the number of used sensors. For this reason the structural modifications are then formulated with respect to point modifications of mass and stiffness associated with the observation points of the constructed modal basis. The problem of assignment of natural frequencies can then be formulated in the form of an inverse problem from the following characteristic equation:

$$\left(\overline{\mathbf{K}} + \overline{\Delta\mathbf{K}} - \overline{\omega_i^2}(\overline{\mathbf{M}} + \overline{\Delta\mathbf{M}})\right)\overline{\boldsymbol{\phi}_i} = 0 \tag{3.3}$$

where $\overline{\mathbf{K}}$ and $\overline{\mathbf{M}}$ are the mass and stiffness matrices related to the experimental observation points, and $\overline{\Delta\mathbf{K}}$ and $\overline{\Delta\mathbf{M}}$ are respectively the corresponding stiffness and mass modifications. In this strategy the structural modifications are concentrated at the experimental observation points of the structure, which is its main limitation. Numerous structural dynamics modification techniques have already been proposed in the literature to solve this type of optimization problem. These techniques consider modifications that are point masses or local stiffness changes that are difficult to translate into physical modifications, which explains the gap between theoretical demonstrations and practical applications observed in the literature.

This problem can be circumvented, as recently presented by Balmes et al [73], by using modal expansion, which is able to combine the high spatial resolution of finite element models and the high fidelity of experimentally identified mode shapes to estimate an extended mode shape.

3.2.3 Modal expansion

In general, expansion methods aim to reconstruct fields on a numerical model from experimentally obtained data. In structural dynamics, the data to be reconstructed on an finite element model are often mode shapes or displacement fields. The goals of such reconstructions are multiple, including: visualization, preparation of tests for model calibration, damage detection, extrapolation of measurements, and enabling the creation of hybrid models [75]. The literature on expansion methods is vast, and we do not attempt to provide an exhaustive list. However, the reader can find more details in [74–76]. In this work, the modal expansion method based on Extended Constitutive Relation Error (ECRE) is used to extrapolate the experimentally identified mode shapes, then with a low spatial resolution of few observation degrees of freedom, to all the degrees of freedom of the corresponding finite element model of the structure. The aim here is to increase the spatial resolution of the experimentally identified mode shapes while maintaining adequate prediction fidelity in order to use them in topology optimization.

In this work only a brief description of modal expansion based on the ECRE method is proposed. The reader can refer to [74, 75, 77, 78] for a more in-depth description of ECRE concepts. Let N_e be the number of degrees of freedom of the finite element model, m the number of experimentally measured modes, $\widehat{\boldsymbol{\phi}_i}$ the $i-$th eigenvector extended from experimental data and $\boldsymbol{\phi}_i$ the $i-$th eigenvector obtained from the FEM. The extended eigenvector contains c degrees of freedom measured with the help of sensors positioned on the structure and $r = N - c$ to be reconstructed. We can then describe model and extended eigenvectors as:

$$\widehat{\boldsymbol{\phi}_i} = \left\{ \begin{array}{c} {}_c\widehat{\boldsymbol{\phi}_i} \\ {}_r\widehat{\boldsymbol{\phi}_i} \end{array} \right\}; \quad \boldsymbol{\phi}_i = \left\{ \begin{array}{c} {}_c\boldsymbol{\phi}_i \\ {}_r\boldsymbol{\phi}_i \end{array} \right\} \tag{3.4}$$

Given these vectors one can write the transformation matrix $\mathbf{L}$ allowing the selection of only the observed degrees of freedom which establishes the following relationship:

$$ {}_c\widehat{\boldsymbol{\phi}_i} = \mathbf{L}\widehat{\boldsymbol{\phi}_i} \tag{3.5}$$

The extended eigenvector based on the ECRE method developed by Ladeveze [77] can be obtained by minimizing the following function:

$$\begin{aligned} g = &\left(\boldsymbol{u}_i - \widehat{\boldsymbol{\phi}_i}\right)^{\mathrm{T}} [\gamma \mathbf{K}] \left(\boldsymbol{u}_i - \widehat{\boldsymbol{\phi}_i}\right) + \left(\boldsymbol{v}_i - \widehat{\boldsymbol{\phi}_i}\right)^{\mathrm{T}} \left[(1-\gamma)\omega_i^2 \mathbf{M}\right] \left(\boldsymbol{v}_i - \widehat{\boldsymbol{\phi}_i}\right) + \ldots \\ &\alpha \left({}_c\widehat{\boldsymbol{\phi}_i} - \mathbf{L}\widehat{\boldsymbol{\phi}_i}\right)^{\mathrm{T}} \mathbf{W} \left({}_c\widehat{\boldsymbol{\phi}_i} - \mathbf{L}\widehat{\boldsymbol{\phi}_i}\right) \end{aligned} \tag{3.6}$$

where $\mathbf{W}$ is the matrix weighting the measured degrees of freedom, γ is a coefficient weighting the errors linked to mass and stiffness, α is a coefficient translating the confidence in the test results, $\boldsymbol{u}_i$ and $\boldsymbol{v}_i$ are the displacement fields defined by:

$$\begin{aligned} \mathbf{K}\boldsymbol{u}_i &= \omega_i^2 \mathbf{M} \boldsymbol{v}_i \\ \left(\boldsymbol{v}_i - \widehat{\boldsymbol{\phi}_i}\right) &= -\frac{\gamma}{1-\gamma} \left(\boldsymbol{u}_i - \widehat{\boldsymbol{\phi}_i}\right) \end{aligned} \tag{3.7}$$

The solution of the minimization of the g function provides the full extended eigenvector and is obtained by solving the following system of equations:

$$\left[\begin{array}{cc} -\left(\mathbf{K} + \frac{\gamma}{1-\gamma}\omega_i^2 \mathbf{M}\right) & \mathbf{K} - \omega_i^2 \mathbf{M} \\ \gamma\left(\mathbf{K} - \omega_i^2 \mathbf{M}\right) & \alpha \mathbf{L}^{\mathrm{T}} \mathbf{W} \mathbf{L} \end{array} \right] \left\{ \begin{array}{c} \widehat{\boldsymbol{\phi}_i} - \boldsymbol{u}_i \\ \widehat{\boldsymbol{\phi}_i} \end{array} \right\} = \left\{ \begin{array}{c} 0 \\ \alpha \mathbf{L}^{\mathrm{T}} \mathbf{W}_m \widehat{\boldsymbol{\phi}_i} \end{array} \right\} \tag{3.8}$$

The solution to this system of equations depends on the value of the α coefficient, a scalar that indicates the confidence in the identified eigenvectors. Due to its lack of physical meaning, the value of the latter is often the subject of discussion and clearly depends on the application case of the ERCE [79]. In this work, it is assumed that the mode shapes are identified with high confidence, a justified hypothesis for plate-type structures with multiple measurement points, and therefore the value of α=0.99 is adopted. In addition, $\gamma = 0.5$ is assumed so that the total modeling error is equally distributed between the mass

error and the stiffness error.

3.2.4 Topology Optimization

In this work, we propose to solve the problem of assignment of natural frequencies from Equation 3.3 directly as a function of the design variable $\mathbf{x}$ that will be defined from the structure topology. For this we assume the material interpolation model of Solid Isotropic Material with Penalization (SIMP) for the FEM elements, which uses a *relative density* of a finite element as only design variable for each element and establish the following proportion between the *relative density* and physical properties [80, 81]:

$$\begin{aligned} \mathbf{E}_e &= x_e^p \mathbf{E}_e^* \\ \mathbf{M}_e &= x_e^q \mathbf{M}_e^* \end{aligned} \tag{3.9}$$

where $x_e\,(0 < x_{\min} \leqslant x_e \leqslant 1)$ is the relative material density of the e-th finite element, $\mathbf{E}_e$ and $\mathbf{M}_e$ are its elasticity and mass matrices expressed in terms of the relative material density, respectively, $\mathbf{E}_e^*$ the elasticity matrix of the corresponding element with the fully solid material and $\mathbf{M}_e$ represents the element mass matrix corresponding to fully solid element; p and q are penalization factors from stiffness and mass, respectively. From the material interpolation model the global mass and stiffness matrices can be rewritten in function of the design variable as $\mathbf{M}(\mathbf{x})$ and $\mathbf{K}(\mathbf{x})$:

$$\begin{aligned} \mathbf{M}(\mathbf{x}) &= \sum_{e=1}^{\mathrm{N_E}} \mathbf{M}_e(x_e) = \sum_{e=1}^{\mathrm{N_E}} x_e^q \mathbf{M}_e^* \\ \mathbf{K}(\mathbf{x}) &= \sum_{e=1}^{\mathrm{N_E}} \mathbf{K}_e(x_e) = \sum_{e=1}^{\mathrm{N_E}} x_e^p \mathbf{K}_e^* \end{aligned} \tag{3.10}$$

where $\mathbf{K}_e^*$ is the stiffness matrix of a finite element with fully solid material and $\mathrm{N_E}$ denotes the total number of finite elements in the admissible design domain.

The sensitivity of the natural frequencies with respect to the design variable for each element can then be determined from the derivation of Equation 3.2 which leads to the following equation[82]:

$$\frac{\partial \omega_i}{\partial x_e} = \frac{1}{2\omega_i} (\boldsymbol{\phi}_i^{\mathrm{T}})_e \left(\frac{\partial \mathbf{K}_e}{\partial x_e} - \omega_i^2 \frac{\partial \mathbf{M}_e}{\partial x_e} \right) (\boldsymbol{\phi}_i)_e \tag{3.11}$$

where $(\boldsymbol{\phi}_i)_e$ is the i-th mode shape associated with e-th finite element. The derivatives of stiffness and mass matrices can be obtained analytically based on the material interpolation model:

$$\begin{aligned} \frac{\partial \mathbf{M}_e}{\partial x_e} &= q x_e^{q-1} \mathbf{M}_e^* \\ \frac{\partial \mathbf{K}_e}{\partial x_e} &= p x_e^{p-1} \mathbf{K}_e^* \end{aligned} \tag{3.12}$$

Assuming that the structure is a thin plate discretized into rectangular elements and considering the formulation based on Kirchhoff's thin plate model, the elementary mass and stiffness matrices are given by [1, 83]:

$$\begin{aligned} \mathbf{M}_e &= \rho h \int_{\mathrm{A}_e} [\mathbf{N}]^{\mathrm{T}} [\mathbf{N}] \mathrm{dA} \\ \mathbf{K}_e &= \frac{h^3}{12} \int_{\mathrm{A}_e} [\mathbf{B}]^{\mathrm{T}} [\mathbf{D}] [\mathbf{B}] \mathrm{dA} \end{aligned} \tag{3.13}$$

where h is the thickness of the plate element, ρ is the material density of the plate and $[\mathbf{N}]$, $[\mathbf{B}]$ and $[\mathbf{D}]$ are respectively the matrices of assumed displacement functions, strain-displacement and material constants for plate element considered. These matrices are presented in detail in Appendix A2.1 of this thesis.

Comparing the elementary mass and stiffness matrices obtained by the SIMP model (Equation 3.10) with the same elementary matrices considering a Kirchhoff thin plate element (Equation 3.13), one can notice that a convenient choice for the penalty factors p and q, which would give a physical interpretation for x_e would be $p = 3$ and $q = 1$. In this case, the variable x_e will represent the variation in the thickness of the plate with respect to the nominal thickness h defined for the element. Therefore, the relative density x_e, which can vary between 0 and 1, interpolates the thickness of each finite element between 0 and h.

The physical interpretation of the design variable with changes in the thickness of the finite elements enables to establish a relationship between structural modifications and the natural frequencies. Therefore, the problem of finding the structural modifications to assign certain natural frequencies can be conveniently formulated as the following topology optimization problem:

$$\begin{aligned} \underset{\boldsymbol{x}}{\text{minimize}} \quad & f(\boldsymbol{x}) = \sum_{i=1}^{\mathrm{M}} \left(\frac{\omega_i(\boldsymbol{x}) - \overline{\omega}_i^{mod}}{\overline{\omega}_i^{mod}} \right)^2 \\ \text{subject to} \quad & \sum_{e=1}^{\mathrm{N}} v_e x_e = \mathbf{v}^{\mathrm{T}} \boldsymbol{x} \leq \mathrm{V}^* \\ & \mathbf{0} < \boldsymbol{x}_{\min} \leq \boldsymbol{x} \leq \mathbf{1} \end{aligned} \tag{3.14}$$

where $f(\boldsymbol{x})$ is the objective function, M is the number of considered modes, $\omega_i(\boldsymbol{x})$ is the i-th natural frequency predicted by the FEM, $\overline{\omega}_i^{mod}$ is the i-th natural frequency assigned to the model during topology optimization, V^* is a volume of the admissible design domain and $\boldsymbol{x}_{\min}$ is the vector of lower bounds of the design variable. It is important to note that for the demonstration case presented here, it is assumed that the modifications will be made through additive manufacturing. This is translated into the optimization by defining the vector of lower bounds as the initial design of the structure, so it can be guaranteed that the new design will not remove any material from the initial one.

The optimization problem will be solved using the moving asymptote method (MMA),

a gradient-based method commonly used for topology optimization due to its known efficiency. However, unlike the traditional approach to topology optimization problems that relies exclusively on information from the FEM of the structure, the methodology based on the self-design manufacturing paradigm considered here will seek to use information extracted from the physical structure, specifically the natural frequencies and mode shapes that can be identified experimentally.

In the context of the demonstration case proposed here, the initial design for the nominal model is assumed to have the natural frequencies precisely assigned. However, due to uncertainties related to the modeling and manufacturing of the physical structure, there is a difference between the natural frequencies predicted by the model and those identified for the physical structure. Therefore, the natural frequencies assigned to the model ($\overline{\omega}^{mod}$) in the topology optimization are defined by the initial natural frequencies of the model plus the difference between the natural frequencies of the physical structure and the desired frequencies to be assigned.

The mode shapes extracted from the structure with a low spatial resolution are used to obtain the expanded mode shapes with the same spatial resolution of the FEM model. These expanded mode shapes are used to compute the sensitivities of the objective function based on Equation 3.11 by replacing the mode shapes obtained from the FEM model ($\boldsymbol{\phi_i}$) with the expanded mode shapes ($\widehat{\boldsymbol{\phi_i}}$). It is noteworthy that the expanded modes are obtained from data extracted directly from the physical structure and typically have a higher fidelity than those from the model. This is important because the mode shapes will directly affect the estimated sensitivities of the objective function and consequently the solution of the problem, since the MMA method used is a gradient-based method. Thus, the goal here is that the solution obtained by the topology optimization based on the model approximates the solution for the physical structure as closely as possible, even in the presence of modeling uncertainties.

Once the new topology has been obtained through the optimization method, the structural modifications needed to implement it in the physical structure can be obtained through the geometric subtraction from the initial topology. In this way, it is possible to determine the regions where more material should be added to the structure. The ultimate goal is that the natural frequencies of the physical structure after the implementation of the modifications approach those frequencies assigned with the required precision. This entire cycle is carried out within a closed-loop process of the self-design manufacturing paradigm, so further cycles may be necessary until the desired goal is achieved.

3.2.5 Methodology Overview

An overview of the methodology proposed in this work is presented in Figure 3.3. The methodology starts with a nominal initial design of the existing physical structure. It is divided into two loops, the so-called inner loop and outer loop. The inner loop corresponds

to the topology optimization, which is in charge of proposing the design modifications and thus driving the developmental plasticity. The outer loop checks the convergence of the natural frequencies assigned in the physical structure after the design modifications have been implemented and restarts a new cycle of the process if necessary until the desired goal is achieved. A detailed description of the main steps of the methodology is presented below:

Finite element analysis: the discretization of the nominal design of the structure is used to build its finite element model, from which the natural frequencies, mode shapes, and mass and stiffness matrices are calculated.

Experimental modal analysis: the natural frequencies and mode shapes of the physical structure are identified through experimental modal analysis considering a fixed number of sensors positioned on the structure. In the application of the numerical case in this work, this step will be replaced by modal analysis in the FE model corresponding to the physical structure for a given number of observation points.

Modal expansion: based on the data from the model and the physical structure, modal expansion of the mode shapes identified with a few observation points is performed using the ECRE method. The expanded modes are then used to feed the sensitivity analysis of the topology optimization represented by the inner loop.

Topology optimization (inner loop): the structural modification optimization problem formulated in the previous section is solved through topology optimization based on the SIMP model and the method of moving asymptotes. At each iteration of the topology optimization loop the natural frequencies are updated for the proposed design and convergence checked. It is important to note that the updating of the expanded mode shapes in the sensitivity analysis occurs only at loop initialization, because it would be impractical in each iteration of the loop, which implies assuming that the design modifications do not cause substantial changes in the structure's mode shapes, a justifiable hypothesis since the modifications are incremental.

Structural modification: based on the design obtained by topology optimization and the physical interpretation of the design variable presented in the previous section, the obtained topology is transformed into a three-dimensional design of the structure. The structural modification is then obtained by geometrically subtracting the new design from the initial design. In this numerical case, these modifications are simulated by changing the design in the model corresponding to the physical structure, but in a real case these modifications can be implemented in practice.

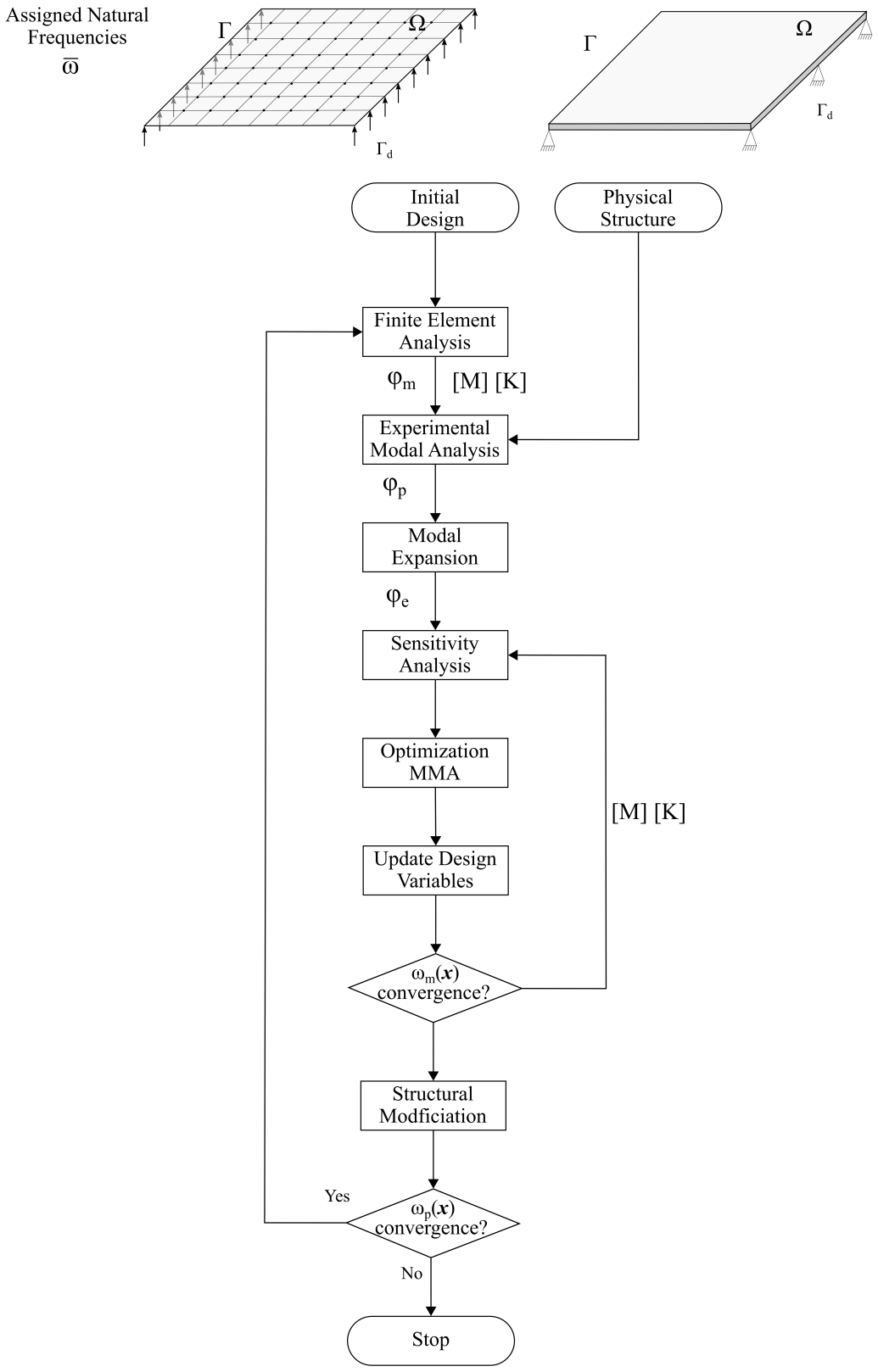

Figure 3.3: Overview of the methodology of structural modification driven by topology optimization for natural frequency assignment.

3.3 Results and discussions

The main goal in the numerical case explored in this chapter is to realize the proposed plate structure with the following first three natural frequencies assigned with high precision: $\overline{\boldsymbol{\omega}}$ = [129.7 213.1 483.8] Hz. By high precision in this case, it is meant an admitted deviation of ±1 Hz from the desired frequencies. In order to demonstrate the methodology proposed for this problem in a simulated environment, two finite element models were created. The first model, called Model I, to simulate the nominal model of the structure and a second model, called Model II, to represent the physical structure supposedly manufactured. The plate has dimensions of 100 × 100 × 2 mm and is simply supported on two sides, with the other two sides free. The FEM models use Kirchhoff plate elements in their formulation and are implemented in Matlab (the codes are available in the repository[1]). For Model I, an ideal simply supported boundary condition is considered and nominal values for the mechanical properties of the material supplied by the manufacturer are used. To simulate a physical structure with Model II, an imperfect boundary condition is considered with different stiffnesses of the plate supports and a variation in the Young's modulus of the structure is introduced. The stiffnesses considered for the boundary conditions on the right and left sides of the plate are uniformly distributed along the length of the respective edge of the plate. All values considered for both models are listed in Table 3.1.

The modifications introduced in Model II are intended to simulate the effect of possible uncertainties in the physical structure. Although the various other sources of uncertainty in the real world can affect the structure and the model itself in different ways, the decision to introduce the modifications only in the boundary conditions and Young's modulus was based on experimental results of the structure fabricated in the past. These past realizations showed variations in natural frequencies and mode shapes similar to those obtained with the values used in the simulations.

The natural frequencies obtained for the two models considering the initial design of the structure are shown in Table 3.2. As can be seen, the natural frequencies of Model I are precisely assigned to the desired frequencies. On the other hand, a significant absolute deviation is observed for Model II, which in this case represents a physical structure manufactured from the same design. This problem is commonly encountered in practice for the development of structures. It will be addressed in this work through the methodology based on the self-design manufacturing paradigm.

The finite element analysis of the two models makes it possible to compare the mode shapes of the three modes shown in Figure 3.4. It can be seen that the modes of the physical structure show significant deformations in the boundary region, due to the support stiffnesses used that allow them to deform - a behavior expected from a non-ideal support boundary condition. The MAC calculated between the modes of the two models shows

[1] https://github.com/jessepaixao/STANTON

	E [GPa]	ρ [kg/m^3]	v	k_{left} [N/m]	k_{right} [N/m]
Model I : "Nominal Model"	2.174	1120	0.35	∞	∞
Model II: "Physical Structure"	0.95 * 2.174	1120	0.35	1e5	10e5

Table 3.1: Mechanical properties of the numerical models used in the demonstration case

	ω_1[Hz]	ω_2[Hz]	ω_3[Hz]
Model I: "Nominal Model"	129.7	213.1	483.8
Model II: "Physical Structure"	124.30	196.4	443.7
Absolute Error	5.4	16.7	40.1

Table 3.2: Natural frequencies of the numerical models for initial design

a significant deviation in the shape of the third mode. Although in this numerical case it is possible to observe the mode shapes representing the physical structure with all degrees of freedom, in practice this is not possible. In a practical case, the mode shapes are obtained from experimental modal analysis with a limited number of observation points. Therefore, in this numerical demonstration, the experimental modal analysis stage is simulated by extracting observations from a mesh of 100 points distributed as shown in Figure 3.5.

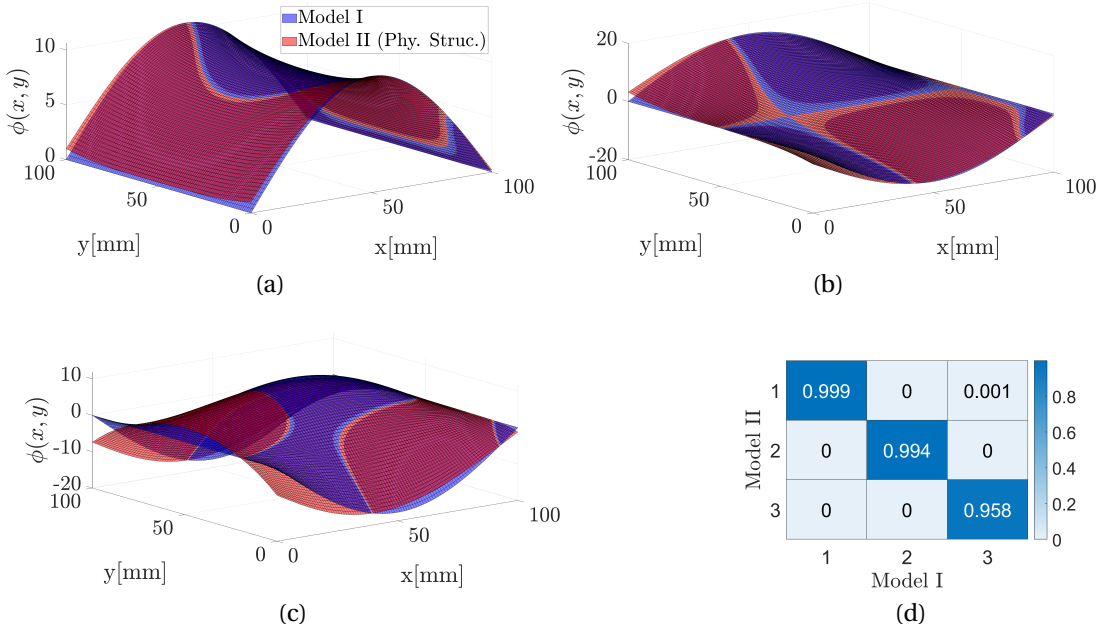

Figure 3.4: Mode shapes and modal assurance criterion analysis of the numerical models in the initial design.

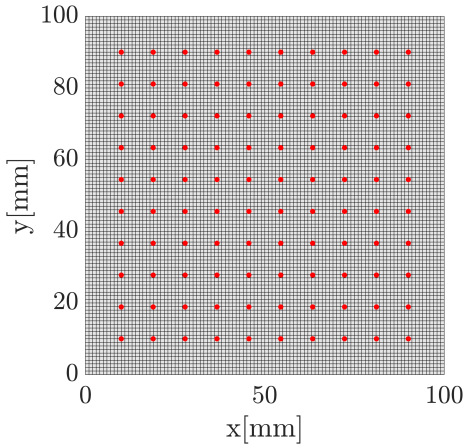

Figure 3.5: Mesh of the plate with observed points for experimental modal analysis.

3.3.1 Application of the proposed methodology

The natural frequencies from Model II (physical structure) and its mode shapes obtained from the observed points (see Figure) are combined with the mode shapes from Model I (nominal model), which are fully observable, to perform the modal expansion based on the ECRE method. Although, in this numerical demonstration case the complete mode shapes of Model II are available, only the deformations extracted from the 100 points in the direction perpendicular to the plate are used for the modal expansion. The modal expansion results shown in Figure 3.6 can be compared with those from Model II (see Figure 3.4), which represents the ground truth in this numerical case. It can be seen in Figures 3.6(a)-(c) that the shapes of the expanded modes are closer to those of Model II than to those of Model I (see Figure 3.4). This is highlighted quantitatively by the MAC shown in Figure 3.6(d), especially for the third mode, which is closer to 1. Therefore, the prediction fidelity of the expanded mode is greater than that of Model I in relation to the shape of the modes, since it takes into account the data from the physical structure. Indeed, this is exactly the aim of using modal expansion in the proposed methodology: to combine the mode shapes extracted from the physical structure (Model II) based on a few observed points, which have good fidelity but low spatial resolution, with the mode shapes extracted (Model I) from the nominal model, which have high spatial resolution but fidelity dependent on the fidelity of the model, to obtain an expanded mode shape with high fidelity and the same spatial resolution as the model.

In the proposed methodology, the natural frequencies and expanded modes of the physical structure are used in the inner loop for the topology optimization of the structural modification. The natural frequencies are used to define the optimization objective, which is given by the current frequency of Model I plus the difference to the frequencies of Model II, information provided in Table 4. The expanded mode shapes are used to update the sensitivity of the structure to the design variable according to Equation 3.11. It is important to note that the expanded modes are updated only at the beginning of the topology optimization loop and kept constant.

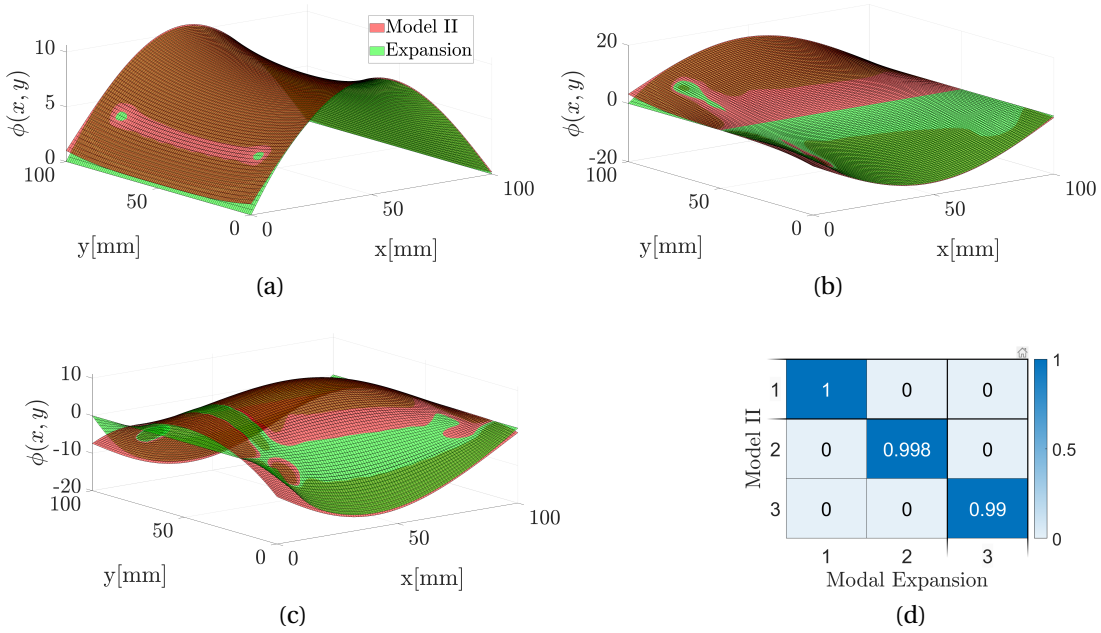

Figure 3.6: Mode shapes and modal assurance criterion analysis of in the initial design.

The results of the topology optimization in the first cycle of the outer loop of the proposed methodology the are shown in Figure 3.7. The topology optimization was based only on Model I with the expanded modes, but since this is a numerical demonstration case, it is also possible to observe the evolution of the natural frequencies of the physical structure (Model II) throughout the process, as shown in Figure 3.7(a). The evolution of the objective function throughout the optimization and the topologies corresponding to some iterations are shown in Figures 3.7(b)-(c), and indicate a clear convergence of the solution for the nominal model. It is interesting to note the asymmetry in the topology obtained on the two supported edges due to the differences in their bearing stiffnesses. More material is distributed on the right edge, which has greater rigidity in the boundary condition than the left edge.

The natural frequencies of the physical structure for the design obtained in the topology optimization of this first cycle are still far from the assigned frequencies (see Table 3.3), especially the third mode. This can be attributed to the uncertainties between the nominal model and the physical structure. Therefore, following the proposed methodology, a new cycle of the outer loop is carried out, in which a modal expansion is performed again with the mode shapes extracted from the physical structure with the design obtained in the first cycle. The results of the topology optimization carried out in the second cycle are presented in Figure 3.8. As can be observed in Figures 3.8(b)-(c), the natural frequencies of the nominal model converge to a solution after 117 iterations. It can be seen in Figure 3.8(c) that the shape of the topology has changed slightly, but the thickness has increased significantly. The natural frequencies of the physical structure with the optimized topology finally attain the assigned frequencies with the desired accuracy, as shown in Table 3.3.

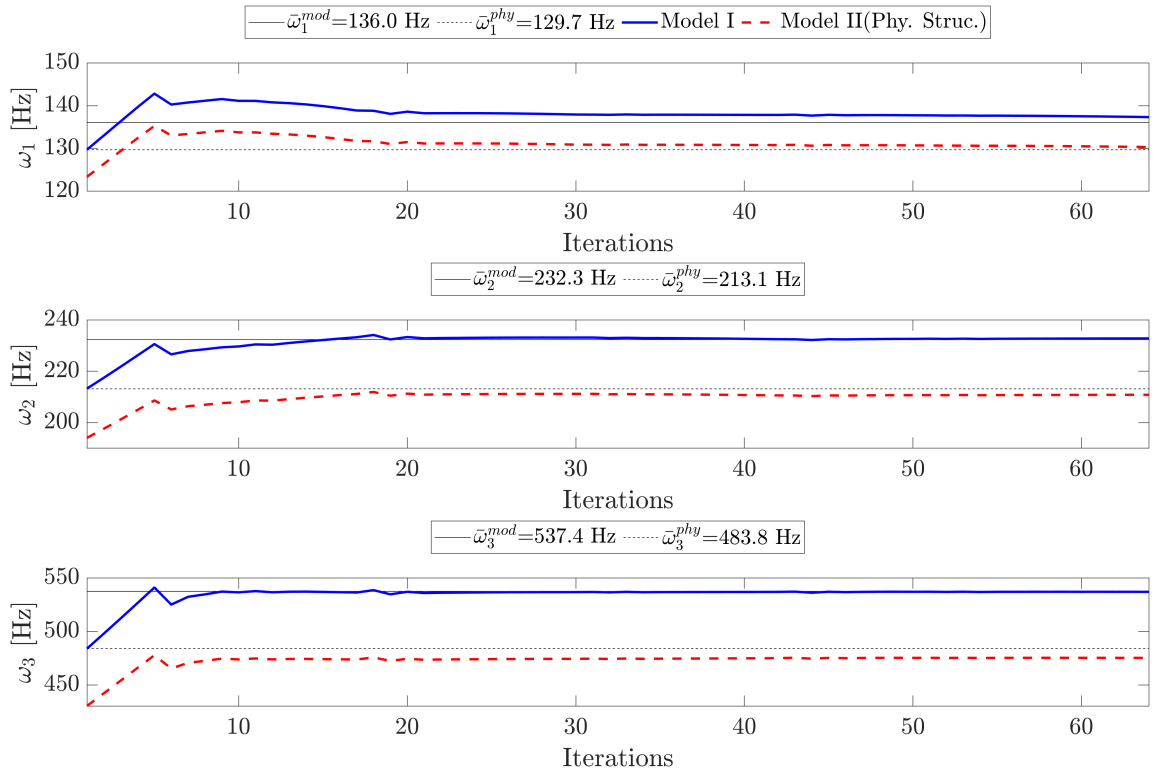

(a) Natural frequencies

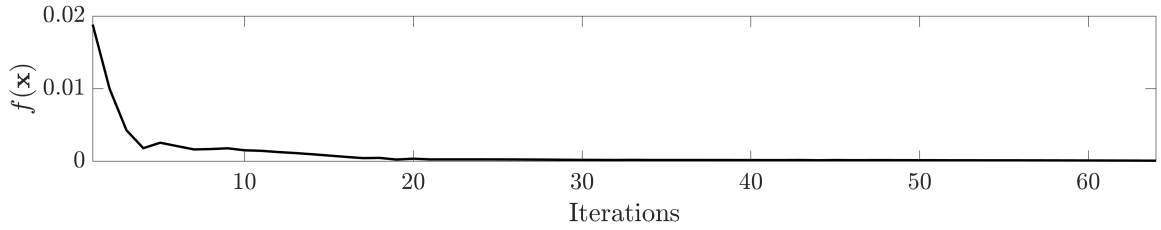

(b) Objective function

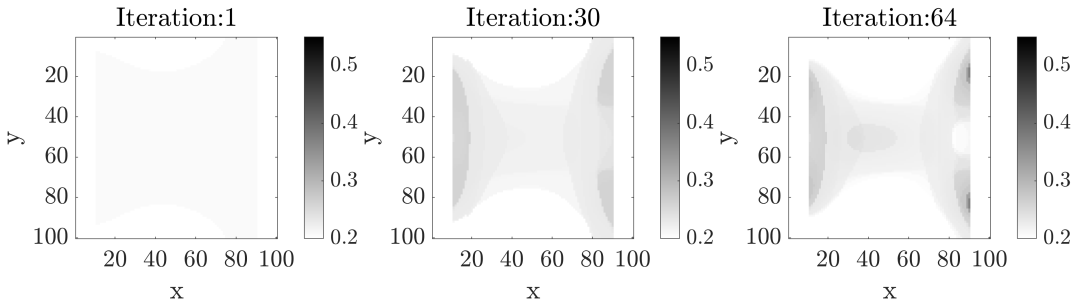

(c) Design topology in iterations: 1, 30 and 64

Figure 3.7: Topology optimization of the first cycle of the proposed methodology.

It is important to remember that in each cycle of the proposed methodology, the design obtained through topology optimization is translated into modifications of the physical structure intended to be implemented through the additive manufacturing process. Although in this numerical case, the practical implementation of these modifications will not be carried out, the three-dimensional visualization of the structure design and the respective modifications are shown in Figure 3.9. Comparing the modifications to the de-

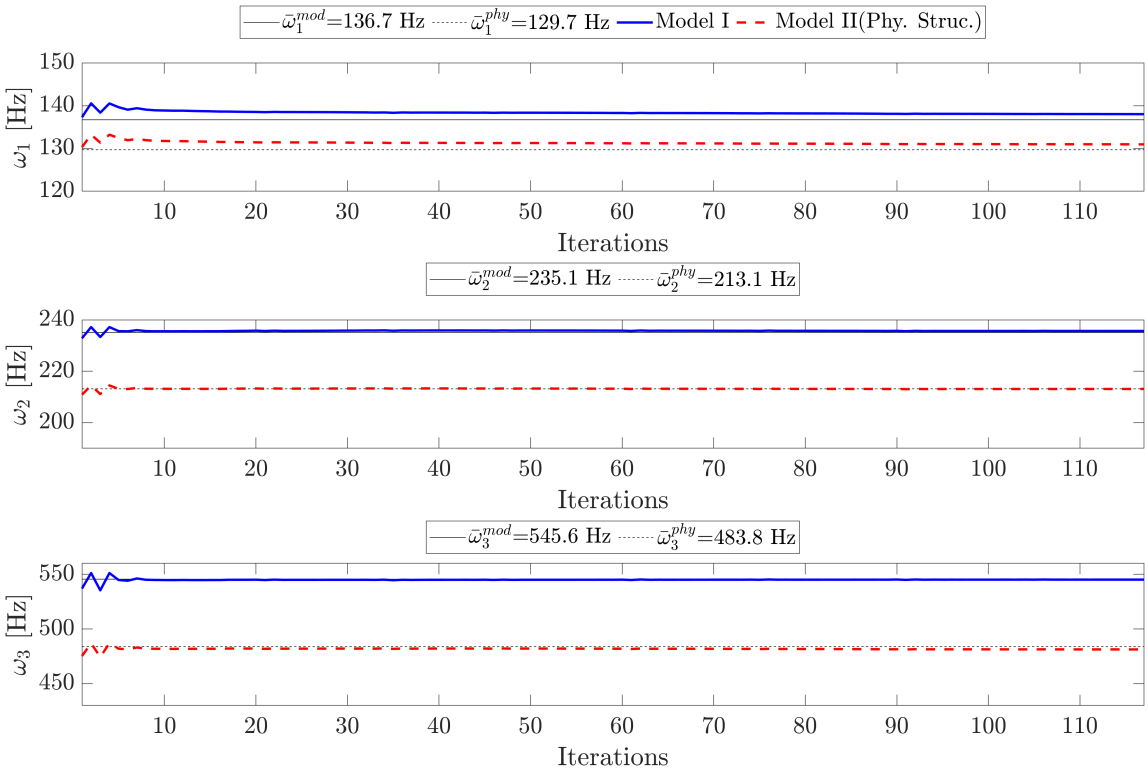

(a) Natural frequencies

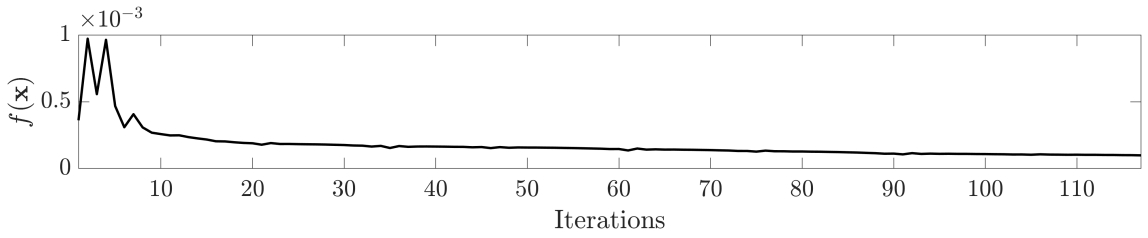

(b) Objective function

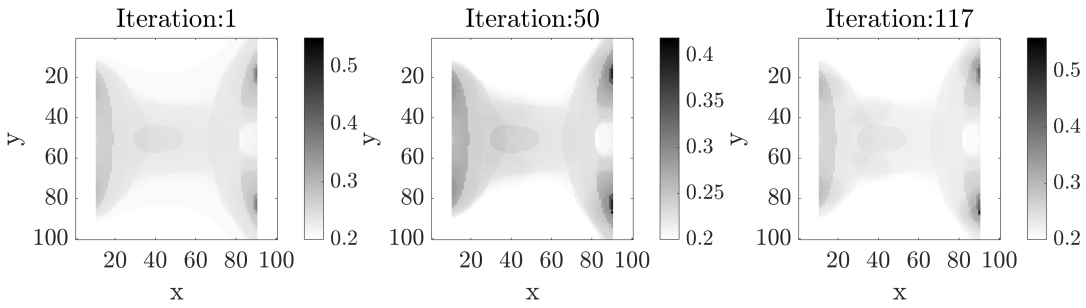

(c) Design topology in iterations: 1,50 and 117

Figure 3.8: Topology optimization of the second cycle of the proposed methodology.

signs of the two cycles, it can be seen that the shape of the modified topology remains similar, but in the second cycle more material is distributed in the areas indicated in yellow, increasing the thickness of the plate in these areas. It is important to remember that in the proposed numerical case, only the possibility of adding more material from the initial design of each cycle is considered, so that the modifications can be carried out through additive manufacturing.

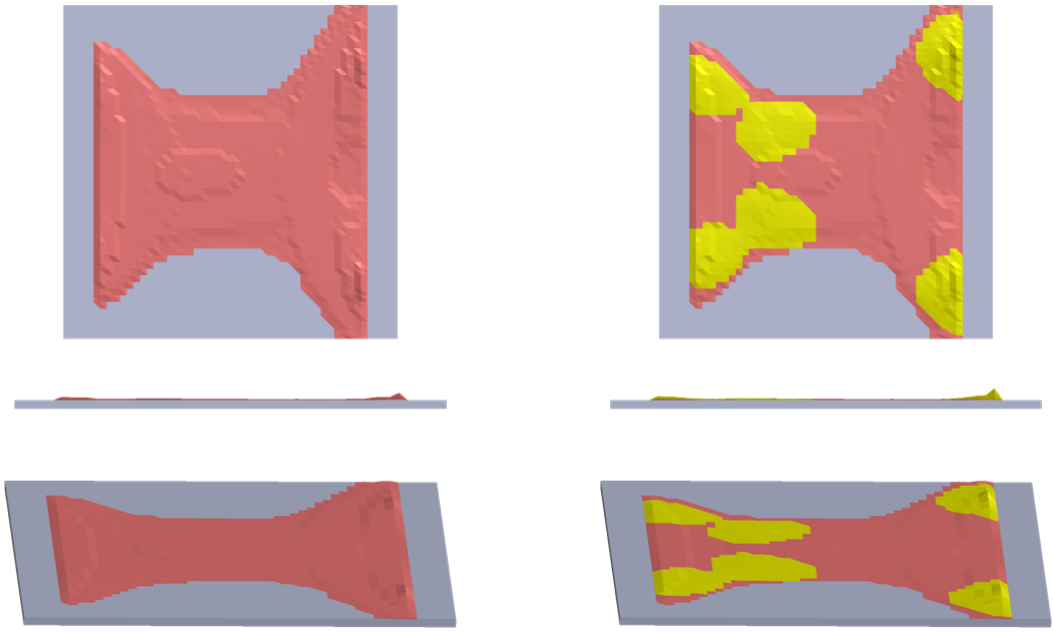

(a) Cycle 1 (b) Cycle 2

Figure 3.9: 3D visualization of the structure with the design generated by topology optimization.

	Initial Design			Cycle 1			Cycle 2		
	$\omega_1[Hz]$	$\omega_2[Hz]$	$\omega_3[Hz]$	$\omega_1[Hz]$	$\omega_2[Hz]$	$\omega_3[Hz]$	$\omega_1[Hz]$	$\omega_2[Hz]$	$\omega_3[Hz]$
Model I: "Nominal Model"	129.7	213.1	483.8	137.2	232.8	537.0	138.3	236.1	544.9
Assigned Frequencies ($\overline{\omega}_n^{mod}$)	-	-	-	136.0	232.3	537.4	136.7	235.1	545.6
Absolute Error	-	-	-	1.2	0.5	0.4	1.6	1.0	0.7
Model II: "Physical Structure"	124.3	196.4	443.7	130.3	210.8	475.3	130.7	213.0	482.9
Assigned Frequencies ($\overline{\omega}_n^{phy}$)	-	-	-	129.7	213.1	483.8	129.7	213.1	483.8
Absolute Error	-	-	-	0.6	2.3	8.5	1.0	0.1	0.9

Table 3.3: Natural frequencies of numerical models after structural modification guided by topology optimization.

3.3.2 Methodology based on the traditional approach of topology optimization without modal expansion

The proposed methodology can be applied without necessarily using modal expansion, directly using the mode shapes from the nominal model of the structure as in the traditional topology optimization approach based on the model exclusively. Therefore, the mode shapes used to feed the topology optimization loop are extracted directly from Model I. The design solution obtained after convergence of the topology optimization loop is then used at the end of each cycle to evaluate the natural frequencies of the phys-

ical structure with the new design (Model II). If the natural frequencies of the physical structure do not meet the established stopping criterion, a new cycle is repeated starting from the last design. This approach is used in this section to compare with the results presented in the last section based on the online topology optimization methodology in order to highlight the advantage of using modal expansion.

The results of the first cycle of topology optimization are shown in Figure 3.10. The evolution of the natural frequencies presented in Figure 3.10(a) a convergence towards the frequencies assigned to the nominal model. However, it can noticed a greater deviation of the natural frequencies of the physical structure with respect to the final objective compared to the previous methodology, especially for the third mode. This becomes quantitatively more evident when analyzing the natural frequencies of the nominal model and the physical structure shown in Table 3.4 for the design obtained by topology optimization in the first cycle. Moreover, it can be observed in Figure 3.10(c) that the topology obtained at the end of the optimization shown in Figure 3.10 is symmetrical, since the model does not take into account the asymmetry in the boundary conditions simulated in the physical structure. Therefore, following the methodology, a new optimization cycle was carried out. Therefore, as in the previously proposed methodology, a new optimization cycle can be performed. It is important to note that in the topology optimization performed here, the mode shapes are updated at each iteration of the optimization, as in the classical topology optimization approach, since the topology optimization is based only on the model, without the modal expansion that requires data from the physical structure.

The results of the second cycle of topology optimization are shown in Figure 3.11. This time, the natural frequencies failed to meet the convergence criterion and the optimization stopped when it reached the limit number of iterations, 200. Figure 3.11(c) shows significant changes in the shape in the topology of the structure and a substantial increase in its thickness. The natural frequencies of the physical structure for the topology obtained in the second cycle are shown in Table 3.4. It can be seen that there is a significant deviation in relation to the assigned frequencies and there is also an increase in this deviation for modes 1 and 2 compared to the first cycle. This fact highlights the importance of using modal expansion in the proposed methodology, which is able to combine the structure of the model and the fidelity of "experimental" data to improve the prediction fidelity of the mode shapes of the structure that directly affect the sensitivity analysis in the optimization problem.

	Cycle 1			Cycle 2					
	$\omega_1[Hz]$	$\omega_2[Hz]$	$\omega_3[Hz]$	$\omega_1[Hz]$	$\omega_2[Hz]$	$\omega_3[Hz]$	$\omega_1[Hz]$	$\omega_2[Hz]$	$\omega_3[Hz]$
Model I: "Nominal Model"	129.7	213.1	483.8	137.4	232.7	537.0	138.3	236.1	550.3
Assigned Frequencies ($\overline{\omega}_n^{mod}$)	-	-	-	136	232.3	537.4	136.5	235.1	550.7
Absolute Error	-	-	-	1.4	0.4	0.4	1.8	1.0	0.5
Model II: "Physical Structure"	124.3	196.4	443.7	130.5	210.7	470.1	131.4	211.1	477.6
Assigned Frequencies ($\overline{\omega}_n^{phy}$)	-	-	-	129.7	213.1	483.8	129.7	213.1	483.8
Absolute Error	-	-	-	0.8	2.4	13.8	1.7	2.0	6.2

Table 3.4: Natural frequencies of numerical models after structural modification guided by the traditional approach of topology optimization without modal expansion.

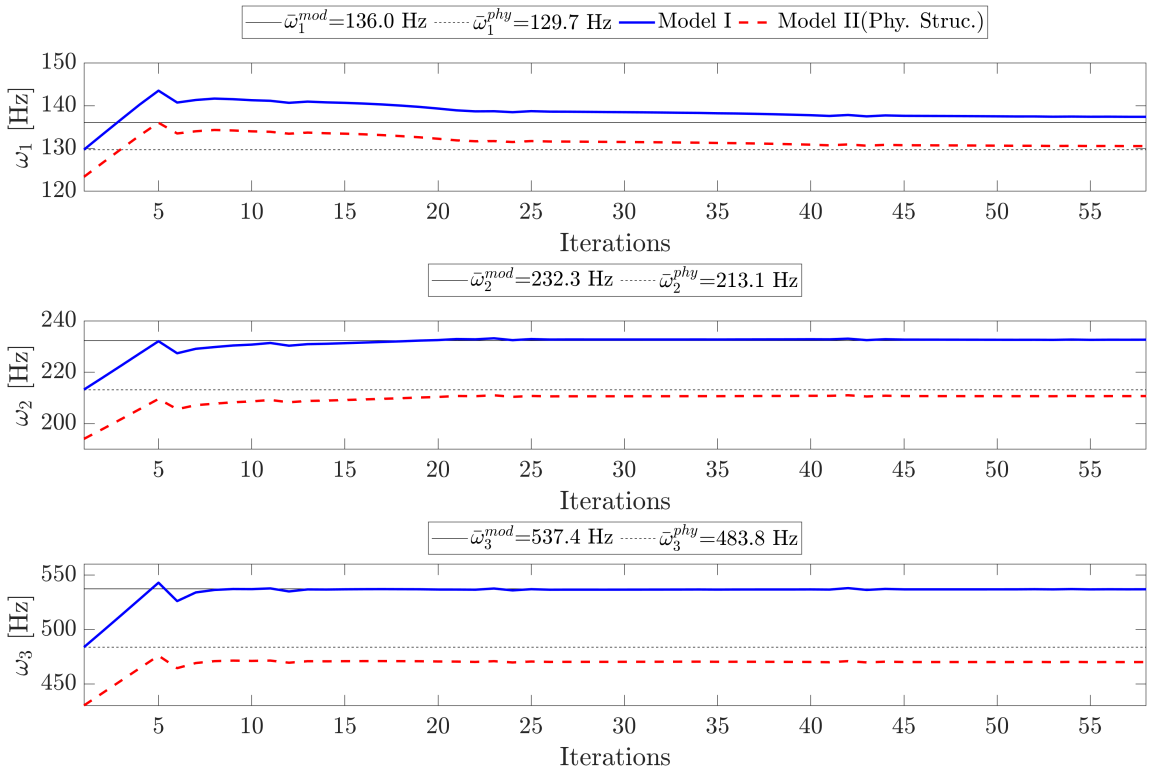

(a) Natural frequencies

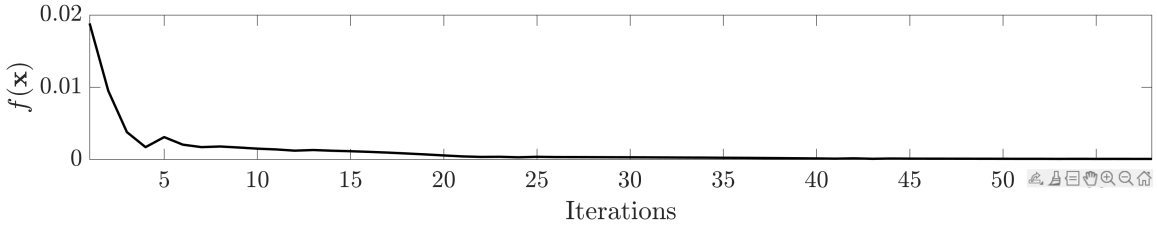

(b) Objective function

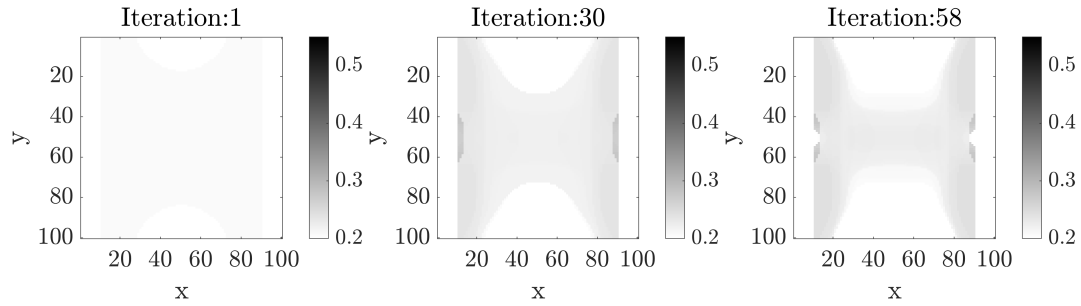

(c) Design topology in iterations: 1,30 and 58

Figure 3.10: Topology optimization of the first cycle of the traditional approach without modal expansion.

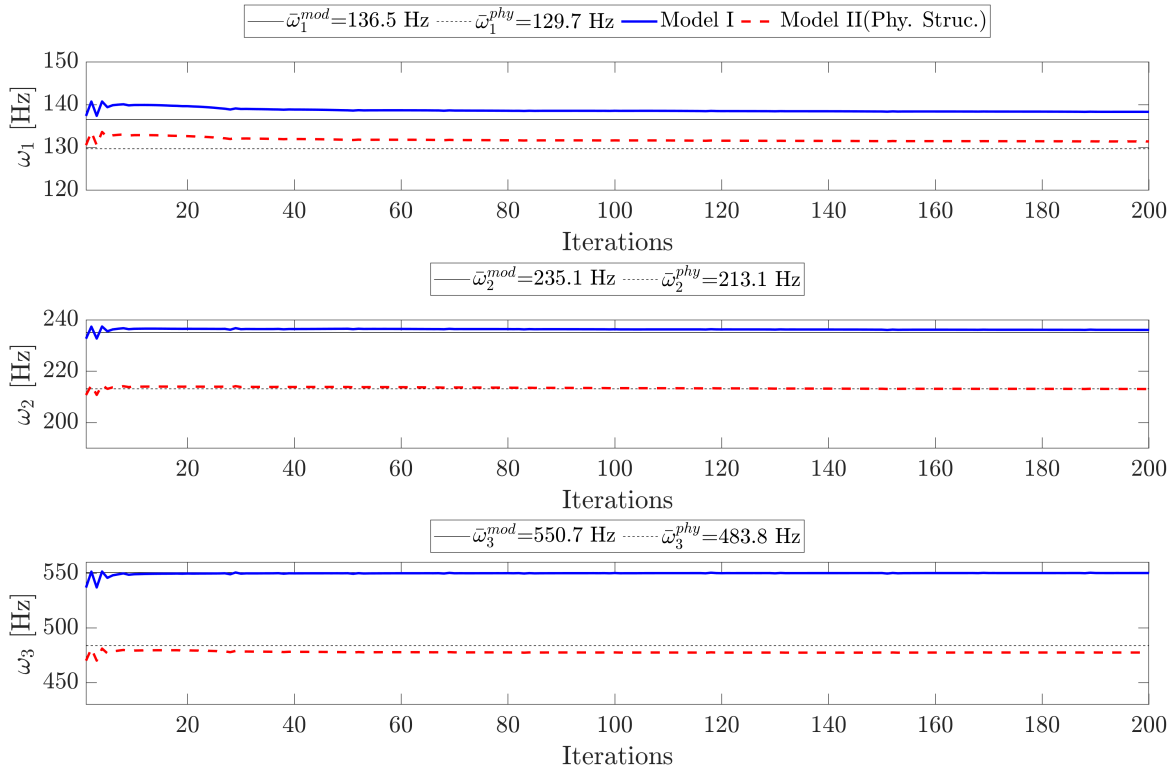

(a) Natural frequencies

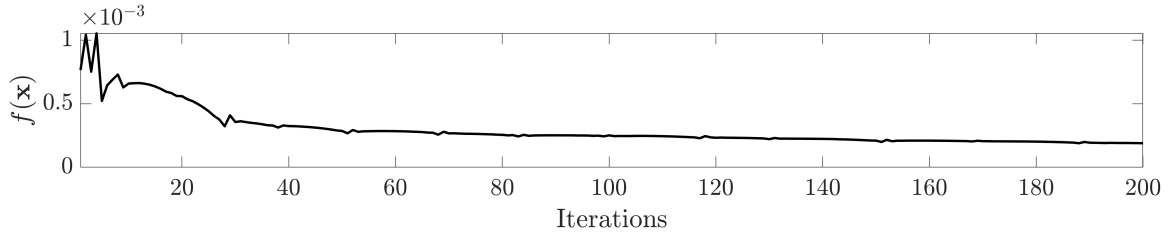

(b) Objective function

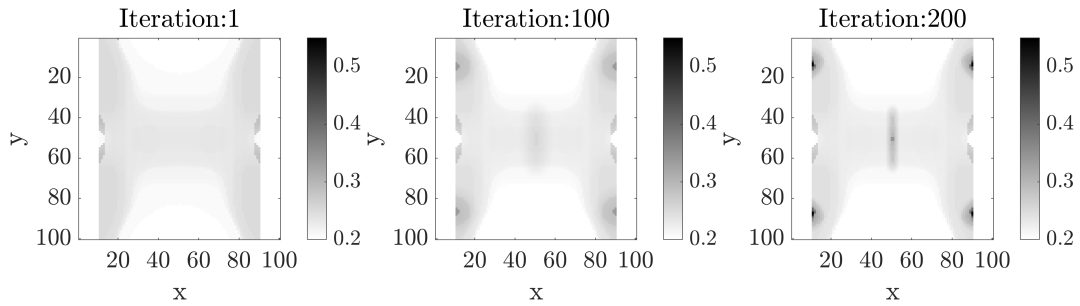

(c) Design topology in iterations: 1,100 and 200

Figure 3.11: Topology optimization of the second cycle of the traditional approach without modal expansion.

3.4 Conclusions

This chapter proposes a new methodology for applying the self-design manufacturing paradigm to the problem of high-precision natural frequency assignment in plate-like structures. The methodology of online topology optimization combines the techniques of modal expansion and topology optimization in a new way to guide the developmental plasticity of the structure within the self-design manufacturing paradigm. The numerical case studied simulates the physical structure through a finite element model with perturbations in its boundary conditions and physical properties, allowing the numerical study of the developmental plasticity of the structure design and an evaluation of the applicability of the methodology in a real case of future application. The numerical results obtained demonstrate the possibility of achieving an accuracy of up to ± 1 Hz in the assignment of three plate-like natural frequencies.

Chapter 4

Self-adaptive Piezoelectric Vibration Absorber with Semi-passive Tunable Resonant Shunt

Contents

4.1 Introduction

The growing demand for more efficient and environmentally friendly structures has led to a current trend toward lightweight structures, often more flexible and making them more susceptible to vibrations. This brings new challenges for current vibration control technologies, which must operate with increasing efficiency and contribute a minimum of mass to the structures on which they are installed [84]. In this context, one such technology that is gaining increasing interest are piezoelectric vibration absorbers (PVA). These devices, invented by Forward [85], employ piezoelectric transducers mounted on or even embedded in a primary structure to convert mechanical energy into electrical energy, which can be dissipated in an appropriate electrical circuit, called a shunt. The first shunt introduced by Forward [85] and one of the most famous is the so-called resonant shunt composed of a resistor and an inductor connected in series or parallel. Since then, different types of passive and active shunt circuits have been developed for single and multi-mode damping of vibrations [84].

The theoretical foundations for the design of resonant PVA shunts were laid by Hagood and Flotow [86] based on the equal-peak design method developed for dynamic vibration dampers (DVA), which is considered to be an equivalent mechanical system. This method provides an approximate solution of values for resistance and inductance to the optimization problem defined by minimizing the H_∞-norm of the system's frequency response function (FRF) considering a single mode. Recently, an analytic closed-form solution to this optimization problem was proposed by Soltani et al [87]. Several other methods for designing resonant circuits have been investigated and proposed in the literature, including more complex shunts and multiple modes of vibration [87–89]. Most of these methods focus on broadband frequency excitation, with the objective of attenuating single or multiple vibration modes as much as possible. Fundamentally, they rely on tuning the electrical resonance frequency to the desired mechanical resonance frequency, in order to maximize the transfer of vibration energy from the primary structure to the shunt circuit, where it is dissipated through electrical damping. Although tuning PVA with resonant drifts can provide important vibration attenuation for low frequency modes, small variations in the resonant frequency of the PVA or the primary structure cause substantial performance degradation [90].

In view of this problem many studies have investigated PVAs with adaptive resonant shunts, which are circuits capable of performing on-line adaptation of their impedance [84]. This type of device is commonly used to improve the robustness of piezoelectric absorbers in operation, which are very sensitive to uncertainties due to operational and environmental conditions. The adaptive shunt circuit is able to change its properties to compensate for possible effects of variation in its resonance frequency or of the structure, ensuring a stable vibration attenuation. For the design of an adaptive shunt two elements are essential: a mechanism to drive its natural frequency and a strategy of control. Hol-

lkamp and Starchville [91] were the pioneers to propose a PVA with an adaptive shunt, capable of automatically adjusting to the resonance frequency of a defined vibration mode using a motorized potentiometer and a synthetic inductor. They proposed a control strategy based on the minimization of the root mean squared value of the time-vibration signal by gradient-search algorithm. Fleming et al [92] applied a similar strategy for the single-mode shunt damping in a cantilevered beam structure using a synthetic impedance controlled by adjusting the relative phase difference between the velocity and the electrical current flowing in the shunt, which was later extended to multi-mode shunt damping by Niederberger et al [93]. More recently, Gardonio et al [94] demonstrated that minimizing the time-averaged vibration response of a mechanical system with a PVA is equivalent to maximizing the time-averaged electric power dissipated by the resonant shunt, which is characterized by a bell-type non-convex surface with a single maximum. From this result they developed an adaptive shunt using a controller based on the extremum seeking algorithm capable of adjusting online the resistance and inductance emulated by an synthetic impedance to maximize the time-averaged electric power dissipated by the PVA [95].

The adaptive PVA shunts proposed in the literature are mostly oriented to structures excited in a broad frequency band, aiming to ensure near-optimal attenuation independent of variations in the natural frequencies of the structure's modes, which usually leads to a frequency response function with equal-peaks. On the other hand, in harmonically excited structures, minimizing the vibration amplitude at each frequency leads to an even more efficient solution by tuning the electrical resonance frequency to the excitation frequency and decreasing the electrical damping as much as possible, creating an anti-resonance [96]. For very low damping, this anti-resonance can practically cancel the steady state vibration amplitude of the structure. This effect can be exploited with adaptive shunt circuits capable of tuning their electrical resonance frequencies by changing their parameters to attenuate structures excited with time-varying harmonic signals. This strategy, known as antiresonance locus, was recently exploited by Audeley et al [96, 97] using in an electromagnetic vibration absorber with adaptive resonant shunt controlled by an electronic chopper with pulse-width modulation. Despite being a well established strategy in the literature and already explored for electromagnetic vibration absorbers, its experimental application to absorbers based on piezoelectric transducers has not yet been investigated and proves to be challenging because the required reduction of the electrical damping of the resonant shunt reduces the stability margin for the control of the system, making it difficult to design a suitable controller. This induces a considerable increase in the electric current, which makes impractical the use of synthetic impedances elements commonly used in adaptive resonant shunts for PVA. Nevertheless, the application of this strategy with piezoelectric transducers has the potential to considerably reduce the mass added to the primary structure compared to electromagnetic transducers, since they are lighter and the resonant circuit that presents more weight can be positioned outside the structure through the electrical connection.

In this chapter, we propose a self-adaptive PVA with semi-passive resonant shunt for vibration attenuation of structures subjected to time-varying harmonic excitations. The main objective of this work is to circumvent the above-mentioned challenges in developing this type of device and to demonstrate the experimental application for vibration attenuation in a demonstrator. We present the development of a tunable resonant shunt composed of a passive inductor with movable ferrite cores and low internal resistance. A simple mechanism to control its inductance and consequently the electrical resonance frequency of the shunt is proposed based on the use of voltage-driven piezoelectric stack actuators capable of regulating the air gap between its ferrite cores. A method for controlling this device based on a machine learning algorithm is then proposed for the problem using a Gaussian Process Regression (GPR) model. This model is used in an offline step for supervised learning of the control signal applied to the resonant shunt to minimize the vibration of the main structure as a function of the excitation frequency, thus providing the self-adaptive capability of its electrical resonance frequency to the time-varying tonal excitation for real-time control. It is important to note that the self-adaptive capability is fundamentally different from that applied in PVA with traditional adaptive shunts, as the system learns how to adapt to changes in excitation frequency by itself through the machine learning model. This type of self-adaptive or self-learning strategy has recently been explored in the literature for other vibration control techniques. Wang et al[98] proposed self-learning tuning method based on artificial neural networks for an electromagnetic vibration absorber with negative stiffness under variable frequency excitation. Song et al [99] investigated the use of a nonlinear autoregressive with exogenous input model for vibration identification and control of a flexural beam with piezoelectric actuators. The GPR model applied in this work was recently explored by Maiworm et al [100, 101] in a control framework for scanning quantum dot microscopy. It is a non-parametric stochastic regression model that allows the learning of complex functions and after its training can be applied for control in the form of a minimization problem, a scenario suitable to the problem addressed in this work.

This chapter is organized as follows: in Section 4.2 a lumped mass model of a single-degree-of-freedom structure connected to a resonant shunt is reviewed and is used to present the theoretical foundations of the strategy for vibration attenuation of harmonically excited structures based on antiresonance locus. A brief description of the semi-passive tunable resonant shunt development and the theoretical concept behind the inductance tuning device based on the air gap between the movable ferrite cores is presented. Then, the self-adaptive control strategy based on the GPR model for the implementation of closed-loop system is presented. The experimental setup for applying the proposed methodology on the demonstrator and the results obtained are presented and discussed in Section 4.3. Finally, the conclusions are summarized in Section 4.4.

4.2 Piezoelectric vibration absorbers

In this section a lumped mass model of a structure connected to a PVA with resonant shunt is presented. This simplified model is sufficient to show the fundamentals of the operation and design of a PVA, as well as the adaptive strategy for vibration attenuation of harmonically excited structures. The fundamentals for the design of the tunable inductance are presented and discussed. Finally, the complete self-adaptive strategy for online control of the system is proposed.

4.2.1 Lumped parameter model of structure with piezoelectric vibration absorber

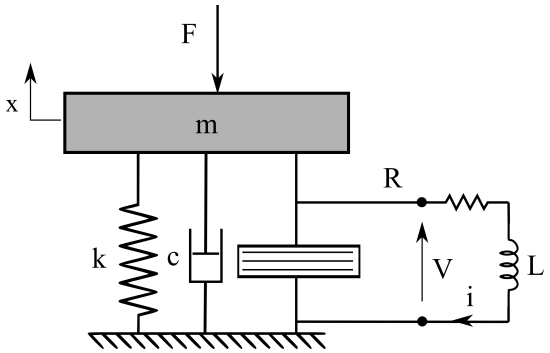

Figure 4.1: Lumped mass model of the structure with the piezolectric vibration absorber.

The lumped mass model of a structure coupled to a piezoelectric transducer connected to a resonant shunt composed of an in inductor and a resistor in series is schematically represented in Figure 4.1. An external force F is applied to the structure, causing a mechanical displacement x and a voltage V across the electrodes of the transducer. The governing equations of the coupled mechanical and electrical systems are given by [90]:

$$\begin{cases} m\ddot{x} + c\dot{x} + k_{oc}x - \theta q = \mathrm{F} \\ \mathrm{L}\ddot{q} + \mathrm{R}\dot{q} + \dfrac{1}{\mathrm{C}^{\varepsilon}} q - \theta x = 0, \end{cases} \tag{4.1}$$

where m, c, k_{oc} represent the mass, damping and stiffness of the structure when the transducer is open-circuited, q is the electric charge displacement, θ is the piezoeletric coupling coefficient and C^{ε} is the piezoelectric capacitance at constant strain.

The electromechanical coupling factor of this system is defined based on the mechanical behavior considering open-circuit ($q = 0$) and short-circuit (V = 0) electrical boundary conditions, and it is given by:

$$k_{\mathrm{c}} = \sqrt{\frac{\omega_{\mathrm{oc}}^2 - \omega_{\mathrm{sc}}^2}{\omega_{\mathrm{sc}}^2}} \tag{4.2}$$

where ω_{oc} and ω_{sc} are the resonance frequencies of the structure with the transducer in open-circuit and short-circuit configurations respectively, and are defined by:

$$\omega_{oc} = \sqrt{\frac{k_{oc}}{m}} \quad \text{and} \quad \omega_{sc} = \sqrt{\frac{k_{sc}}{m}} = \sqrt{\frac{k_{oc} - \theta^2 C^{\varepsilon}}{m}} \tag{4.3}$$

The electromechanical coupling defined by Equation 4.2 is an important factor considered for shunt circuit design because it represents the efficiency of strain energy conversion into electrical energy. Furthermore, it can be easily identified experimentally through the frequencies of the structure in open and closed circuit, which allows to mitigate modeling uncertainties [90].

The dynamic behavior of the electric circuit RL can be characterized by the resonance frequency (ω_e) and the electrical damping (ξ_e), which are obtained by:

$$\omega_e = \frac{1}{\sqrt{LC^{\varepsilon}}}, \quad \xi_e = \frac{R}{2}\sqrt{\frac{C^{\varepsilon}}{L}} \tag{4.4}$$

The frequency response function of this model can be computed from the Fourier transform of the Equation 4.1 and results in:

$$H(\omega) = \frac{X(\omega)}{F(\omega)} = \frac{-\omega^2 L + i\omega R + \frac{1}{C_p^{\varepsilon}}}{\left(-\omega^2 m + i\omega c + K_{oc}\right)\left(-\omega^2 L + i\omega R + \frac{1}{C^{\varepsilon}}\right) - \theta^2} \tag{4.5}$$

Based on the FRF, the problem of vibration attenuation considering a large band excitation can be described as an optimization problem, where one wants to minimize the H_∞-norm, for example the FRF maximum amplitude. Hagood and Flotow [86] studied this problem for a system without structural damping and showed that an approximate solution can be obtained by applying a method analogous to that used for tuned mass dampers, which is commonly known as equal-peak design method. This solution leads to the inductance and resistance values shown below:

$$L_{ep} = \frac{1}{C^{\varepsilon}\omega_{oc}^2} \quad \text{and} \quad R_{ep} = \sqrt{\frac{3}{2}}\frac{k_c}{C^{\varepsilon}\omega_{oc}} \tag{4.6}$$

This solution shows no significant difference for systems with low structural damping (below 10%) as demonstrated by Thomas et al [89]. It leads to a FRF with two peaks of equal amplitudes around the resonance frequency of the mechanical system with a substantial amplitude attenuation compared to the system with an open-circuit transducer (or without PVA) as presented in Figure 4.2. However, small variations in the properties of the shunt or the structure can cause an important increase in the maximum amplitude. It should be remarked that this solution considers a broadband frequency excitation near the mode and constant properties of the shunt.

4.2.2 Adaptive shunt based on antiresonance locus

In considering a harmonic excitation of the structure of known frequency Ω and an adaptive resonant shunt in which the inductance and resistance can be varied, a more efficient attenuation can be obtained using a different strategy, the antiresonance locus [97]. This strategy can be inferred from the FRF presented in Equation 4.5. The electromechanical coupling of the transducer induces a term in the numerator of the equation. For a given excitation frequency (Ω) and assuming null electrical resistance, one can show that the FRF is zero for :

$$L_{adaptive} = \frac{1}{C^{\varepsilon}\Omega^2} \tag{4.7}$$

This occurs due to the existence of an antiresonance, in which the excitation force counteracts the force generated by the electromechanical coupling, making the structure remain at rest [97]. By increasing the electrical resistance in the circuit, some of the energy is dissipated as heat, reducing the attenuation effect on the antiresonance. If the electrical resistance remains small, the maximum attenuation is obtained for the inductance given by Equation 4, for which $\Omega = \omega_e$. Therefore, by applying this strategy for a harmonic excitation varying within a frequency range one can drastically attenuate the vibration amplitude of the structure as presented in Figure 4.2.

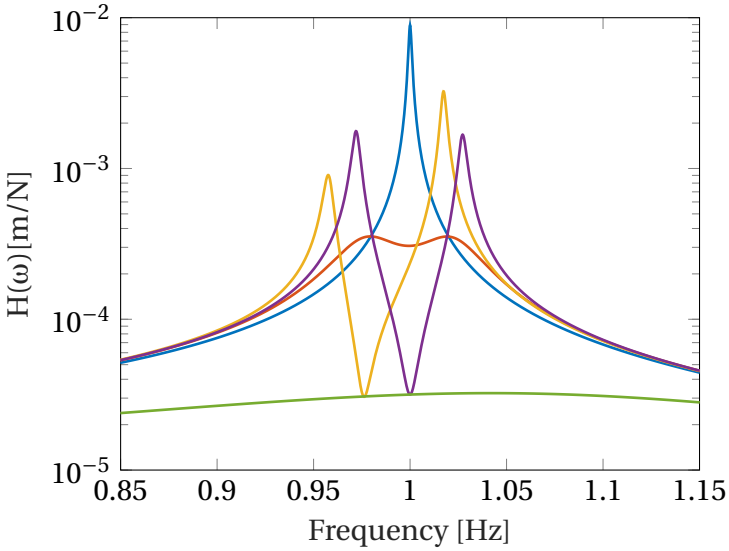

Figure 4.2: Frequency response function of primary system with an open-circuit transducer (—) and with resonant shunt circuit : $L = L_{ep}$ and $R = R_{ep}$ (—); $L = L_{ep}$ and $R = 0.1R_{ep}$ (—); $L = 0.9L_{ep}$ and $R = 0.1R_{ep}$ (—); $L = \frac{1}{C^{\varepsilon}\Omega^2}$ and $R = 0.1R_{ep}$ (—).

The application of this strategy depends on controlling of the resonance frequency of the electrical circuit through the inductance and a circuit with low electrical resistance. Although these two issues can be solved using a synthetic impedance to emulate the resistance and the inductance, this type of active circuit has instability problems along with other limitations already discussed previously. To circumvent these limitations, we pro-

pose the use of a semi-passive device that will be discussed in the next subsection.

4.2.3 Semi-passive tunable inductor

The major difficulty in using passive resonant circuits is related to the high values of inductance required for attenuation of low frequency modes - usually in the order of tens of H - which are difficult to find commercially or present impractical dimensions [102]. A passive inductor is a simple device, typically consisting of a coil of wire, which can be wound around a core made of different materials such as iron, ferrite, or air. This electrical component stores energy in a magnetic field when a current flows though the coil. The inductance depends on the number of turns in the coil, the core geometry, and the core material and it is given by [102]:

$$\mathrm{L} = \mu_e \mu_0 \frac{\mathrm{A}_e}{l_e} \mathrm{N}^2 \tag{4.8}$$

where N is the number of turns in the coil, A_e is the effective cross-sectional area, l_e represents the effective magnetic path length, μ_e and μ_0 are respectively the permeabilities in the core material and vacuum. The term $\mathrm{A}_l = \mu_e \mu_0 \frac{\mathrm{A}_e}{l_e}$ is known as the inductance factor and is commonly provided by the manufacturer. Based on this factor and the desired inductance, the number of turns of wire required can be calculated using Equation 4.8. The selection of the wire material and the wire section must take into consideration the maximum current and energy stored in the inductor as detailed in [102].

The resistance of the wire, which is proportional to its length and inversely proportional to its cross-sectional area, can be non-negligible for high inductances. To obtain a high quality factor one must seek a compromise between the wire diameter and the type of ferrite core selected, which directly affects the wire length needed to obtain a defined inductance. Therefore, in this work the high quality factor Q was obtained through the compromise between these design aspects in order to reduce to a minimum the wire resistance and consequently the electrical damping.

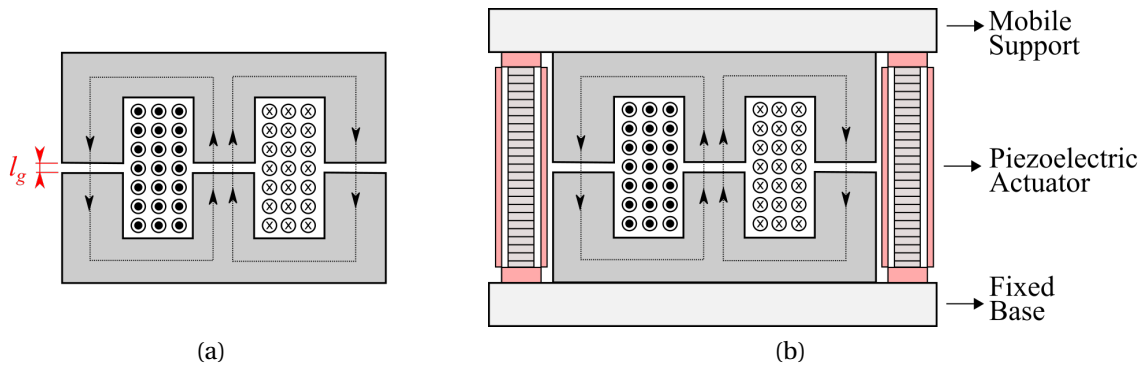

Figure 4.3: Inductance with air-gap scheme.

The use of high permeability magnetic cores allows the manufacture of high induc-

tance with a reduced number of windings according to the Equation 4.8, thus making them more compact as proposed by [102]. Although this allows the fabrication of the inductors necessary for the resonant circuit, these devices have constant inductance. In order to realize a device with tunable inductance, necessary to implement the antiresonance locus strategy, we will investigate the effect caused by the air gap between the ferrite cores.

The effects of the presence of an air gap between the cores of the inductors have been well studied in the literature. It is commonly exploited to improve the design of these devices, since it increases the saturation current, allows the storage of more energy, and decreases the sensitivity of the inductor to variations in the magnetic properties of the cores [103]. Under the assumption of a homogeneous flux density distribution in the air gap and cross-sectional area of the core equal to that of the gap l_g, the inductance is given by [103]:

$$L = \mu_0 A_e \left[\frac{\mu_e}{l_e} + \frac{1}{l_g} \right] N^2 \tag{4.9}$$

It is worth noting the impact of air gap on inductance. According to Equation 4.9, it is clear that an increase in the air gap leads to a reduction in inductance. This equation is valid if the air gap length is much smaller than the dimensions of the core cross-section, a condition for which the homogeneous flux density distribution hypothesis is satisfied. Small variations in the air gap can cause significant variations in inductance, thus requiring a precise control mechanism. For this purpose, we propose the use of the system illustrated in Figure 4.3(b) composed of two piezoelectric stack actuators capable of controlling the air gap between the cores with micrometer precision and two mechanical supports attached to the cores. The piezoelectric stack actuators allow the upper core to be displaced by the force transmitted through the mobile support. The displacement is imposed by applying a constant voltage on the piezoelectric stacked actuators.

4.2.4 Self-adaptive PVA based on machine learning control

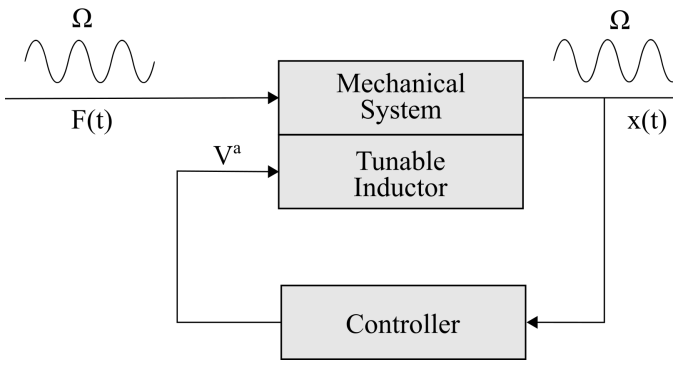

Figure 4.4: General schematic representation of the closed-loop control structure.

Having designed the semi-passive tunable inductor presented in the previous sub-

section, it can be used in a closed-loop system to implement the vibration attenuation based on the antiresonance locus approach. A diagram with all of the components of this system is illustrated in Figure 4.4. Recall that the main goal of the self-adaptive strategy proposed here is to minimize the vibration of the mechanical structure for a given harmonic excitation by controlling the tunable inductance through the applied voltage on the piezoelectric stack actuators.

As discussed for the simplified lumped mass model, the solution of this optimization problem is based on the strategy of an antiresonance locus considering a small resistance and adaptive inductance, leading to Equation 4.7, where the optimal inductance depends on the excitation frequency and represents the condition in which the frequency of the electrical circuit coincides with the excitation frequency. Although this solution can be directly related to the mechanism of inductance tuning through the air gap between the ferrite cores, it is important to note that this variable is driven by the voltage applied to the piezoelectric actuators, which has an unknown relationship with the air gap. To address this problem, we propose an approach based on machine learning control.

Machine learning control has recently been formalized by Duriez et al [104] as a generic model-free strategy for controlling nonlinear systems, although one of the first works using this type of technique was reported by Fleming and Purshouse [105] in the past. In this approach, the control problem is formulated as an optimization with respect to a cost function that can be evaluated using the system's measured outputs. The control objective is to minimize the defined cost function within the space of the control laws. The controller is formulated based on a machine learning algorithm that is trained on an off-line learning loop using data from simulations or experiments. It is then used to minimize the objective in the online closed-loop control system [106]. Different machine learning algorithms have been used with this approach, including: genetic algorithms, reinforcement learning, artificial neural networks, and support vector machines [104, 107].

In this work we propose to use the Gaussian Process Regression (GPR) model, a machine learning algorithm that has attracted attention due to its stochastic formulation and ability to describe nonlinear functions. We propose to use the GPR model in an off-line loop for the supervised learning, where a training data set under operational conditions is provided and the model learns by itself the relationship between the observed variables, which is a priori unknown. This model is then used in the closed-loop system using a controller, based on the machine learning approach to determine the applied voltage for each excitation frequency, in order to minimize the vibration amplitude of the structure. This novel self-adaptive strategy to control the resonant shunt is illustrated in Figure 4.5 and presented in detail in what follows.

In the problem presented in this chapter, the cost function is the time-averaged RMS of the vibration of the mechanical system that depends on the excitation frequency (Ω) and the applied voltage of the piezoelectric actuators (V^a) of the tunable inductance, and is expressed as $J(\Omega, V^a)$. This type of cost function was already explored with adaptive

resonant shunts and is justified by its smooth behavior, less susceptible to noise than the maximum vibration amplitude, and the existence of a global minimum point as reported by Fleming and Moheimani [92].

Consider a data set available for training where you have noisy observations of the time-averaged RMS response $\mathbf{J} = (\mathrm{J}_1, \ldots, \mathrm{J}_\mathrm{N})^\mathrm{T}$ of the mechanical system for a set of applied actuator voltage $\mathbf{V}^{\boldsymbol{a}} = \{\mathrm{V}_1^a, \ldots, \mathrm{V}_\mathrm{N}^a\}$ and excitation frequencies $\boldsymbol{\Omega} = \{\Omega_1, \ldots, \Omega_\mathrm{N}\}$. Adopting the notation of Rasmussen[108], let $\boldsymbol{x} = [\mathbf{V}^{\boldsymbol{a}}, \boldsymbol{\Omega}]^\mathrm{T}$ denote a matrix of multivariate training inputs, and $\boldsymbol{y} = [\mathbf{J}]$ denote the corresponding vector of training outputs. Assuming that these observations can be expressed following regression model :

$$y_i = f(x_i) + \varepsilon, \quad \varepsilon \sim \mathcal{N}\left(0, \sigma^2\right) \tag{4.10}$$

where f is a unknown function and ε is a Gaussian distributed noise with zero mean and variance σ^2. Various methods can be used to solve this classic regression problem. We propose in this work to apply, the GPR model, a non-parametric stochastic model that has been recently explored for control problems of this type. Thus, the function f can be written as [108]:

$$f(\boldsymbol{x}) \sim \mathcal{GP}\left(\mu(\boldsymbol{x}), r\left(\boldsymbol{x}, \boldsymbol{x}'\right)\right) \tag{4.11}$$

where $\mu(\boldsymbol{x})$ and $r\left(\boldsymbol{x}, \boldsymbol{x}'\right)$ are respectively the mean and covariance functions of the distribution over functions described by the Gaussian process. An effective and common choice for the covariance function is the squared-exponential function which is adopted in this work. The training of the model for the dataset is performed by maximizing the marginal likelihood function using a gradient-based optimizer, which for the sake of clarity, is not detailed here. The interested reader is invited to consult [108, 109]. In addition, the code used for implementation is available on the github repository[1].

The main aim of the GPR model is to make predictions for new input data that are not in the training data. Given a new input vector, $\boldsymbol{x}_*$, one can estimate the distribution over functions of a new point y_* given the previous observations as [108]:

$$f_*(\boldsymbol{x}_*) \sim \mathcal{N}\left(\mu_*\left(\boldsymbol{x}_*\right), r_*\left(\boldsymbol{x}_*, \boldsymbol{x}_*'\right)\right) \tag{4.12}$$

where

$$\begin{aligned} \mu_*\left(\boldsymbol{x}_*\right) &= r_*^\mathrm{T}\left(\boldsymbol{x}^*, \boldsymbol{x}\right)\left[\mathrm{R}\left(\boldsymbol{x}, \boldsymbol{x}\right) + \sigma_n^2 \mathbf{I}\right]^{-1} \boldsymbol{y}, \\ r_*\left(\boldsymbol{x}_*, \boldsymbol{x}_*'\right) &= r\left(\boldsymbol{x}_*, \boldsymbol{x}_*\right) - r\left(\mathbf{x}_*, \mathbf{x}\right)^\top \left(\mathrm{R} + \sigma_n^2 \mathbf{I}\right)^{-1} r\left(\boldsymbol{x}, \boldsymbol{x}_*\right). \end{aligned} \tag{4.13}$$

are the posterior mean and variance of the GPR model, $\mathbf{I}$ is the identity matrix, σ_n^2 is a hyperparameter and R is a matrix whose i,j-th element is equal to $r(x_i, x_j)$.

Assuming that the posterior mean of GPR model adequately represents the cost func-

[1] https://github.com/jessepaixao/SPARTA

tion $J(\Omega, V^a)$, it can be used to control the voltage applied to the piezoelectric actuators in order to minimize the vibration of the structure by solving the following minimization problem:

$$\bar{V}^a(\Omega) = \underset{V^a}{\operatorname{argmin}}\, \mu_*(\Omega, \mathbf{V^a}) \tag{4.14}$$

This problem can be solved for a given excitation frequency by interpolating the GPR model within the training range and selecting the voltage to be applied to the piezoelectric actuators that provides the lowest value for the cost function. The complete closed-loop system based on the machine learning control approach is presented in the diagram of Figure 4.5.

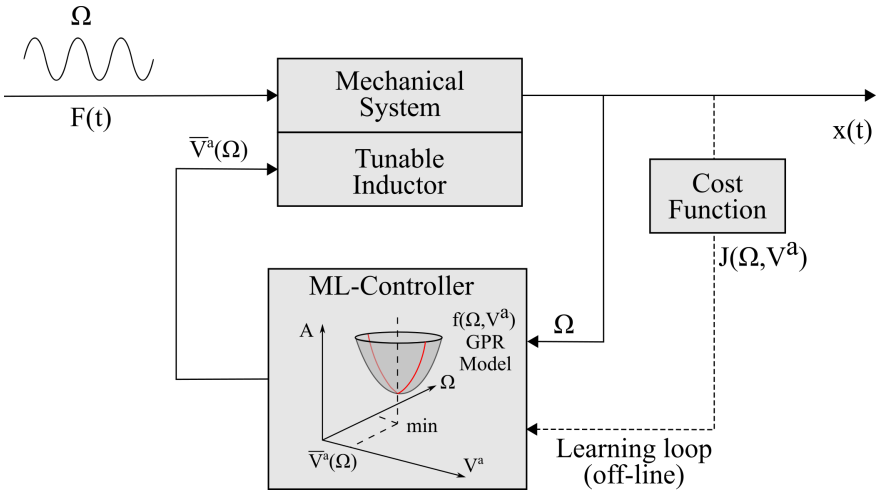

Figure 4.5: Proposed self-adaptive strategy for the the closed-loop operation of the PVA with semi-passive tunable inductor based on the machine learning control approach using GPR model for vibration attenuation of a harmonically excited structure.

4.3 Experimental validation of the self-adaptive vibration absorber

In this section the experimental application of the proposed strategy is presented for a simplified aircraft prototype. This mechanical structure is used only as a demonstrator for the validation of the methodology for vibration reduction. The design and realization of the resonant shunt and the passive tunable inductor are discussed. Then, the self-adaptive strategy is utilized for the vibration attenuation of the airplane prototype considering a swept harmonic excitation and the results obtained are discussed.

4.3.1 Experimental Setup

A photograph of the experimental apparatus is provided in Figure 4.6(a). The simplified aircraft mockup was suspended on a test rig by flexible cables to simulate free-free boundary conditions. Two piezoelectric patches were glued to the airplane wings, the first used for vibration attenuation connected to the shunt circuit, denoted PZT2, and another employed as a collocated sensor to measure the voltage, denoted as PZT1. A schematic representation detailing all components and the integration of the experimental setup is shown in Figure 4.6(b), where three subsystems can be identified: the so-called testing subsystem highlighted in red, responsible for the excitation and vibration measurement of the structure to perform the tests; the named control subsystem highlighted in blue, an active circuit responsible for controlling the shunt circuit; and lastly the resonant shunt subsystem highlighted in green, a passive circuit.

The testing subsystem is managed by a computer dedicated to signal analysis and integrated with the Polytec controller. The structure is excited using an electrodynamic shaker positioned close to PZT 1 and the applied excitation force is measured using a load cell PCB type 208C01. The transverse velocity is measured at the point shown in Figure 4.6(a), the tip of the wing to which the excitation is applied, using the Polytec Laser Doppler vibrometer PSV-500 Xtra 1D. The control subsystem is managed by the Raspberry Pi with the add-on boards MCC 128 and MCC 152 manufactured by Measurement Computing, dedicated respectively for acquisition and analog signal generation. A voltage divider is used to adjust the voltage measurement at PZT2 to the acquisition card limits of plus or minus 10V. The piezoelectric actuators in charge of the inductance variation are controlled by the signal generated in the MCC-152 card, which is amplified with a gain of 20 in the Cedrat LA75B power amplifier. The resonant circuit consisting only of the tunable inductor is connected to PZT2 and mounted right next to the aircraft prototype. The machine learning control algorithm for closed-loop operation in the experimental tests performed are implemented on the Raspberry Pi.

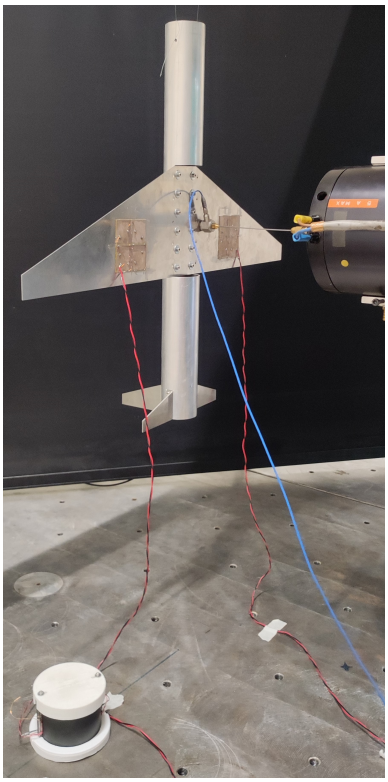

(a)

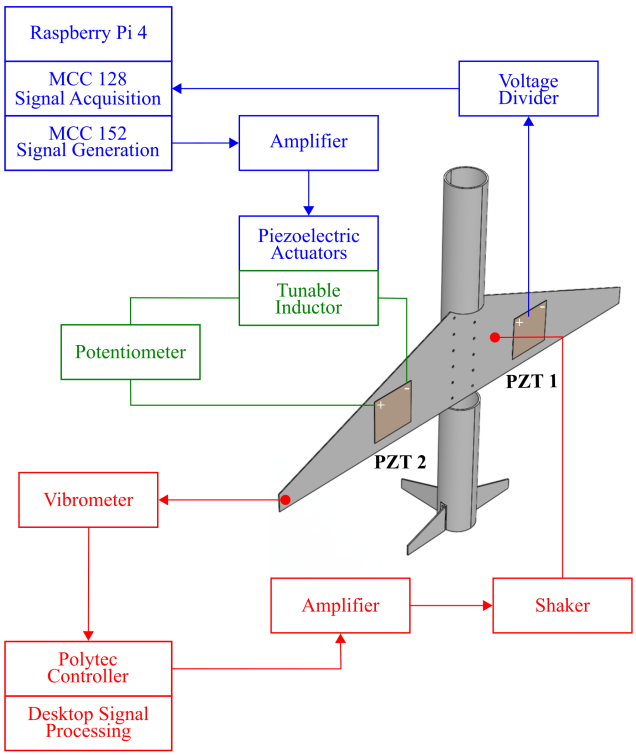

(b)

Figure 4.6: (a) Photograph and (b) schematic representation of the experimental setup.

4.3.2 Design and manufacturing of tunable passive inductor

The choice of the position and dimensions of the piezoelectric patches presented in Figure 4.6 were based on the finite element model of the aircraft prototype, already detailed in a previous publication [110]. An initial parametric study of the position was performed to maximize the electromechanical coupling of the piezoelectric patches in relation to the third bending mode of the airplane. The choice of this symmetric mode was based on a compromise between its frequency and the inductance required to tune the PVA. It should be noted that in the case of choosing an asymmetric mode, the positioning of the PZTs to ensure a colocalization would be different. The width and length dimensions of the patches were chosen to maximize the piezoelectric capacitance, aiming to reduce the inductance required that, according to Equation 4.6, is inversely proportional to the piezoelectric capacitance.

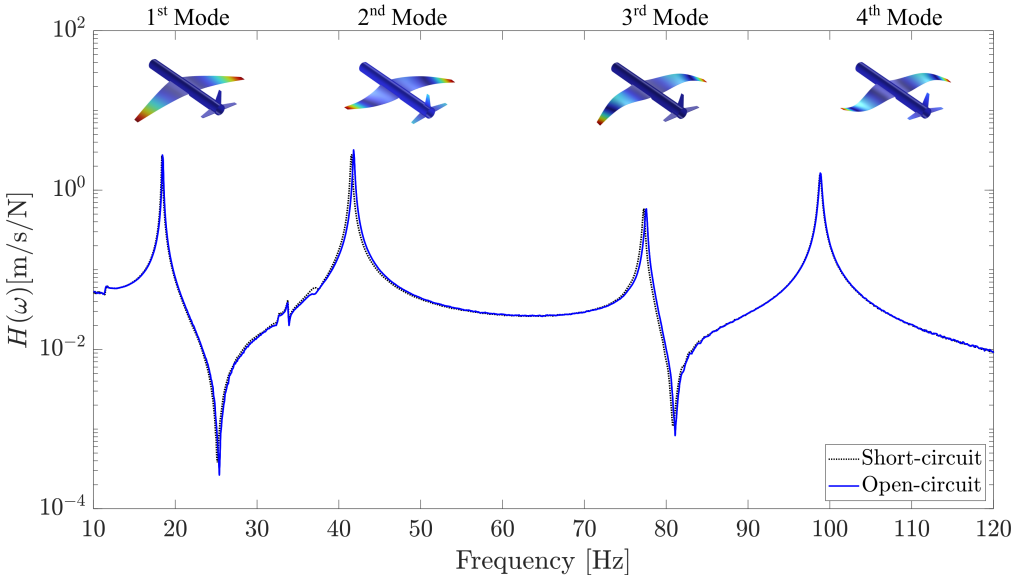

Figure 4.7: Mobility frequency response function and corresponding mode shapes for short-circuit and open-circuit patch configurations.

The initial design of the resonant circuit was performed considering constant inductance, given by Equation 4.6. The electromechanical coupling was estimated using Equation 4.3 and the natural frequencies obtained from the experimental FRFs shown in Figure 4.7 for the piezoelectric transducers in open-circuit and closed-circuit conditions. The value of the piezoelectric capacitance at constant strain was measured experimentally using an impedance analyzer. From the estimated experimental parameters and using Equation 4.6, an inductance of 28.64 H and a resistance of 1533.18 Ω were obtained for the equal-peak design solution. All the numerical values are summarized in Table 4.1.

The inductance and resistance estimates for the solution based on the equal-peaks method was used as a starting point for the tunable inductor design. Among the various commercially available ferrite cores, the T26 ferrite was chosen because it offers a suitable compromise between inductance factor and maximum saturation current. Based on

Table 4.1: Numerical values for the experimental estimated paramters.

ω_{oc}[Hz]	ω_{sc}[Hz]	k_c	C^{ε} [nF]	L_{ep} [H]	R_{ep} [Ω]	A_l [μH/tr^2]
77.56	77.25	0.0897	147	28.64	1533.18	10

the initial values of inductance an resistance and the inductance factor supplied by the manufacturer of the T26 ferrite cores it is possible to calculate the number of windings required to make the coil, which was 1692 turns. However, since the tunable inductance is controlled by the air gap between the cores that reduces its value, the winding was manufactured with a higher number of turns to allow the inductance to be piloted within a margin of plus or minus 10 percent of the calculated initial value. Thus, the coil was manufactured using an automatic winding machine with 1900 turns. The inductor was assembled using the coil and the T26 ferrite cores along with piezoelectric stack actuators. The inductance measured using a LCR meter for the assembled inductor without air gap between the cores was 35.5 H with a quality factor of 181.3, which is equivalent to a DC resistance of 95 Ω. It can be observed that the measured inductance is considerably higher than that estimated using the numerical model. This was expected for the device assembly without air gap, since the inductor coil was manufactured with a higher number of turns to ensure the required margin of variation for the inductance, which was intentionally foreseen as the inductance is reduced as the air-gap increases. A photograph of the tunable inductor including the fixed base and movable support additively fabricated using PLA and the piezoelectric actuators is shown in Figure 4.8(a).

The characterization of the relationship between the inductance and the applied voltage in the piezoelectric actuators was performed using the experimental setup schematized in Figure 4.8(b). A voltage generator was used to apply a constant signal varying from 0 to 5 V with a step of 0.5 V, while an LCR meter was used to measure the inductance at each level. This test was repeated three times and the results obtained are shown in Figure 4.8(c). Note in this curve that with increasing applied voltage, raising the space between the ferrite core proportionally, initially induces a linear variation in inductance, as predicted by Equation 4.9. However, as the gap increases, the magnetic flux lines start to bulge out around the gap, causing a reduction in effective air gap reluctance and consequently an increase in inductance, a phenomenon known as the fringing effect, which explains the change in trend of the curve. For more details on fringing effect the interested reader can refer to [103, 111].

4.3.3 Self-adaptive control based on Gaussian Process Regression

The application of the proposed self-adaptive strategy requires an initial supervised learning step performed off-line. The aircraft prototype is submitted to an automated data collection process for training the GPR model. Using the test and control subsystem si-

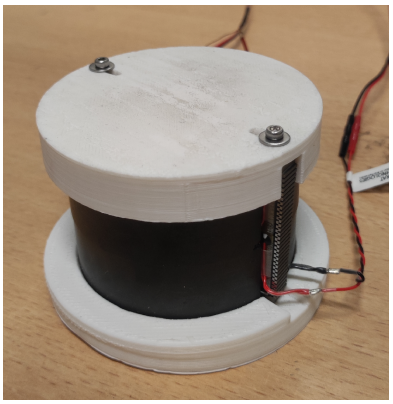

(a)

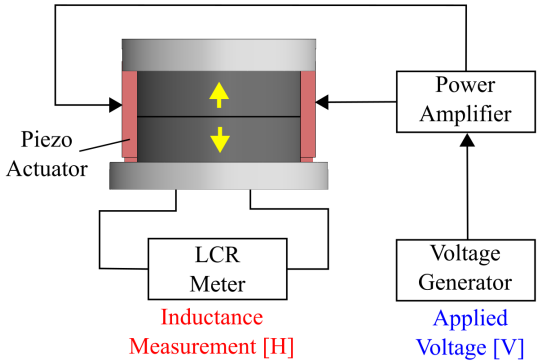

(b)

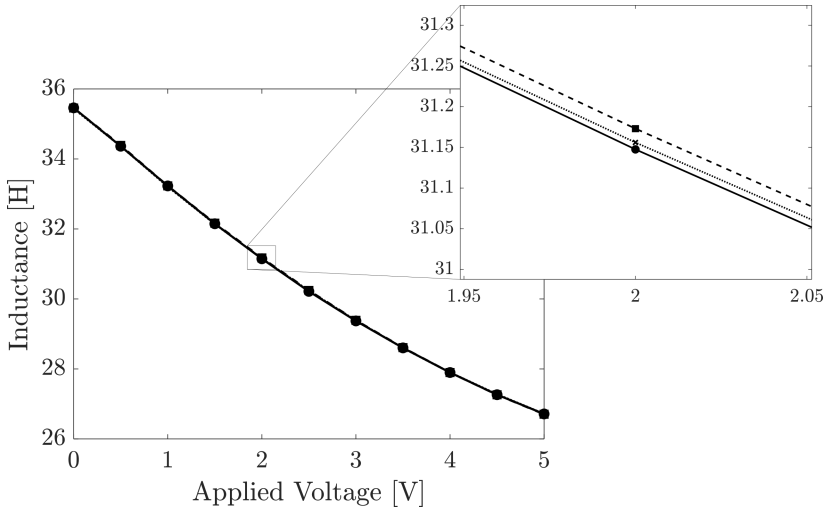

(c)

Figure 4.8: Experimental characterization of variable inductance as a function of applied voltage on the stack : test 1 (- - -), test 2 (—) and test 3 (.....).

multaneously, a constant amplitude harmonic excitation signal is applied to the shaker and the excitation frequency is varied from 70 to 85 Hz with a step of 0.5 Hz. For each frequency the voltage applied to the piezoelectric stack actuators is varied from 0 to 5 V with a step of 0.25 V, for a total of 651 test configurations. For each configuration the structure is excited for 2 seconds followed by 1s of rest, and the synchronized acquisition of the time signals of velocity measured by the vibrometer and voltage at the PZT1 is performed. This

process, which is fully automated, takes approximately 32 minutes.

Samples of the time signals for the wing velocity measured by the vibrometer and voltage at PZT1 for an excitation frequency of 70 Hz and applied voltage on the piezoelectric actuators of 0 V are presented in Figure 4.9. The time-averaged RMS values of the signals for all experimentally tested conditions as a function of excitation frequency and applied voltage on the stack are represented through the surface plots presented in Figure 4.10. It can be observed by analyzing the surface presented in Figure 4.10(a) that the RMS value of the velocity has a smooth behavior in relation to the excitation frequency, with the existence of minimum operating points - highlighted by the blue dots - as a function of the voltage applied to the piezoelectric stack actuators that directly controls the resonance frequency of the electric circuit. It is important to note that the minimum points for the velocity surface coincide exactly with the minimum points for the voltage values in PZT 1. This is because the two surfaces have a remarkably similar shape. This fact can be quantitatively verified by calculating the distance between the two normalized surfaces, which have a maximum distance of 0.0028. Therefore, it allows the use of the voltage signal measured at PZT 1 to evaluate the cost function, which is considerably more practical for the implementation in practice than the velocity measured by the vibrometer, since the transducer is already installed in the structure and can be readily measured. Hence, hereafter the measured velocity by the vibrometer will only be used for validation of the implemented control system.

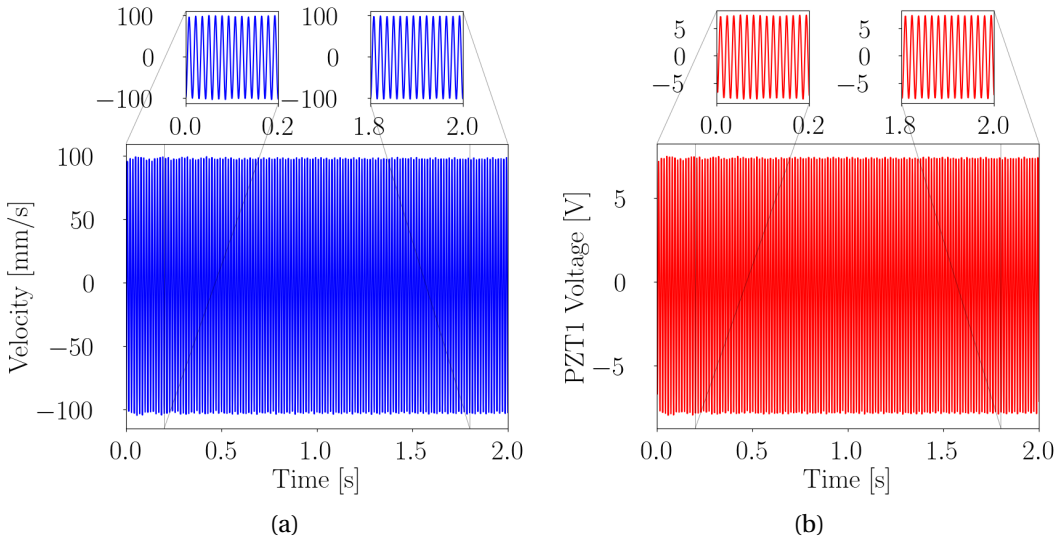

Figure 4.9: Time signals of velocity at measured point by the vibrometer and voltage in PZT 1 for 75 Hz excitation frequency and 0V applied to piezoelectric stack actuators.

A total of five tests were performed to collect experimental data in the mentioned configurations. The data sets from four of these tests were used to train the GPR model, considering the excitation frequency and the applied voltage on the piezoelectric actuators as input variables and the RMS voltage value at PZT 1 as output. The experimental data used for training and the predicted mean of the trained model is presented in Figure 4.11.

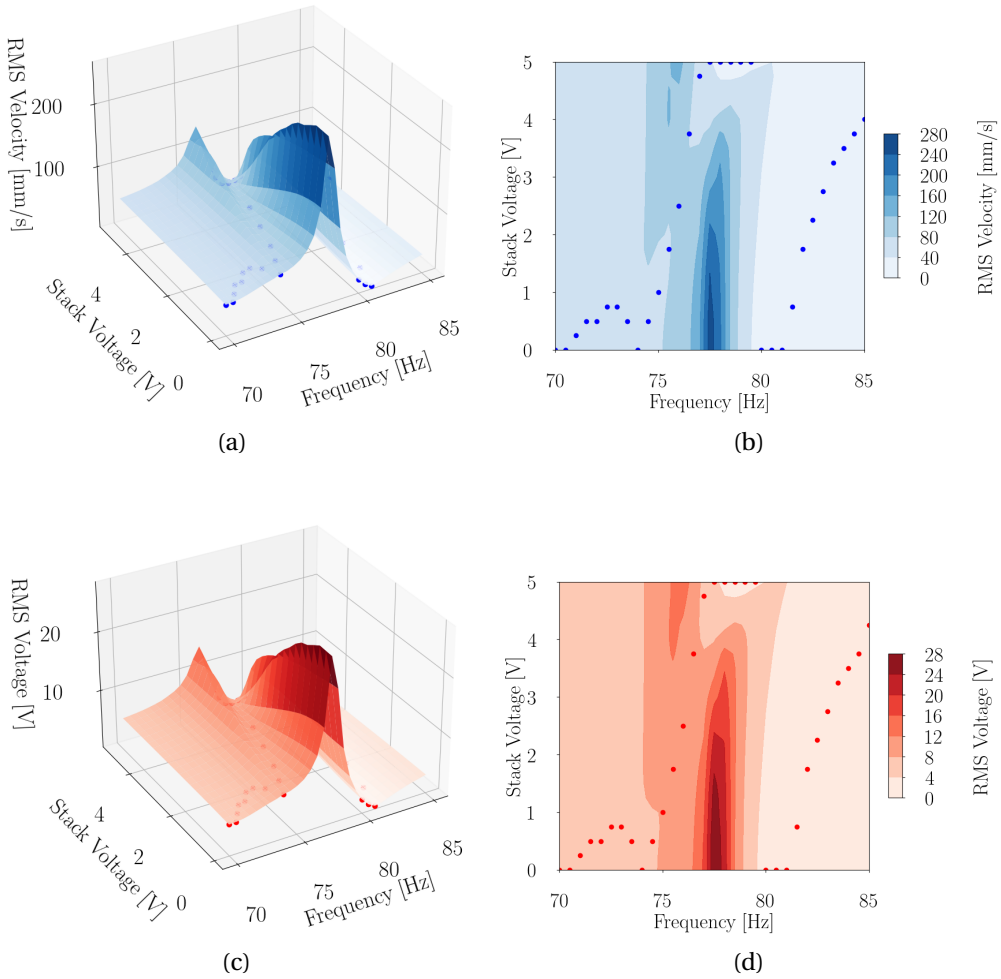

Figure 4.10: Experimental surfaces obtained for the RMS value of velocity (a - b) and voltage at PZT 1 (c - d) as a function of excitation frequency and applied voltage on the piezoelectric actuators for the first test performed.

The model validation was performed using Root-Mean Squared Error (RMSE) criterion based on leave-one-out cross-validation method, for which the last data set from the five was used. The maximum RMSE between the RMS voltage of PZT 1 experimentally observed and predicted by the model obtained was of 0.038. This low RMSE value is a strong indicator of adequate prediction the trained GPR model.

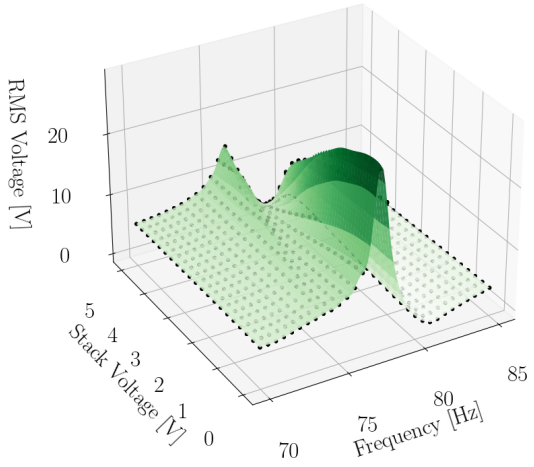

Figure 4.11: Predicted mean ( )by the GPR model trained with the experimental data (●) used for training from four of the five tests.

Closed-loop control based on the trained GPR model

Once the GPR model has been trained in the off-line learning loop, the self-adaptive control strategy can be tested in closed-loop. The test subsystem is used to excite the structure with a swept-sine signal with frequency varying linearly from 70 Hz to 85 Hz and a duration of 120 seconds. The machine learning control algorithm based on the trained GPR model is implemented on the Raspberry Pi, responsible for the control subsystem that runs independently. The voltage acquisition at PZT 1 is performed at a frequency of 2500 Hz and with a duration of 0.5 s. For each voltage time signal acquired the frequency is estimated using the fast Fourier transform based on the parabolic interpolation approach, which provides improved frequency resolution for harmonic signals [112]. The signal frequency is then used as input to the GPR model, which is used to estimate the voltage that must be applied to the piezoelectric actuators to minimize the stress on PZT 1 and consequently the vibration in the structure. This whole process takes place in a closed-loop online on the Raspberry Pi board.

The experimental results of the self-adaptive control strategy is compared to the solution provided by the equal-peak design, in which the inductance is kept constant regardless of the operating conditions. This solution is obtained experimentally by adjusting the tunable inductance to the condition where the experimental FRF of the system has two equal-peaks around the mode of interest. The results obtained for these two strategies are presented in Figure 4.12. An attenuation gain of 3.07 dB (equivalent to an amplitude reduction of approximately 30%) is obtained by comparing the maximum amplitudes can be observed for the self-adaptive strategy for frequencies around the third mode, which can be explained by the antiresonance locus at the excitation frequency. In particular, at

the resonant frequency of the mode of interest, the two solutions perform similarly, which is to be expected, since in this case the excitation frequency coincides with the frequency of the mode for which equal-peak method solution is based. The peak in the velocity response at 80s is due to the drastic decrease in the voltage applied to the piezoelectric actuators, causing a sharp decrease in inductance. This causes a transient response of the system, which soon becomes stable, but that should be further investigated.

The voltage signal applied to the tunable inductor has a relationship with the electrical resonance frequency of the shunt whose trend can be inferred from its inductance. With the increase of the applied voltage, it is expected a decrease in inductance (see Figure 4.8) and consequently an increase in the electric resonance frequency of the shunt (see Equation 4.4). Thus, the analysis of the time signal of the voltage applied to the actuators indicates that there was an overall increase in resonance of the electrical circuit from 0 to approximately 60 s, following approximately the same trend of the excitation frequency. However, one can question the behavior of the sharp reduction of the applied voltage around 80 s which indicates a reduction of the electric resonance frequency as the excitation frequency increases. Although this behavior cannot be explained regarding the antiresonance locus strategy presented in the previous section for the lumped mass model, it is important to note that this experimental application involves a complex structure with multiple modes, some of which are close to each other (see mode 3 and 4 in Figure 4.7). Moreover, the nonlinear effects of the semi-passive tunable inductor as well as uncertainties, are difficult to take into account in the traditional model-based control approach. This justifies and strengthens the advantages of the model-free approach based on the machine learning control method presented here.

The machine learning control strategy proposed in this work is applicable for the operation of the structure under operating conditions within the conditions used in training of the GPR model, which limits its application in more challenging scenarios susceptible to unforeseen variations in environmental and operating conditions. However, recent works involving the use of GPR models has already shown the possibility of updating a trained model with data obtained during operation in a way that allows the adaptation of the controller in case of structural changes [113]. Alternatively, the application of gradient-based optimization methods for the online controlling of the input variable of the closed-loop system as applied in the past may be envisaged [92]. Another interesting type of machine learning control strategy that could also be applied in this case is the reinforcement learning approach based on neural networks, in which the algorithm performs an automatic training step to tune the controller. This strategy was initially explored as a control method for the demonstration case studied here, however, the main difficulty encountered was in choosing the appropriate parameters for the neural network used, which failed to converge in the learning process in the tests carried out. Nevertheless, a recent study presented by Febvre et al [114] using this strategy has shown promising results for the control of piezoelectric transducers' networks in vibration attenuation.

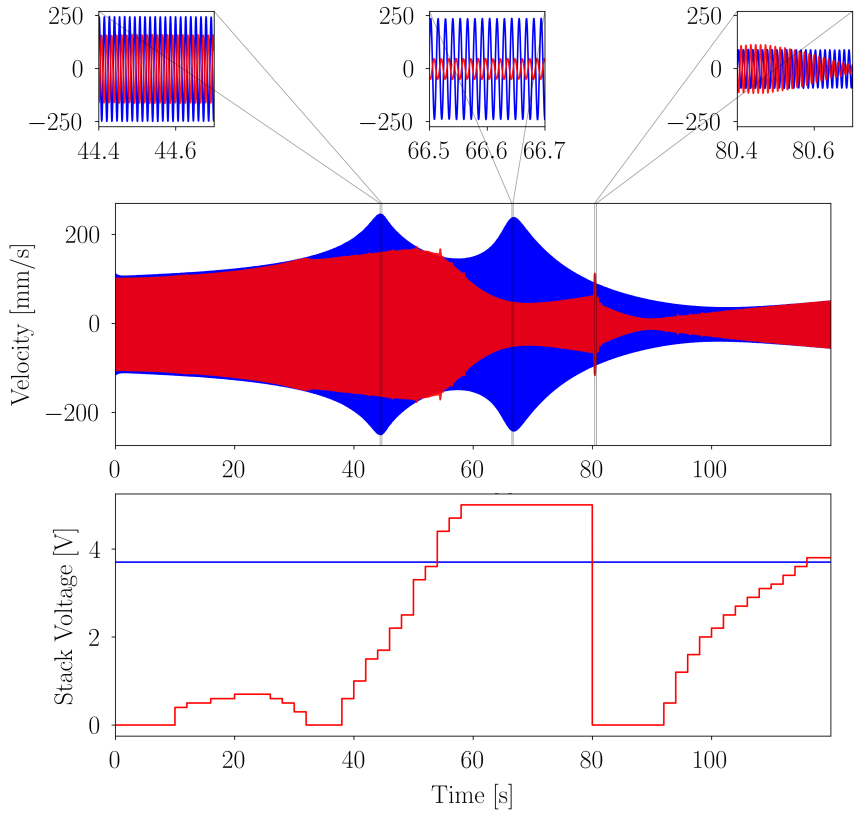

Figure 4.12: Closed-loop experimental application of the self-adaptive strategy based on the trained GPR model (—) compared to the solution provided by the equal-peak method (—), in which inductance remains constant.

4.4 Conclusions

In this chapter a self-adaptive PVA with semi-passive resonant shunt for the vibration attenuation of harmonically excited structures is proposed. This technique has many advantages. A resonant shunt composed only of passive components circumvents the main limitation of the widely used synthetic impedances, in particular the problem of instability. In addition, the inductance of the novel high-Q tunable inductor can be controlled by the application of a simple constant voltage signal, unlike the devices with similar capabilities based on SSD and PWM techniques that require signals at high-switching frequencies. Moreover, the proposed self-adaptive strategy based on machine learning control does not require a physical model of the closed-loop system since it employs a supervised learning approach via a GPR model to learn how to control the semi-passive tunable inductor to achieve the maximum vibration attenuation as function of the excitation frequency. The application of this strategy was demonstrated experimentally on a simplified airplane mockup. The results show a significant improvement of approximately 3.07 dB (equivalent to an amplitude reduction of approximately 30%) in vibration attenuation for a swept sine excitation compared to a traditional resonant shunt with fixed inductance. Future applications to the attenuation of vibrations in rotating machinery are envisaged as well as an extension to the case of random excitations.

Conclusions and Perspectives

In this thesis, a paradigm shift in structural design has been investigated based on the introduction of the bio-inspired concept of developmental plasticity has been explored in the context of high performance dynamic structures. The analogy of this bio-concept to engineering applications is achieved through the proposed new paradigms: the self-design manufacturing paradigm and the self-adaptive structures paradigm. New methodological and experimental solutions have been developed based on these two paradigms to enable their application in three demonstration cases of known structural dynamics problems: the design of mechanical vibration absorbers, the assignment of natural frequencies, and the attenuation of vibration with piezoelectric vibration absorbers.

The implementation of the self-design manufacturing paradigm relies on the integration of the manufacturing process, a real-time measurement system, and a decision algorithm for modifying the initial design in a closed-loop system to provide developmental plasticity during the manufacturing of a structure. Thus, the first contribution of this work was the development of the methodology and experimental solution for its application, combining the additive manufacturing process, an *in-situ* laser vibrometer system and a closed-loop control system to guide the modifications based on experimental data presented in Chapter 2. The methodology was applied to a demonstration case of fabricating a beam-like vibration absorber inserted into a plate, with the aim of achieving an enhanced attenuation performance near to the theoretical solution for each sample manufactured. This case allowed to demonstrate for the first time the feasibility of this paradigm with current technologies, and the results achieved in improving the attenuation of the manufactured devices served to highlight the advantages of this paradigm over the traditional one.

A major challenge in providing developmental plasticity for the fabrication of a structure is related to the complex technological integration required of the manufacturing process, measurement system and decision-making, since most manufacturing processes are based on the traditional paradigm, which seeks to reproduce the nominal design of the structure as accurately as possible. Although this challenge was surmounted in the first demonstration case with the experimental system developed, the design modifications to the structure were limited to predefined shapes and to only two possible regions of the absorber through a simple decision algorithm. This was the main limitation of the methodology proposed for this first demonstration case. Hence, in order to tackle this

limitation through a decision-making algorithm capable of proposing modifications with less constraints, a new methodology was proposed in the Chapter 3 for application to the problem of assigning natural frequencies with high precision.

The second contribution of this work refers to the so-called online topological optimization methodology applied to the problem of assigning the natural frequencies of a plate-like structure based on the self-design manufacturing paradigm. This methodology proposes an intelligent algorithm to guide the developmental plasticity of the structure through structural modifications with fewer constraints through an approach based on topology optimization. Unlike the traditional topology optimization approach based exclusively on the prediction of physical models, online topological optimization proposes the combination of this approach with modal expansion technique, which makes it possible to incorporate data extracted from the physical structure to improve the fidelity of the proposed solution. This feature is essential for achieving high precision in applications with performance that is very sensitive to uncertainties, as in the case of the problem of assignment of natural frequencies explored. Although the demonstration of this methodology was carried out using only numerical simulations, the proposed demonstration case of assigning the first three natural frequencies of a plate was formulated considering various aspects of the practical implementation in the experimental apparatus developed in Chapter 1 based on the additive manufacturing process. The numerical results demonstrated the possibility of achieving an accuracy of $\pm$ 1 Hz in the assignment of frequencies for the case explored and the comparison made with the traditional topology optimization approach based solely on the model without modal expansion highlighted the importance of taking into account information extracted directly from the physical structure in this context.

In the last part of this thesis, the concept of developmental plasticity, which focuses on modeling and manufacturing uncertainties, was extended to the operation of the structure in order to deal with uncertainties related to its functioning, through the so-called operational plasticity with the paradigm of self-adaptive structures. This paradigm was applied to the problem of vibration attenuation using a piezoelectric absorber, a new semi-passive resonant shunt with tunable inductance. The device is based on a tunable inductor made with ferrite cores and which has its inductance controlled through the effect of air space between the cores using piezoelectric stack actuators. This concept, which has not yet been explored in the literature, represents the third contribution of this work and allowed the experimental implementation of the proposed methodology. Although the concept of adaptability for piezoelectric absorbers in operation has already been explored in the literature, it is generally applied in order to improve the robustness of vibration attenuation by making the device less sensitive to operating or design uncertainties. The proposed paradigm seeks to explore adaptability from the point of view of the concept of operational plasticity, in the sense of using the device's sensitivity to operational uncertainties to adapt it to the operating condition.

Perspectives

The research carried out in this thesis served mainly to introduce the concepts of developmental and operational plasticity through the proposed paradigm shift with simple demonstration cases to highlight the advantages and limitations arising from the introduction of these concepts in the development of engineering structures. Although the feasibility of the proposed paradigms in the current technological state has been demonstrated, several challenges and issues have been highlighted and should be tackled in future work.

A major challenge to implementing developmental plasticity in the self-design manufacturing paradigm is technological. Current manufacturing processes are designed to execute a design from start to finish without modification. The experimental implementation using the 3D printer in Chapter 2 was only possible by developing a program to generate the routine for printing modifications to an already printed structure, which requires a calibration or recognition stage of the existing part within the machine. Although this experimental solution worked for the demonstration case in Chapter 2 with modifications of simple predefined shapes, it will not work properly for more complex structural modifications, such as those provided by the online topology optimization method in Chapter 3, mainly due to the problem of debonding of printed layers and destruction of existing layers. These problems may be related to the low geometric accuracy of the machine and the configuration of printing parameters for structural changes to an existing structure. It is therefore envisioned to implement the methodology using a more accurate 3D printer and to carry out a study of the printing parameters and optimization of the printing path for structural modifications to an existing part.

Moreover, the two demonstration cases of the self-adaptive manufacturing paradigm were limited to applications involving only the additive manufacturing process due to technological limitations. However, other types of manufacturing processes may be envisaged, such as subtractive manufacturing. Hybrid additive/subtractive manufacturing in particular, which combines these two manufacturing processes, could enhance the capacity for structural modifications and consequently the developmental plasticity in the proposed paradigm. Therefore, this is a prospect to be explored in the future.

One of the major limitations of the online topology optimization methodology proposed in Chapter 3 is related to its high computational cost, a common problem with topology optimization methodologies. In addition, there is the computational cost of the modal expansion technique. These can be a limiting factors for applying this methodology to larger, more complex structures. In this sense, a possible solution would be to explore model reduction techniques, which are already being explored to speed up topology optimization methods. A second solution envisioned is to study the application of machine learning algorithms to solve optimization with gradient free methods. A recent work proposed by Deng et al [115] revealed promising results in reducing computational

time of topology optimization with the application of a method based on deep neural network, called self-directed online learning optimization.

In the application of the self-adaptive structures paradigm in Chapter 4 to the case of attenuation using the piezoelectric absorber, a new tunable inductance device was presented. This device was able to generate a high inductance values of the order of tens of H and with a tunability in the order of ± 10 % of the nominal inductance. The tuning range was limited by the gap between the ferrite cores controlled by the piezoelectric stack actuators. After a certain distance between the cores, the variation in inductance becomes non-linear. In this sense, it would be interesting to investigate the behavior of the inductance for larger distances between the cores in order to determine the maximum limits of inductance variation. This information would be useful in studying the possibility of using this type of device to attenuate multiple modes.

Moreover, the attenuation strategy adopted for the piezoelectric absorber demonstration case was limited to the case of harmonically excited structures. Therefore, a natural extension of this work in the future would be to study the application to the case of a broadband excitation. In addition, the vibration attenuation was based on the antiresonance locus approach. As the attenuation caused by the antiresonance for the shunt circuit used depends on reducing its resistance, an interesting point to be investigated to improve the attenuation performance would be how to reduce this internal resistance of the shunt circuit inductance, increasing the Q factor. One possibility envisioned but still limited by technological factors would be the use of superconducting wires.

The control algorithm using the Gaussian Process model for the proposed piezoelectric absorber is based on supervised learning and requires an offline training stage of the structure under similar operating conditions. In practical applications, this training step can be difficult to carry out and, in addition, in the case of unexpected changes outside the training domain, it can generate undesired behavior. In this context, the use of techniques that allow online learning or learning adaptation in real-time, a topic that has recently been widely investigated [113, 116], is envisioned for the future.

Bibliography

[1] M. Petyt, *Introduction to Finite Element Vibration Analysis*. Cambridge University Press, 2010.

[2] N. Cross, *Engineering Design Methods: Strategies for Product Design*. Wiley, 2021.

[3] C. Soize, *Uncertainty Quantification: An Accelerated Course with Advanced Applications in Computational Engineering*. Springer, 2017.

[4] G. I. Schueller and H. A. Jensen, "Computational methods in optimization considering uncertainties - an overview," *Computer Methods in Applied Mechanics and Engineering*, vol. 198, pp. 2–13, Nov. 2008.

[5] C. Zang, M. Friswell, and J. Mottershead, "A review of robust optimal design and its application in dynamics," *Computers & Structures*, vol. 83, pp. 315–326, Jan. 2005.

[6] G. I. Schueller, "On the treatment of uncertainties in structural mechanics and analysis," *Computers and Structures*, vol. 85, pp. 235–243, Mar. 2007.

[7] Y. Ben-Haim and F. M. Hemez, "Robustness, fidelity and prediction-looseness of models," *Proceedings of the Royal Society A: Mathematical, Physical and Engineering Sciences*, vol. 468, pp. 227–244, Sept. 2012.

[8] F. Kiakojouri, V. De Biagi, and L. Abbracciavento, "Design for Robustness: Bio-Inspired Perspectives in Structural Engineering," *Biomimetics*, vol. 8, p. 95, Feb. 2023.

[9] B. Sieriebriennikov and R. J. Sommer, "Developmental Plasticity and Robustness of a Nematode Mouth-Form Polyphenism," *Frontiers in Genetics*, vol. 9, p. 382, Sept. 2018.

[10] A. Hot, T. Weisser, and S. Cogan, "An info-gap application to robust design of a pre-stressed space structure under epistemic uncertainties," vol. 91, pp. 1–9, 2017.

[11] M. Khammash, "An engineering viewpoint on biological robustness," *BMC Biology*, vol. 14, p. 22, Dec. 2016.

[12] Z. Huan, G. Zhenghong, X. Fang, and Z. Yidian, "Review of Robust Aerodynamic Design Optimization for Air Vehicles," *Archives of Computational Methods in Engineering*, vol. 26, pp. 685–732, July 2019.

[13] H.-G. Beyer and B. Sendhoff, "Robust optimization – A comprehensive survey," *Computer Methods in Applied Mechanics and Engineering*, vol. 196, pp. 3190–3218, July 2007.

[14] G.-J. Park, T.-H. Lee, K. H. Lee, and K.-H. Hwang, "Robust Design: An Overview," *AIAA Journal*, vol. 44, pp. 181–191, Jan. 2006.

[15] S. Moritz Göhler, T. Eifler, and T. J. Howard, "Robustness Metrics: Consolidating the Multiple Approaches to Quantify Robustness," *Journal of Mechanical Design*, vol. 138, p. 111407, Nov. 2016.

[16] Y. Ben-Haim, *Information-gap Decision Theory : Decisions Under Severe Uncertainty*. London: Academic Press, 2nd ed., 2006.

[17] L. Dell'Elce, E. Gourc, and G. Kerschen, "A robust equal-peak method for uncertain mechanical systems," *Journal of Sound and Vibration*, vol. 414, pp. 97–109, feb 2018.

[18] G. Calafiore and M. C. Campi, "Uncertain convex programs: randomized solutions and confidence levels," *Mathematical Programming*, vol. 102, pp. 25–46, 2005.

[19] J. Ormondroyd and J. Den Hartog, "The theory of the dynamic vibration absorber," *Trans., ASME, Applied Mechanics*, vol. 50, pp. 9–22, 1928.

[20] J. Kim, T. H. Lee, Y. Song, and T. H. Sung, "Robust design optimization of fixed-fixed beam piezoelectric energy harvester considering manufacturing uncertainties," *Sensors and Actuators A: Physical*, vol. 260, pp. 236–246, 2017.

[21] L. Adamson, S. Fichera, and J. Mottershead, "Receptance-based robust eigenstructure assignment," *Mechanical Systems and Signal Processing*, vol. 140, p. 106697, June 2020.

[22] J. A. G. M. Visser, J. Hermisson, G. P. Wagner, L. A. Meyers, H. Bagheri-Chaichian, J. L. Blanchard, L. Chao, J. M. Cheverud, S. F. Elena, W. Fontana, G. Gibson, T. F. Hansen, D. Krakauer, R. C. Lewontin, C. Ofria, S. H. Rice, G. V. Dassow, A. Wagner, and M. C. Whitlock, "Perspective: Evolution and detection of genetic robustness," *Evolution*, vol. 57, pp. 1959–1972, Sept. 2003.

[23] P. Wojtaszek, *Mechanical Integration of Plant Cells and Plants*. Springer Berlin Heidelberg, 1 ed., Jan. 2011.

[24] B. C. Nicoll and D. Ray, "Adaptive growth of tree root systems in response to wind action and site conditions," *Tree Physiology*, vol. 16, pp. 891–898, Nov. 1996.

[25] B. Moulia, C. Coutand, and J.-L. Julien, "Mechanosensitive control of plant growth: bearing the load, sensing, transducing, and responding," *Frontiers in Plant Science*, vol. 6, p. 52, Feb. 2015.

[26] W. Tan, "Water level control for a nuclear steam generator," *Nuclear Engineering and Design*, vol. 241, pp. 1873–1880, May 2011.

[27] S. Barbarino, O. Bilgen, R. M. Ajaj, M. I. Friswell, and D. J. Inman, "A review of morphing aircraft," *Journal of Intelligent Material Systems and Structures*, vol. 22, pp. 823–877, Aug. 2011.

[28] K. Yi, G. Matten, M. Ouisse, and E. Sadoulet-reboul, "Programmable metamaterials with digital synthetic Programmable metamaterials with digital synthetic impedance circuits for vibration control," *Smart Materials and Structures*, Jan. 2020.

[29] C. M. Shaffer, A. Deo, A. Tudor, R. Shenoy, C. D. Danesh, D. Nathan, L. L. Gamble, D. J. Inman, and Y. Chen, "Self-Programming Synaptic Resistor Circuit for Intelligent Systems," *Advanced Intelligent Systems*, p. 2100016, May 2021.

[30] L. Asarian, V. Gloy, and N. Geary, "Homeostasis," in *Encyclopedia of Human Behavior (Second Edition)* (V. Ramachandran, ed.), pp. 324–333, San Diego: Academic Press, second edition ed., Mar. 2012.

[31] E. W. Chehab, E. Eich, and J. Braam, "Thigmomorphogenesis: A complex plant response to mechano-stimulation," *Journal of Experimental Botany*, vol. 60, pp. 43–56, Dec. 2009.

[32] A. J. Teichtahl, A. E. Wluka, P. Wijethilake, Y. Wang, A. Ghasem-Zadeh, and F. M. Cicuttini, "Wolff's law in action: A mechanism for early knee osteoarthritis," *Arthritis Research and Therapy*, vol. 17, pp. 1–9, Sept. 2015.

[33] M. Sitti, "Physical intelligence as a new paradigm," *Extreme Mechanics Letters*, vol. 46, p. 101340, July 2021.

[34] S. Li and K. W. Wang, "Plant-inspired adaptive structures and materials for morphing and actuation: a review," *Bioinspiration & Biomimetics*, vol. 12, p. 011001, Dec. 2016.

[35] D. Moorhouse, B. Sanders, M. V. Spakovsky, and J. Butt, "Benefits and design challenges of adaptive structures for morphing aircraft," *The Aeronautical Journal*, vol. 110, pp. 157–162, Mar. 2006.

[36] V. Cavalieri, A. De Gaspari, and S. Ricci, "Optimization of compliant adaptive structures in the design of a morphing droop nose," *Smart Materials and Structures*, vol. 29, p. 075020, July 2020.

[37] R. Y. Zhong, X. Xu, E. Klotz, and S. T. Newman, "Intelligent manufacturing in the context of industry 4.0: A review," *Engineering*, vol. 3, pp. 616–630, Oct. 2017.

[38] M. Eugeni, T. Quercia, M. Bernabei, A. Boschetto, F. Costantino, L. Lampani, A. M. Spaccamela, A. Lombardo, M. Mecella, L. Querzoni, R. Usinger, M. Aliprandi, A. Stancu, M. Ivagnes, G. Morabito, A. Simoni, A. Brandão, and P. Gaudenzi, "An industry 4.0 approach to large scale production of satellite constellations. The case study of composite sandwich panel manufacturing," *Acta Astronautica*, vol. 192, pp. 276–290, Mar. 2022.

[39] I. A. Okaro, S. Jayasinghe, C. Sutcliffe, K. Black, P. Paoletti, and P. L. Green, "Automatic fault detection for laser powder-bed fusion using semi-supervised machine learning," *Additive Manufacturing*, vol. 27, pp. 42–53, May 2019.

[40] C. Liu, A. C. C. Law, D. Roberson, and Z. J. Kong, "Image analysis-based closed loop quality control for additive manufacturing with fused filament fabrication," *Journal of Manufacturing Systems*, vol. 51, pp. 75–86, 2019.

[41] L. Lu, J. Hou, S. Yuan, X. Yao, Y. Li, and J. Zhu, "Deep learning-assisted real-time defect detection and closed-loop adjustment for additive manufacturing of continuous fiber-reinforced polymer composites," *Robotics and Computer-Integrated Manufacturing*, vol. 79, p. 102431, 2023.

[42] S. Jayasinghe, P. Paoletti, C. Sutcliffe, J. Dardis, N. Jones, and P. L. Green, "Automatic quality assessments of laser powder bed fusion builds from photodiode sensor measurements," *Progress in Additive Manufacturing*, pp. 1–18, 2022.

[43] K. Y. Au-yeung, B. Yang, L. Sun, K. Bai, and Z. Yang, "Super Damping of Mechanical Vibrations," *Scientific Reports*, pp. 1–10, 2019.

[44] H. Frahm, "Device for damping vibrations of bodies." US Patent 989958, April 1909.

[45] X. Lu, Q. Zhang, D. Weng, Z. Zhou, S. Wang, S. A. Mahin, S. Ding, and F. Qian, "Improving performance of a super tall building using a new eddy-current tuned mass damper," *Structural Control and Health Monitoring*, vol. 24, no. 3, p. e1882, 2017. e1882 STC-15-0170.R1.

[46] S. Elias and V. Matsagar, "Research developments in vibration control of structures using passive tuned mass dampers," *Annual Reviews in Control*, vol. 44, pp. 129–156, 2017.

[47] K. K. Reichl and D. J. Inman, "Lumped mass model of a 1d metastructure for vibration suppression with no additional mass," *Journal of Sound and Vibration*, vol. 403, pp. 75–89, 2017.

[48] K. K. Reichl, *Active metastructures for light-weight vibration suppression.* PhD thesis, University of Michigan, 2018.

[49] O. Abdeljaber, O. Avci, S. Kiranyaz, and D. J. Inman, "Optimization of linear zigzag insert metastructures for low-frequency vibration attenuation using genetic algorithms," *Mechanical Systems and Signal Processing*, vol. 84, pp. 625–641, 2017.

[50] G. Raze, *Piezoelectric Digital Vibration Absorbers for Multimodal Vibration Mitigation of Complex Mechanical Structures.* PhD thesis, Universite de Liege, 2021.

[51] T. Asami, O. Nishihara, and A. M. Baz, "Analytical solutions to hinf and h2 optimization of dynamic vibration absorbers attached to damped linear systems," *Journal of Vibration and Acoustics*, vol. 124, pp. 284–295, 03 2002.

[52] O. Nishihara and T. Asami, "Closed-Form Solutions to the Exact Optimizations of Dynamic Vibration Absorbers (Minimizations of the Maximum Amplitude Magnification Factors) ," *Journal of Vibration and Acoustics*, vol. 124, pp. 576–582, 09 2002.

[53] G. Calafiore and M. C. Campi, "Uncertain convex programs: randomized solutions and confidence levels," *Mathematical Programming*, vol. 102, no. 1, pp. 25–46, 2005.

[54] P. Dumond, D. Monette, F. Alladkani, J. Akl, and I. Chikhaoui, "Simplified setup for the vibration study of plates with simply-supported boundary conditions," *MethodsX*, vol. 6, no. July, pp. 2106–2117, 2019.

[55] S. Cantero-Chinchilla, A. T. Fabro, H. Meng, W.-J. Yan, C. Papadimitriou, and D. Chronopoulos, "Robust optimised design of 3D printed elastic metastructures: A trade-off between complexity and vibration attenuation," *Journal of Sound and Vibration*, vol. 529, no. September 2021, p. 116896, 2022.

[56] D. Beli, A. T. Fabro, M. Ruzzene, and J. R. F. Arruda, "Wave attenuation and trapping in 3d printed cantilever-in-mass metamaterials with spatially correlated variability," *Scientific Reports*, no. March, pp. 1–12, 2019.

[57] A. T. Fabro, H. Meng, and D. Chronopoulos, "Uncertainties in the attenuation performance of a multi-frequency metastructure from additive manufacturing," *Mechanical Systems and Signal Processing*, vol. 138, p. 106557, 2020.

[58] F. Demoly, M. L. Dunn, K. L. Wood, H. J. Qi, and J.-C. André, "The status, barriers, challenges, and future in design for 4d printing," *Materials & Design*, vol. 212, p. 110193, 2021.

[59] R. Belotti, H. Ouyang, and D. Richiedei, "A new method of passive modifications for partial frequency assignment of general structures," *Mechanical Systems and Signal Processing*, vol. 99, pp. 586–599, Jan. 2018.

[60] L. Zhang, T. Zhang, H. Ouyang, T. Li, and M. You, "Natural frequency assignment of a pipeline through structural modification in layout optimization of elastic supports," *Journal of Sound and Vibration*, p. 117702, Apr. 2023.

[61] R. Sedaghati, A. Suleman, and B. Tabarrok, "Structural Optimization with Frequency Constraints Using the Finite Element Force Method," *AIAA Journal*, vol. 40, pp. 382–388, Feb. 2002.

[62] M. Fischer, D. Kennedy, and C. Featherson, "Multilevel Optimization of a Composite Aircraft Wing Using Viconopt MLO," in *9th AIAA/ISSMO Symposium on Multidisciplinary Analysis and Optimization*, (Atlanta, Georgia), American Institute of Aeronautics and Astronautics, Sept. 2002.

[63] X. Huang, Z. Zuo, and Y. Xie, "Evolutionary topological optimization of vibrating continuum structures for natural frequencies," *Computers and Structures*, vol. 88, no. 5-6, pp. 357–364, 2010.

[64] J.-H. Zhu, W.-H. Zhang, and L. Xia, "Topology Optimization in Aircraft and Aerospace Structures Design," *Archives of Computational Methods in Engineering*, vol. 23, pp. 595–622, Dec. 2016.

[65] J. E. Mottershead and Y. M. Ram, "Inverse eigenvalue problems in vibration absorption: Passive modification and active control," *Mechanical Systems and Signal Processing*, vol. 20, pp. 5–44, Jan. 2006.

[66] J. T. Weissenburger, "Effect of Local Modifications on the Vibration Characteristics of Linear Systems," *Journal of Applied Mechanics*, vol. 35, pp. 327–332, June 1968.

[67] R. J. Pomazal and V. W. Snyder, "Local Modifications of Damped Linear Systems," *AIAA Journal*, vol. 9, pp. 2216–2221, Nov. 1971.

[68] G. Lallement and S. Cogan, "Parametric Identification Based on Pseudo-Tests," in *Modal Analysis and Testing* (J. M. M. Silva and N. M. M. Maia, eds.), pp. 265–280, Dordrecht: Springer Netherlands, 1999.

[69] J. Mottershead and G. Lallement, "Vibration Nodes, and the Cancellation of Poles and Zeros by Unit-Rank Modifications to Structures," *Journal of Sound and Vibration*, vol. 222, pp. 833–851, May 1999.

[70] O. Zarraga, I. Ulacia, J. M. Abete, and H. Ouyang, "Receptance based structural modification in a simple brake-clutch model for squeal noise suppression," *Mechanical Systems and Signal Processing*, vol. 90, pp. 222–233, June 2017.

[71] H. Liu, H. Gao, and Y. Ma, "Receptance-based assignment of dynamic characteristics: A summary and an extension," *Mechanical Systems and Signal Processing*, vol. 145, p. 106913, Nov. 2020.

[72] R. Belotti, D. Richiedei, and A. Trevisani, "Multi-domain optimization of the eigenstructure of controlled underactuated vibrating systems," *Structural and Multidisciplinary Optimization*, vol. 63, pp. 499–514, Jan. 2021.

[73] G. Martin, E. Balmes, T. Chancelier, S. Thouviot, and R. Lemarie, "A Structural Dynamics Modification Strategy based on Expanded Squeal Operational Deflection Shapes," in *EuroBrake 2022 - Technical Content*, FISITA, 2022.

[74] A. Deraemaeker, *Sur la maîtrise des modèles en dynamique des structures à partir de résultats d'essais.* PhD thesis, Ecole Normale Supérieure, 2001.

[75] A. Kuczkowiak, S. Cogan, M. Ouisse, E. Foltête, and M. Corus, "Robust expansion of experimental mode shapes under epistemic uncertainties," in *Model Validation and Uncertainty Quantification, Volume 3* (H. S. Atamturktur, B. Moaveni, C. Papadimitriou, and T. Schoenherr, eds.), (Cham), pp. 419–427, Springer International Publishing, 2014.

[76] E. Balmes, "Review and evaluation of shape expansion methods," in *International Modal Analysis Conference*, vol. 4062, pp. 555–561, 2000.

[77] P. Ladeveze and D. Leguillon, "Error estimate procedure in the finite element method and applications," *SIAM Journal on Numerical Analysis*, vol. 20, no. 3, pp. 485–509, 1983.

[78] I. Isasa, A. Hot, S. Cogan, and E. Sadoulet-Reboul, "Model updating of locally nonlinear systems based on multi-harmonic extended constitutive relation error," *Mechanical Systems and Signal Processing*, vol. 25, no. 7, pp. 2413–2425, 2011.

[79] P. Ladevèze, G. Puel, A. Deraemaeker, and T. Romeuf, "Validation of structural dynamics models containing uncertainties," *Computer Methods in Applied Mechanics and Engineering*, vol. 195, no. 4, pp. 373–393, 2006. Adaptive Modeling and Simulation.

[80] D. Tcherniak, "Topology optimization of resonating structures using SIMP method," *International Journal for Numerical Methods in Engineering*, vol. 54, pp. 1605–1622, Aug. 2002.

[81] M. P. Bendsøe and O. Sigmund, *Topology optimization: theory, methods, and applications.* Berlin ; New York: Springer, 2003.

[82] D. Giannini, F. Braghin, and N. Aage, "Topology optimization of 2D in-plane single mass MEMS gyroscopes," *Structural and Multidisciplinary Optimization*, vol. 62, no. 4, pp. 2069–2089, 2020. Publisher: Structural and Multidisciplinary Optimization.

[83] A. Ugural, *Plates and Shells: Theory and Analysis, Fourth Edition*. Applied and Computational Mechanics, CRC Press, 2017.

[84] J. Gripp and D. Rade, "Vibration and noise control using shunted piezoelectric transducers: A review," *Mechanical Systems and Signal Processing*, vol. 112, pp. 359–383, Nov. 2018.

[85] R. L. Forward, "Electronic damping of vibrations in optical structures," *Appl. Opt.*, vol. 18, pp. 690–697, Mar 1979.

[86] N. W. Hagood and A. v. Flotow, "Damping of structural vibrations with piezoelectric materials and passive electrical networks," *Journal of Sound and Vibration*, vol. 146, no. 2, pp. 243–268, 1991.

[87] P. Soltani, G. Kerschen, G. Tondreau, and A. Deraemaeker, "Piezoelectric vibration damping using resonant shunt circuits: An exact solution," *Smart Materials and Structures*, vol. 23, no. 12, 2014.

[88] S.-M. Kim, S. Wang, and M. J. Brennan, "Dynamic analysis and optimal design of a passive and an active piezo-electrical dynamic vibration absorber," *Journal of Sound and Vibration*, vol. 330, no. 4, pp. 603–614, 2011.

[89] O. Thomas, J. Ducarne, and J.-F. Deü, "Performance of piezoelectric shunts for vibration reduction," *Smart Materials and Structures*, vol. 21, p. 015008, Jan. 2012.

[90] G. Raze, *Piezoelectric Digital Vibration Absorbers for Multimodal Vibration Mitigation of Complex Mechanical Structures*. PhD thesis, University of Liege, 2021.

[91] J. J. Hollkamp and J. Thomas F. Starchville, "A self-tuning piezoelectric vibration absorber," *Journal of Intelligent Material Systems and Structures*, vol. 5, no. 4, pp. 559–566, 1994.

[92] A. J. Fleming and S. O. R. Moheimani, "Adaptive piezoelectric shunt damping," *Smart Materials and Structures*, vol. 12, p. 36, jan 2003.

[93] D. Niederberger, A. Fleming, S. O. R. Moheimani, and M. Morari, "Adaptive multimode resonant piezoelectric shunt damping," *Smart Materials and Structures*, vol. 13, p. 1025, jul 2004.

[94] P. Gardonio, G. Konda Rodrigues, L. Dal Bo, and E. Turco, "Extremum seeking online tuning of a piezoelectric vibration absorber based on the maximisation of the shunt electric power absorption," *Mechanical Systems and Signal Processing*, vol. 176, p. 109171, Aug. 2022.

[95] G. Konda Rodrigues, P. Gardonio, L. Dal Bo, and E. Turco, "Piezoelectric patch vibration control unit connected to a self-tuning RL-shunt set to maximise electric power absorption," *Journal of Sound and Vibration*, vol. 536, p. 117154, Oct. 2022.

[96] M. Auleley, O. Thomas, C. Giraud-Audine, and H. Mahé, "Enhancement of a dynamic vibration absorber by means of an electromagnetic shunt," *Journal of Intelligent Material Systems and Structures*, vol. 32, pp. 331–354, Feb. 2021.

[97] M. Auleley, C. Giraud-Audine, H. Mahé, and O. Thomas, "Tunable electromagnetic resonant shunt using pulse-width modulation," *Journal of Sound and Vibration*, vol. 500, p. 116018, May 2021.

[98] X. Wang, D. Wang, F. Li, Y. Zhang, Z. Xu, T. Wang, G. Fu, and C. Lu, "Self-learning vibration absorber with negative electromagnetic stiffness for variable vibration," *International Journal of Mechanical Sciences*, vol. 248, p. 108225, June 2023.

[99] H. Song, X. Shan, L. Zhang, G. Wang, and J. Fan, "Research on identification and active vibration control of cantilever structure based on NARX neural network," *Mechanical Systems and Signal Processing*, vol. 171, p. 108872, May 2022.

[100] M. Maiworm, *Gaussian process in control : model predictive control with guarantees and control of scanning quantum dot microscopy*. PhD thesis, Otto-von-Guericke-Universität Magdeburg, Fakultät für Elektrotechnik und Informationstechnik, 2021.

[101] M. Maiworm, C. Wagner, R. Temirov, F. S. Tautz, and R. Findeisen, "Two-degree-of-freedom control combining machine learning and extremum seeking for fast scanning quantum dot microscopy," in *2018 Annual American Control Conference (ACC)*, pp. 4360–4366, 2018.

[102] B. Lossouarn, M. Aucejo, J. F. Deu, and B. Multon, "Design of inductors with high inductance values for resonant piezoelectric damping," *Sensors and Actuators, A: Physical*, vol. 259, pp. 68–76, 2017. Publisher: Elsevier B.V.

[103] V. Valchev and A. Van den Bossche, *Inductors and Transformers for Power Electronics*. CRC Press, 2018.

[104] T. Duriez, S. L. Brunton, and B. R. Noack, *Machine Learning Control – Taming Nonlinear Dynamics and Turbulence*, vol. 116 of *Fluid Mechanics and Its Applications*. Cham: Springer International Publishing, 2017.

[105] P. Fleming and R. Purshouse, "Evolutionary algorithms in control systems engineering: a survey," *Control Engineering Practice*, vol. 10, pp. 1223–1241, Nov. 2002.

[106] S. L. Brunton and J. N. Kutz, *Data-Driven Science and Engineering: Machine Learning, Dynamical Systems, and Control*. Cambridge University Press, 1 ed., Jan. 2019.

[107] R. Li, B. R. Noack, L. Cordier, J. Borée, and F. Harambat, "Drag reduction of a car model by linear genetic programming control," *Experiments in Fluids*, vol. 58, p. 103, Aug. 2017.

[108] C. E. R. . C. K. I. Williams, *Gaussian Processes for Machine Learning*. Massachusetts Institute of Technology, 2006. ISSN: 10236090.

[109] K. Worden and P. Green, "A machine learning approach to nonlinear modal analysis," *Mechanical Systems and Signal Processing*, vol. 84, pp. 34–53, 2017. Recent advances in nonlinear system identification.

[110] E. Bachy, K. Jaboviste, E. Sadoulet-Reboul, N. Peyret, G. Chevallier, C. Arnould, and E. Collard, "Investigations on the performance and the robustness of a metabsorber designed for structural vibration mitigation," *Mechanical Systems and Signal Processing*, vol. 170, p. 108830, May 2022.

[111] M. Frivaldsky, M. Pipiska, M. Zurek-Mortka, and D. Andriukaitis, "PFC Inductor Design Considering Suppression of the Negative Effects of Fringing Flux," *Applied Sciences*, vol. 12, p. 6815, July 2022.

[112] M. Gasior and J. Gonzalez, "Improving fft frequency measurement resolution by parabolic and gaussian spectrum interpolation," in *AIP Conference Proceedings*, vol. 732, pp. 276–285, American Institute of Physics, 2004.

[113] A. Cully, J. Clune, D. Tarapore, and J.-B. Mouret, "Robots that can adapt like animals," *Nature*, vol. 521, no. 7553, pp. 503–507, 2015.

[114] *Artificial Intelligence for Active Vibration Control Optimization on Smart Structures*, vol. ASME 2023 Conference on Smart Materials, Adaptive Structures and Intelligent Systems of *Smart Materials, Adaptive Structures and Intelligent Systems*, 09 2023.

[115] C. Deng, Y. Wang, C. Qin, Y. Fu, and W. Lu, "Self-directed online machine learning for topology optimization," *Nature Communications*, vol. 13, p. 388, Jan. 2022.

[116] A. Lederer, A. J. O. Conejo, K. A. Maier, W. Xiao, J. Umlauft, and S. Hirche, "Gaussian process-based real-time learning for safety critical applications," in *International Conference on Machine Learning*, pp. 6055–6064, PMLR, 2021.

Appendix A1

Appendix Chapter 2

A1.1 Details of experimental setup

In this appendix, the experimental setup developed for the application of the self-design manufacturing paradigm is detailed. The main dimensions of the beam-like absorber inserted in the plate and its support structure are shown in Figure A1.1. As can be noted, the simply supported boundary condition was ensured by means of a V-groove supporting the plate which prevents translation movements, but allows rotation in the perpendicular direction of the main vibration of the plate.

Photographs detailing the assembly of the support structure are shown in Figure A1.2. The support structure presents a considerable distance between the base and the plate to allow for the positioning of a loudspeaker underneath the plate, which is responsible for its excitation in the experimental modal analysis. The cavities on the sides of the support structure are required to allow the wires connected to the loudspeaker to pass through. This design idea was inspired by a recent paper published by Dumond et al [54].

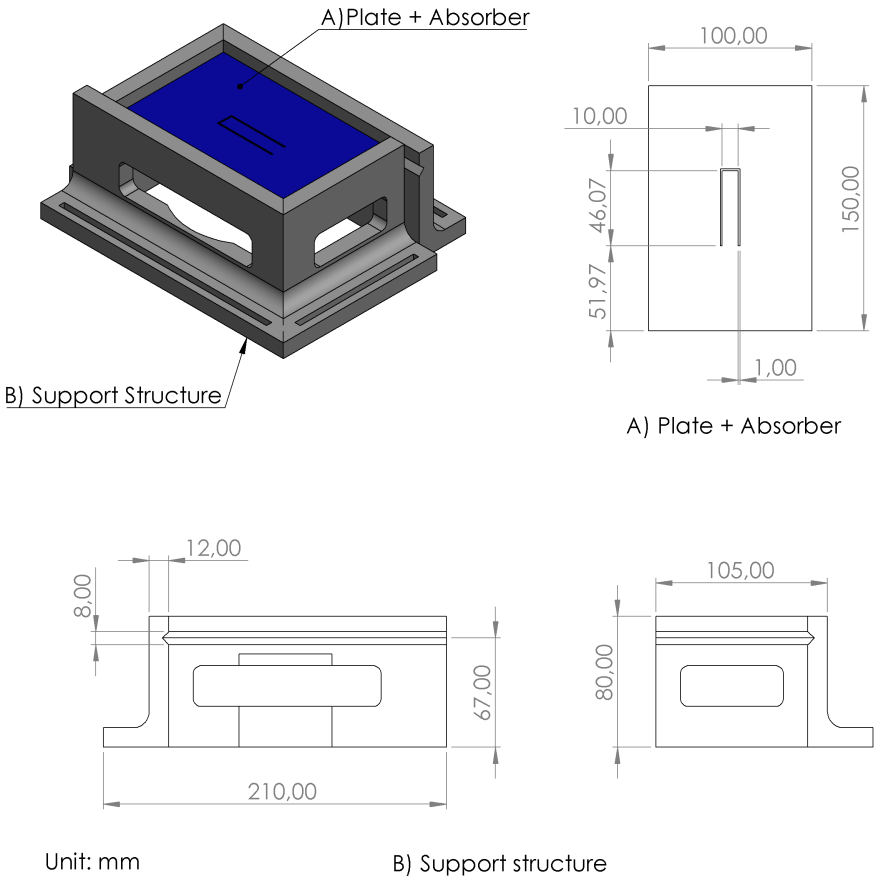

Figure A1.1: Dimensions of the structure constructed in the demonstration case of the beam-like vibration absorber inserted in a plate.

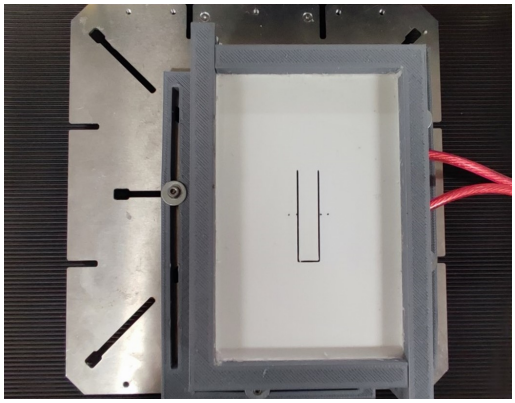

(a)

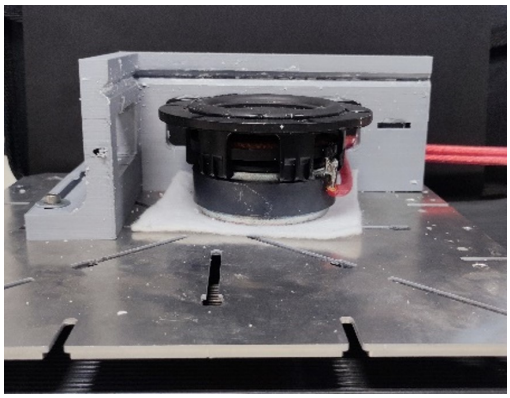

(b)

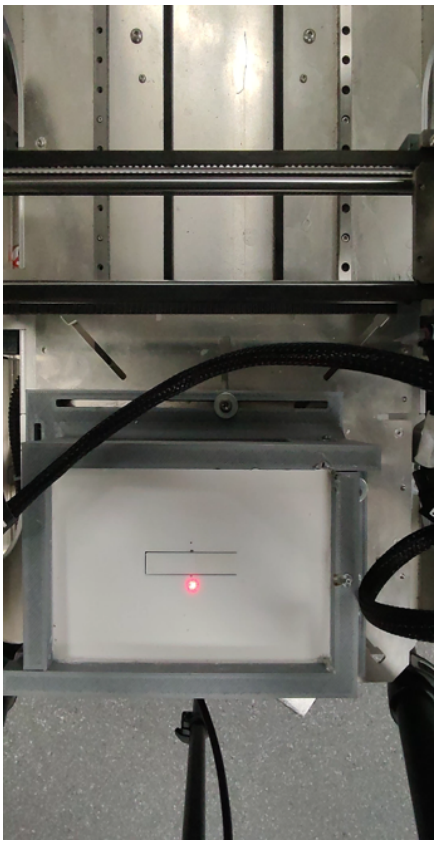

(c)

Figure A1.2: Photographs of details of the experimental assembly of the support structure and plate.

Appendix A2

Appendix Chapter 3

A2.1 Flexural vibration of thin plate bending elements

This appendix section presents the details of the formulation of the elementary mass and stiffness matrices for the finite element model of thin plate-like structures presented in [1] and used in this work in Chapter 3. Plate structures can be analyzed by dividing the plate into a set of two-dimensional finite elements called plate bending elements. The elements considered in the plate-like structure studied in this work are rectangular in shape.

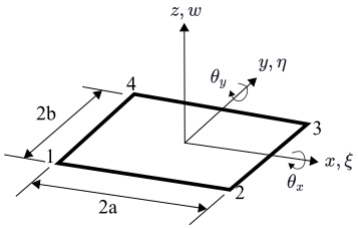

Figure A2.1: Geometry of a rectangular plate bending element. Adapted from [1].

An illustration of the shape geometry of the element considered is shown in Figure A2.1.Each node in a plate element has three degrees of freedom: the displacement normal to the plane of the plate, w, and two rotations, θ_x and θ_y. This element is commonly referred to as the ACM element and its displacement function can be represented by following polynomial :

$$\begin{aligned} w =& \alpha_1 + \alpha_2\xi + \alpha_3\eta + \alpha_4\xi^2 + \alpha_5\xi\eta + \alpha_6\eta^2 \\ &+ \alpha_7\xi^3 + \alpha_8\xi^2\eta + \alpha_9\xi\eta^2 + \alpha_{10}\eta^3 + \alpha_{11}\xi^3\eta + \alpha_{12}\xi\eta^3 \end{aligned} \tag{A2.1}$$

This expression can written in the following matrix form:

$$\begin{aligned} w &= \begin{bmatrix} \mathbf{N}_1(\xi,\eta) & \mathbf{N}_2(\xi,\eta) & \mathbf{N}_3(\xi,\eta) & \mathbf{N}_4(\xi,\eta) \end{bmatrix} \{\mathbf{w}\}_e \\ &= \lfloor \mathbf{N}(\xi,\eta) \rfloor \{\mathbf{w}\}_e \end{aligned} \tag{A2.2}$$

where

$$\mathbf{N}_j^{\mathrm{T}}(\xi,\eta) = \begin{bmatrix} \frac{1}{8}\left(1+\xi_j\xi\right)\left(1+\eta_j\eta\right)\left(2+\xi_j\xi+\eta_j\eta-\xi^2-\eta^2\right) \\ (b/8)\left(1+\xi_j\xi\right)\left(\eta_j+\eta\right)\left(\eta^2-1\right) \\ -(a/8)\left(\xi_j+\xi\right)\left(\xi^2-1\right)\left(1+\eta_j\eta\right) \end{bmatrix} \tag{A2.3}$$

$$\{\mathbf{w}\}_e^{\mathrm{T}} = \begin{bmatrix} w_1 & \theta_{x1} & \theta_{y1} & \cdots & w_4 & \theta_{x4} & \theta_{y4} \end{bmatrix} \tag{A2.4}$$

A2.1.1 Element mass matrix

Based on the kinetic energy of the element, the element mass matrix is defined by [1]:

$$[\mathbf{m}]_e = \int_{\mathrm{A}_e} \rho h \lfloor \mathbf{N} \rfloor^{\mathrm{T}} \lfloor \mathbf{N} \rfloor \mathrm{dA} \tag{A2.5}$$

A2.1.2 Element stiffness matrix

Based on the strain energy of the element, the element stiffness matrix is defined :

$$[\mathbf{k}]_e = \int_{\mathrm{A}_e} \frac{h^3}{12} [\mathbf{B}]^{\mathrm{T}} [\mathbf{D}] [\mathbf{B}] \mathrm{dA} \tag{A2.6}$$

where the strain-displacement matrix **B** is given by:

$$[\mathbf{B}] = \begin{bmatrix} \frac{\partial^2}{\partial x^2} \\ \frac{\partial^2}{\partial y^2} \\ 2\frac{\partial^2}{\partial x \partial y} \end{bmatrix} \lfloor \mathbf{N} \rfloor = \begin{bmatrix} \frac{1}{a^2} & \frac{\partial^2}{\partial \xi^2} \\ \frac{1}{b^2} & \frac{\partial^2}{\partial \eta^2} \\ \frac{2}{ab} & \frac{\partial^2}{\partial \xi \partial \eta} \end{bmatrix} \lfloor \mathbf{N}(\xi,\eta) \rfloor \tag{A2.7}$$

A2.2 Case study of topology optimization approach

In this appendix section we present a case study of the application of the topology optimization based on the traditional paradigm to the problem of natural frequency assignment of a plate-like structure. The experimental application presented in this case study helps to highlight the challenges of applying this approach to the problem of assigning natural frequencies with high precision, which was addressed in Chapter 3 of this thesis based on the self-design manufacturing paradigm.

The illustrative problem proposed in this case study consists of the design and fabrication of a thin aluminium plate of 90x90 mm with a variable thickness profile and with its first three natural frequencies assigned to 524, 655 and 786 Hz respectively, considering free boundary condition. The combination of these frequencies produces the sound of a *Do major* chord and has a frequency ratio of 1, 1.25 and 1.5, respectively, relative to the first. This particular frequency ratio produces a consonant sound that is attractive to the human ear. Slight variations in this frequency ratio can produce a much less attractive dissonant sound. Therefore, in this merely illustrative context, high precision in frequency assignment is very important.

	E [GPa]	ρ [kg/m^3]	v
FEM Model	71	2700	0.34

Table A2.1: Material properties of the finite element model.

Mode	FEM Model		Manufactured Plate	
	ω_n [Hz]	ω_1/ω_n	ω_n [Hz]	ω_1/ω_n
1	404.1	1.00	394.5	1.00
2	591.9	1.46	597.6	1.51
3	756.0	1.87	764.4	1.94

Table A2.2: Comparison of the natural frequencies of the FEM model and the manufactured plate for the initial plate design with constant thickness of 1mm.

In this case study, the aim of applying the topology optimization method is to determine the thickness profile of the plate in order to assign the desired natural frequencies. Initially, an aluminium plate of 90x90 mm with a constant thickness of 1 mm is considered. A finite element model of this structure considering solid elements was built using the Partial Differential Equation Toolbox in Matlab. The material properties considered for the model are shown in Table A2.1. The first three eigenfrequencies obtained from this model are shown in Table A2.2. To validate the model, this same plate was manufactured (see Figure A2.2) and experimental modal analysis was carried out to obtain its eigenfrequencies, which are shown in Table A2.2. As can be seen, the model predicts the natural frequencies of the plate with a low error of less than 3%.

The topology optimization problem is formulated in a similar way to the one presented in Section 2, based on the SIMP model and the physics interpretation of the relative density as the thickness of the plate elements. The MMA method is also used here to solve the optimization problem. The goal is to obtain a plate design based solely on the finite element model of the structure with the natural frequencies precisely assigned. Once this design has been obtained, the plate is manufactured in a separate step according to the sequential life cycle of the traditional structure development paradigm. The formulation of the topology optimization problem is presented below:

Figure A2.2: Photograph of the constant thickness plate manufactured.

$$\begin{aligned} \underset{\boldsymbol{x}}{\text{minimize}} \quad & f(\boldsymbol{x}) = \sum_{i=1}^{\mathrm{M}} \left(\frac{\omega_i(\boldsymbol{x}) - \overline{\omega}_i}{\overline{\omega}_i} \right)^2 \\ \text{subject to} \quad & \sum_{e=1}^{\mathrm{N}} v_e x_e = \mathbf{v}^{\mathrm{T}} \boldsymbol{x} \leq \mathrm{V}^* \\ & 0 < x_{min} \leq x_e \leq 1 \end{aligned} \tag{A2.8}$$

where $\omega_i(\boldsymbol{x})$ is the i-th natural frequency for the current topology, $\overline{\omega_i}$ the i-th natural frequency assigned, M is number of modes considered, N is the number of finite elements of ht model and V^* is a volume of the admissible design domain and $x_m in$ is the lower bound of the design variable. In this case study, the minimum thickness of the plate is defined as 1 mm by setting the lower limit of the relative density of each element x_e to 0.1, since the thickness of the plate element considered is $h = 10$ mm.

The results of the topology optimization are shown in Figure A2.4. It can be observed the convergence of the objective function after 40 iterations. The evolution of the topology throughout the optimization is shown in Figure A2.4(c). The final topology obtained is transformed into a solid geometry whose graphical representation is shown in Figure A2.3(a). This solid geometry was fabricated in a CNC machining center used to mill the part from a 10 mm thick aluminum plate which was then cut using the wire electrical discharge machining process, see the photograph in A2.3(b). The natural frequencies identified by the experimental modal analysis of the manufactured plate are presented in Table A2.3. Although the natural frequencies of the FEM model are precisely assigned to the defined frequencies, there is a significant deviation for the frequencies of the plate manufactured with the optimized topology. A deviation of this order was unexpected, since a much less significant deviation was found for the initial case with constant thickness. A plausible explanation for this was revealed through detailed analysis of the part and the manufacturing process. A small angular cutting deviation was found on the flat face of the plate, which is associated with the cutting stage of the plate by the wire electrical discharge machining process. Although this deviation can be corrected with other manufacturing processes such as grinding, this was not the aim of this case study but rather to show the challenges of manufacturing this type of structure with precisely assigned frequencies in a real environment subject to the traditional product development paradigm. In addition, despite a significant deviation in the absolute values of the natural frequencies, it can be seen that the frequency rates were close to those expected.

Mode	Assigned Frequencies		FEM Model		Manufactured Plate	
	ω_n	ω_1/ω_n	ω_n	ω_1/ω_n	ω_n	ω_1/ω_n
1	524	1.00	524.1	1.00	631.3	1.00
2	655	1.25	654.2	1.25	842.0	1.33
3	786	1.50	786.7	1.50	1005.2	1.59

Table A2.3: Comparison of the natural frequencies of the FEM model and the manufactured physical structure for the design obtained by topology optimization.

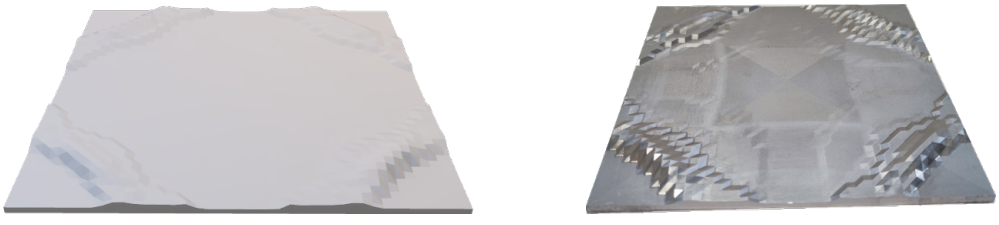

(a) 3D model (b) Manufactured plate

Figure A2.3: (a) 3D graphic representation of the plate design obtained by topology optimization and a photograph of the corresponding manufacturing board.

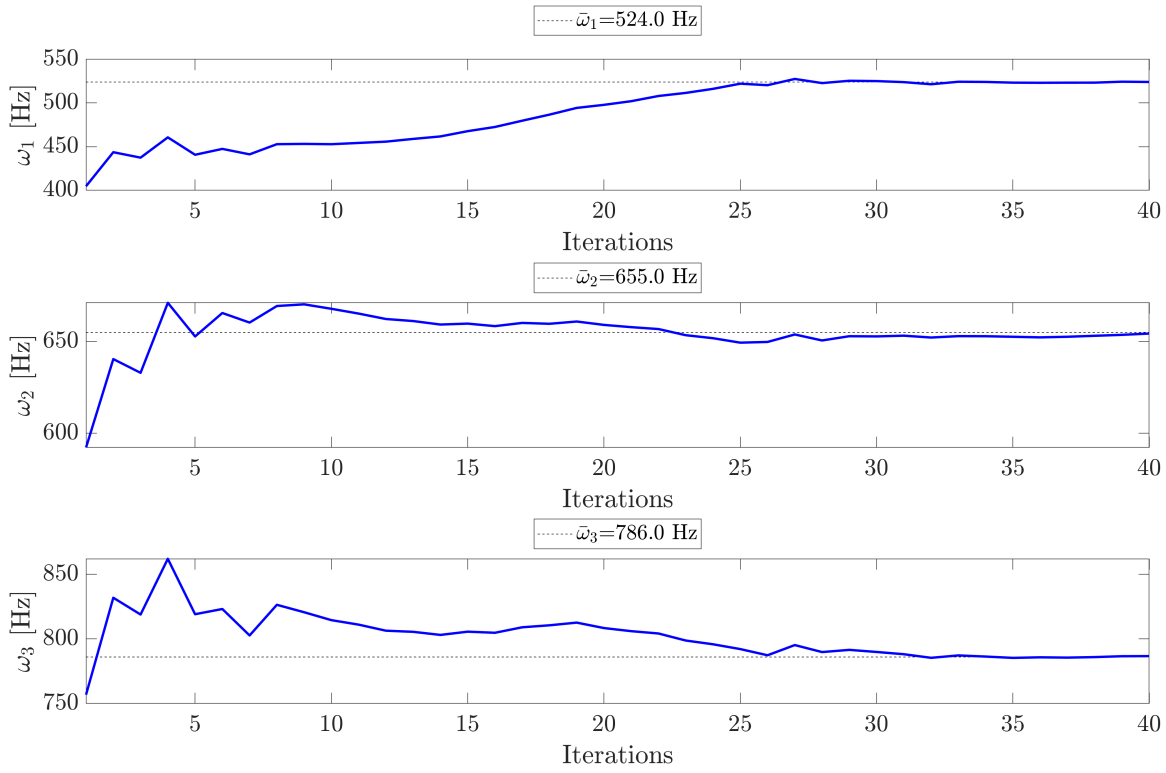

(a) Natural frequencies

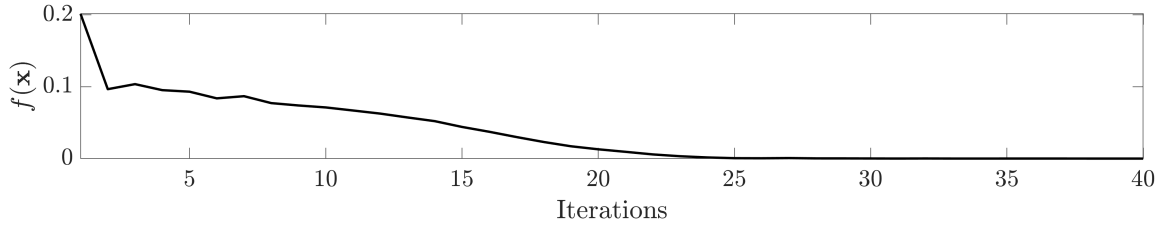

(b) Objective function

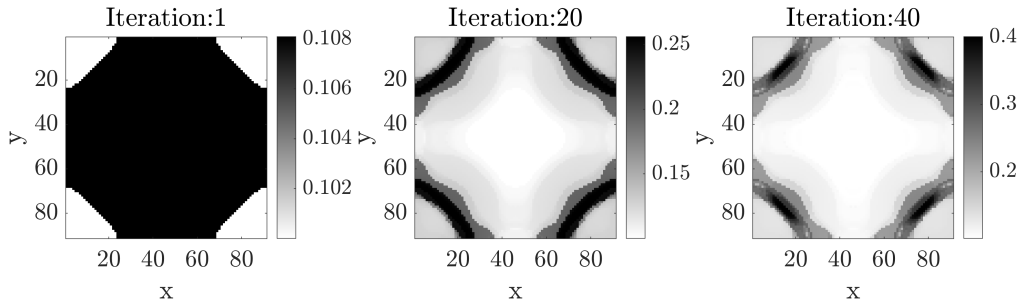

(c) Design topology in iterations: 1, 30 and 64

Figure A2.4: Topology optimization.

Titre : Paradigmes de conception auto-adaptative pour le développement de structures à haute performance : du processus de fabrication au contrôle des vibrations en temps réel

Mots clés : Structures auto-adaptatives, Optimisation Topologique, Conception Robuste, Vibrations, Structures intelligentes, Incertitudes

Résumé : Le développement de structures d'ingénierie complexes s'appuie fortement sur l'*intelligence computationnelle* sous la forme de modèles prédictifs basés sur la physique et sur le concept de robustesse face aux incertitudes pour soutenir les décisions de conception. Cette approche nécessite que les incertitudes liées à la modélisation, à la fabrication et au fonctionnement de la structure soient explicitement prises en compte, ce qui conduit inévitablement à un compromis entre performance et robustesse. Ce point est particulièrement important pour les applications à haut enjeu, car pour une conception candidate donnée, les modifications apportées afin d'avoir une conception robuste tout en garantissant une performance acceptable aboutissent à des conceptions sous-optimales avec une performance dégradée. Pour contourner cette situation, cette thèse propose d'étudier un changement de paradigme dans la façon dont les incertitudes sont gérées à travers le concept bio-inspiré de plasticité développementale, qui vise à fournir à la structure la capacité d'adapter sa conception tout au long de sa fabrication et de son fonctionnement. Dans ce contexte, deux paradigmes sont proposés : le paradigme des structures auto-architecturantes pour traiter les incertitudes pendant le processus de fabrication, et le paradigme des structures auto-adaptatives pour traiter les incertitudes affectant la phase de fonctionnement. Le paradigme des structures auto-architecturantes se fonde sur un processus en boucle fermée entre la conception et la fabrication en tirant parti de *l'intelligence physique* sous la forme d'observations expérimentales en temps réel. Ce paradigme est exploré dans deux problèmes d'application de la dynamique des structures : premièrement, la réalisation d'un absorbeur de vibrations à haute performance et deuxièmement, l'assignation des fréquences propres avec une haute précision. Dans le premier problème, le paradigme proposé est appliqué à la réalisation d'une plaque avec un absorbeur en forme de poutre introduit pour réduire les vibrations sur la base du critère de performance dit equal-peak. La démonstration expérimentale est réalisée à l'aide d'une imprimante 3D équipée d'un système de test de vibration en ligne et pilotée par un algorithme de décision basé sur des données expérimentales. Les performances d'une population de plaques auto-architecturées sont comparées à celles de leurs homologues standardisés afin de mettre en évidence les avantages et les limites du paradigme proposé. Dans le second problème, le paradigme de structures auto-architecturantes est appliqué à un cas de démonstration numérique pour la réalisation d'une plaque dont les trois premières fréquences naturelles sont assignées avec haute précision à l'aide d'une méthodologie originale qui combine l'expansion modale et l'optimisation topologique. Dans le paradigme des structures auto-adaptatives, le concept de plasticité développementale est étendu pour traiter les incertitudes pendant le fonctionnement des structures grâce à la stratégie d'opération auto-adaptative. Ce paradigme est traduit dans le développement d'un absorbeur de vibrations piézoélectrique auto-adaptatif avec un shunt résonant accordable analogique, exploité expérimentalement pour la réduction des vibrations d'un prototype d'avion.

Université Bourgogne Franche-Comté
32, avenue de l'Observatoire
25000 Besançon

Title : Self-adaptive design paradigms for the development of high-performance systems: from the manufacturing process to real-time vibration control

Keywords : Self-adaptive structures, Topology optimization, Robust design, Vibration, Smart Structures, Uncertainties

Abstract : The development of complex engineering structures relies heavily on *computational intelligence* in the form of science-based predictive models and on the concept of robustness to uncertainties to support design decisions. This approach requires that modeling, manufacturing, and operational uncertainties be explicitly considered and leads to an inevitable trade-off of performance for robustness. This point is particularly important for high-performance applications, because for a given candidate design, modifications made to ensure acceptable performance under uncertainty result in sub-optimal designs with degraded performance. To remedy this situation, this thesis proposes to investigate a paradigm shift in the way uncertainties are handled in the development of structures through the bio-inspired concept of developmental plasticity, which aims to provide the structure with the ability to adapt its design throughout its fabrication and its operation. Two paradigms are proposed: the self-design manufacturing paradigm to address uncertainties during the fabrication of structures; and the self-adaptive design paradigm to tackle uncertainties affecting structure operation. The application of the self-design manufacturing paradigm is achieved by closing the loop between the design and manufacturing processes by leveraging *physical intelligence* in the form of real-time experimental observations. This paradigm is explored in two challenging structural dynamics application problems: first, the realization of a high-performance vibration absorber, and second, the assignment of natural frequencies with high accuracy. In the first problem, the proposed paradigm is applied to the realization of a simply supported plate with a beam-like absorber introduced to reduce vibrations based on an equal peak performance criterion. The experimental demonstration is performed using a low-cost 3D printer driven by a simple decision algorithm and equipped with an online vibration testing system. The performances of a small population of self-designed plates are compared to those of their standardized counterparts to highlight the advantages and limitations of the proposed paradigm. In the second problem, the self-design manufacturing paradigm is applied to a numerical demonstration case of the realization of a simply supported plate with the first three natural frequencies accurately assigned using a methodology that combines structural modification driven by topology optimization. In the second paradigm proposed in this thesis, the concept of developmental plasticity is extended to deal with uncertainties during the operation of structures through the self-adaptive design strategy. This paradigm is exploited in the development of a self-adaptive piezoelectric vibration absorber with analog tunable resonant shunt, experimentally demonstrated in the vibration reduction of an aircraft prototype.

Université Bourgogne Franche-Comté
32, avenue de l'Observatoire
25000 Besançon